Implementation of a Fuzzy Logic Based Set-Point Modulation Scheme with SVC System Applications

By:

Steven Lawrence Howell

A thesis submitted to the Faculty of Graduate Studies of

The University of Manitoba

in partial fulfillment of the requirements for the degree of:

Master of Science

Department of Electrical and Computer Engineering

University of Manitoba

Winnipeg, Manitoba

Acknowledgements

I would like to express my sincere gratitude to Dr. Shaahin Filizadeh for his guidance and support throughout the completion of my research. It was a privilege to work under his supervision.

I wish to thank Dr. David Jacobson and Mr. Pei Wang from Manitoba Hydro and Dan Kell from TransGrid Solutions (TGS) for their guidance and knowledge regarding the Ponton SVC system.

I would also like to thank the academic and technical staff of the Electrical and Computer Engineering department, and specifically Mr. Erwin Dirks and Dr. Aniruddha Gole, for their help and technical discussions.

Dedication

To my family and friends for their support.

Abstract

This thesis introduces a novel online set-point modulation (SPM) technique that employs fuzzy logic to adjust the timing and magnitude of control system set-points. After first applying fuzzy logic-enabled SPM to underdamped second order systems for testing purposes, the new scheme is then applied to an electromagnetic transient simulation model of Manitoba Hydro's existing Ponton SVC system, and the results are then compared to the original SVC system that uses traditional control approaches. Conclusions show that fuzzy logic-based SPM improves the controlled voltage's transient overshoot response to changes in the voltage set-point.

Table of Contents

List of Figures

List of Tables

List of Symbols

α	thyristor firing angle
ζ	damping ratio of a second order system
θ	power factor angle
$\mu(x)$	membership function
σ	thyristor conduction interval
ψ	phase shift of second order system response
ω	angular frequency
ω_0	system nominal frequency
ω_d	damped frequency of a second order system
ω_n	natural frequency of a second order system
ω_r	resonant frequency
ac	alternating current
B	susceptance
C	capacitance
CLR	current limiting reactor
FC-TCR	fixed capacitor-thyristor controller reactor
FIS	fuzzy inference system
G	conductance
GPG	gate pulse generator
I_{rms}	root mean squared current
j	imaginary number
K_I	integral gain

K_p	proportional gain
K_{sl}	SVC droop
L	inductance
M_p	overshoot of a second order system
P	real power
PLL	phase locked loop
pf	power factor
pu	per unit
Q	reactive power
S	apparent power
SPAA	set-point automatic adjustment
SPAACE	set-point automatic adjustment-correction enabled
SPM	set-point modulation
SVC	static var compensator
T_d	oscillation period of a second order system response
t_p	time to peak of a second order system
TCR	thyristor controlled reactor
TSC	thyristor switched capacitor
V_m	voltage magnitude
V_{rms}	root mean squared voltage
Y	admittance
Z	integer
¬	complement

$\Rightarrow$	implication
$\cap$	intersection operator
$\cup$	union operator

Chapter 1 Introduction

Transmission lines conduct electrical power over the distances that separate energy sources such as generating stations from demand centers such as cosmopolitan areas. Although these transmission lines must transmit more energy as power demand increases, cost and regulatory restrictions often render new transmission line construction infeasible, thereby necessitating more efficient use of existing transmission infrastructure [**1**].

Alternating current (ac) transmission systems transmit *apparent power*, which comprises both real, or *active*, and imaginary, or *reactive*, components in order to meet customer demand, or *load*. Real power is dissipated in the course of providing everyday functions such as heating, lighting, and electric motor operation. Some real power is also lost due to the resistance of the transmission line.

In contrast to the apparent power's real component, its reactive component does not dissipate but is instead temporarily stored throughout the transmission system in the form of electric and magnetic fields. Although technically incorrect, such reactive power storage is colloquially said to be *generated* or *consumed*. A component that stores energy in the form of electric fields is capacitive and is said to *generate*, or *inject*, *reactive power*. A component that stores energy in the form of magnetic fields is inductive and is said to *absorb*, or *consume reactive power*.

Although transmission lines exhibit both capacitive and inductive traits depending upon the amount of current flowing in the line [**2**], practical transmission lines tend to be inductive and therefore absorb rather than generate reactive power [**3**]. This is because

utilities load transmission lines to their maximum allowable limit during peak load periods in order to maximize asset utilization, and inductive characteristics become increasingly predominant as a transmission line carries more apparent power. Moreover, in addition to the transmission line's physical characteristics, the majority of load connected to the ac transmission system's terminal end is also inductive, which causes a further voltage drop at the terminal end of the transmission line. Reactive power is therefore absorbed both throughout the transmission line and at its terminal ends, as illustrated in Figure 1.1.

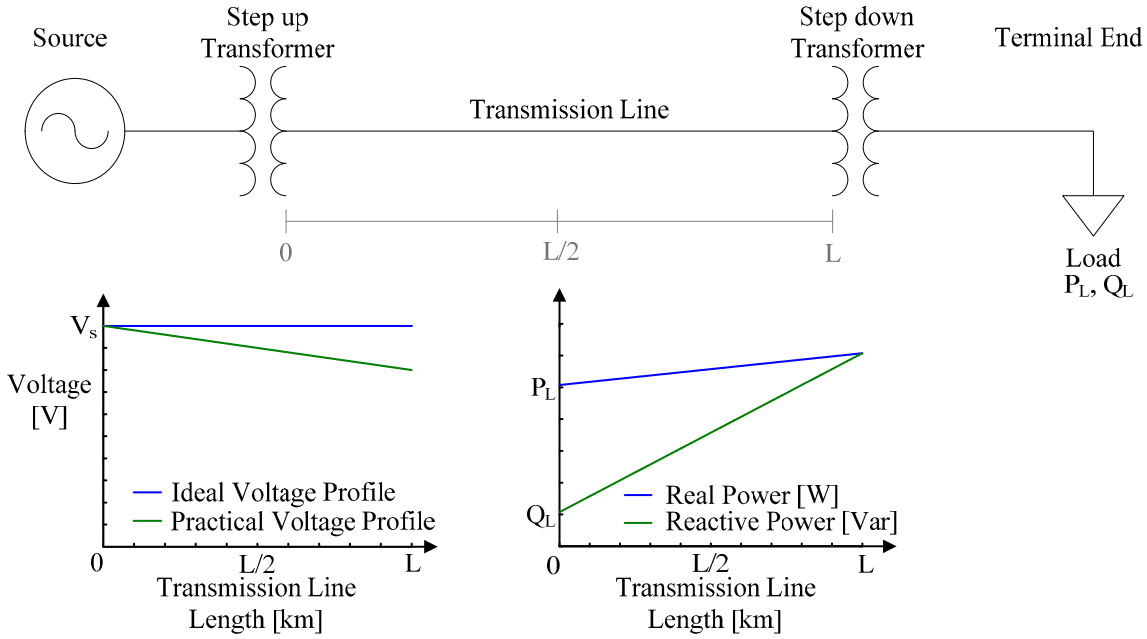

Figure 1.1: Transmission system without reactive power compensation

Although non-dissipative power is precluded from producing useful output, reactive power's presence helps maintain system voltage stability and is therefore necessary for the electrical system's successful operation. Despite this, the transmission line's fixed apparent power capacity results in reactive power storage reducing the amount of real power that can be transmitted and also decaying the *voltage profile* along the line.

Utilities therefore try to maximize real power transmission while supplying reactive power locally instead of transmitting it.

Reactive power compensation refers to the set of corrective measures undertaken to improve the transmission system's reactive power utilization. These methods employ reactive elements that can be either fixed or controllable in nature depending upon system requirements. Figure 1.2 illustrates *transmission line compensation's* ability to provide local reactive power through either series or shunt reactive elements that are connected somewhere along a transmission line. These elements alter the transmission line's voltage profile by either reducing its reactive power consumption or by causing it to behave as a reactive power source [**4**].

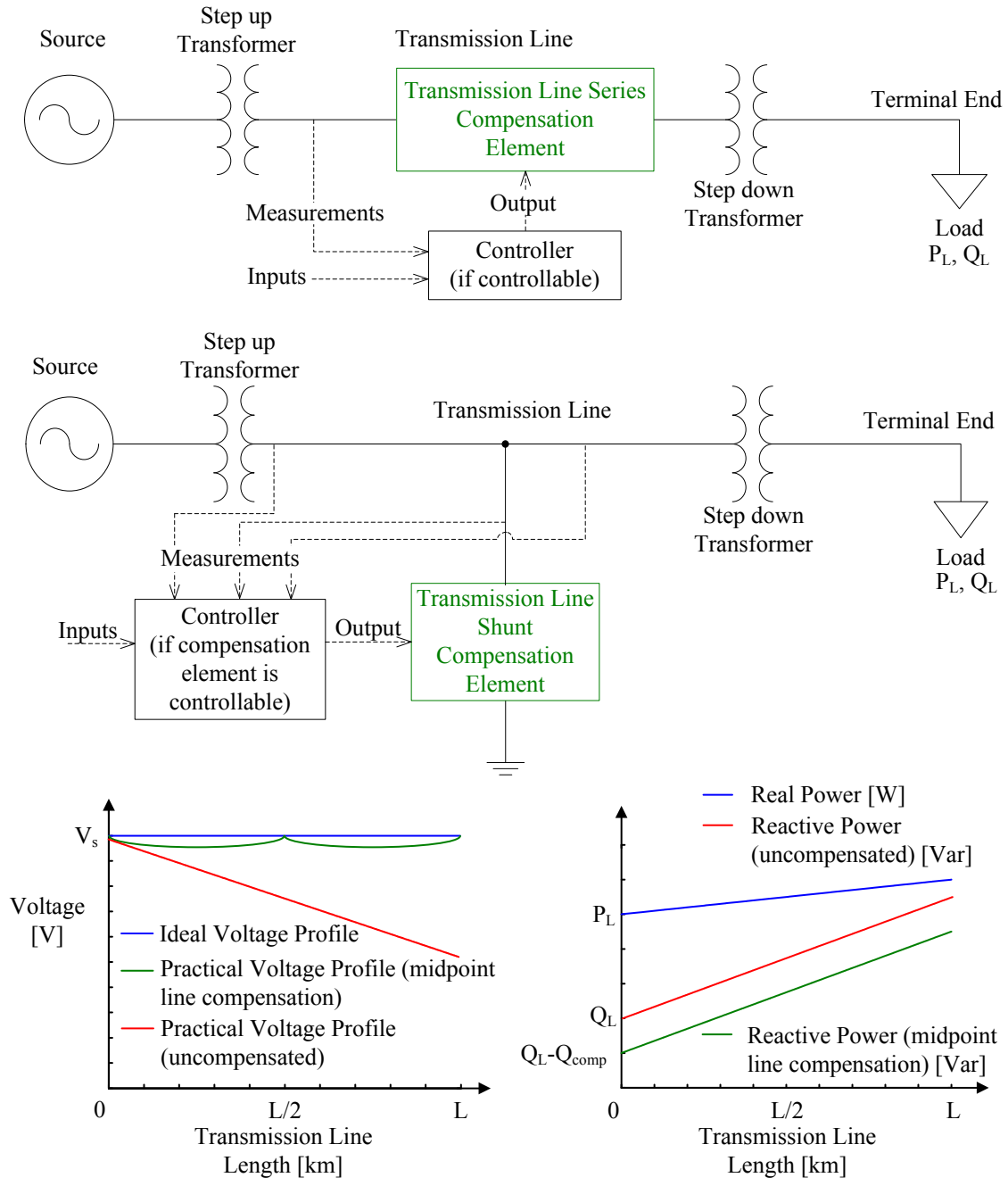

Figure 1.2: Series and shunt compensated transmission line configurations

Although transmission line compensation reduces the amount of reactive power absorbed along the line, transmission capacity continues to be consumed in supplying the reactive power that is required to support the load. The *load compensation* configuration in Figure 1.3 mitigates this phenomenon by adjusting the terminal voltage. Load

compensation reduces the transmission line's reactive power requirement by adding either reactive power sources or sinks, normally in shunt, at the line's terminal end in order to locally meet the load's required reactive power. This approach reduces the amount of reactive power that must be transmitted to support the load, but the transmission line itself remains highly inductive and therefore continues to absorb reactive power.

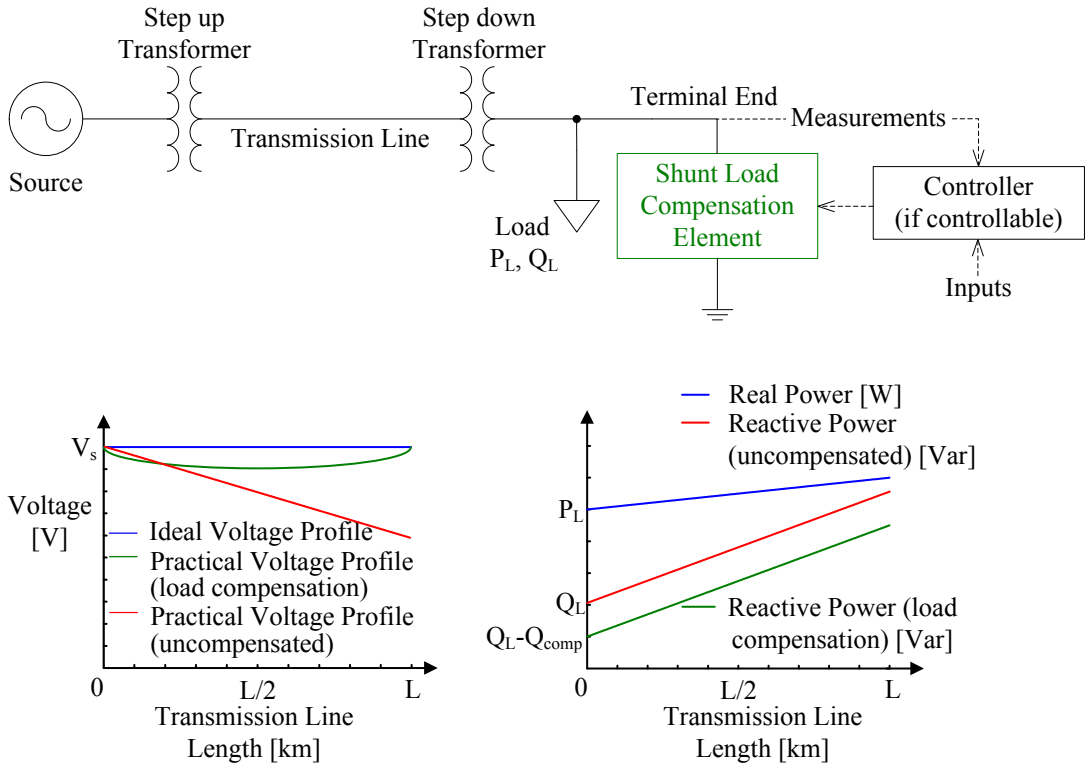

Figure 1.3: Load compensation configuration

Although systems would ideally employ both transmission line and load compensation, cost considerations normally prohibit such a combination, and so the compensation method shown in Figure 1.4 is rarely employed. Specific system objectives dictate the type of reactive power compensation techniques that are actually implemented.

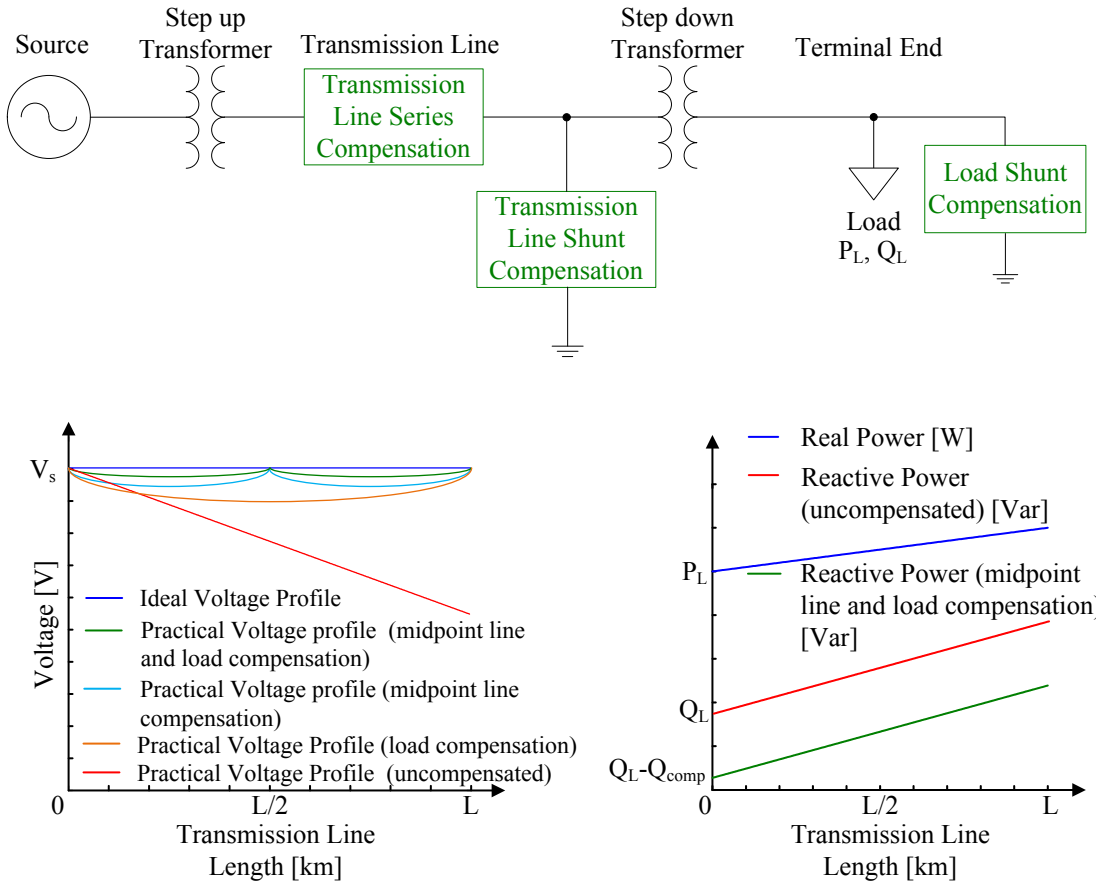

Figure 1.4: System with both transmission line and load compensation

1.1 Objectives of Reactive Power Compensation

Providing reactive power compensation is essential along long transmission lines for maintaining terminal voltages within acceptable limits, enhancing the power system's stability, and increasing the system's power transfer capability [**2**]. Capacitors and other switched passive elements suffice as compensation devices when relatively wide voltage ranges are acceptable. However, controllable elements such as *static var compensators* (SVCs) are employed when more restricted voltage ranges are required.

Reactive power compensation device controllers compare user-defined inputs to measured system parameters and then adjust the reactive power elements' characteristics in order to meet predetermined objectives. For example, a controller that must maintain a

specified system voltage compares a provided voltage reference value, V_{ref}, with the measured system voltage, $V_{measured}$. Depending upon the voltage difference, V_e, between them, the controller then signals the device to generate or absorb reactive power in order to maintain the desired voltage, V_{ref}. A simplified block diagram of an SVC voltage controller is illustrated in Figure 1.5.

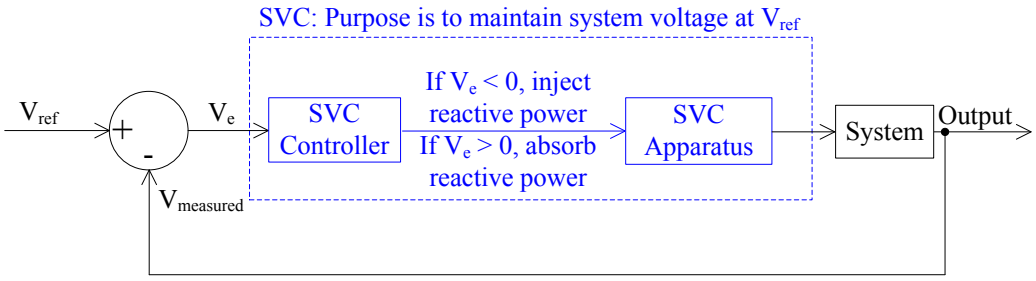

Figure 1.5: Block diagram of an SVC voltage controller

1.2 Controller Tuning for Reactive Power Compensators

The *controller response* describes the speed and accuracy with which the controller obtains its objectives. Controller designs involve trading off improved settling time with overshoot and undershoot considerations. This tradeoff can be adjusted by varying the control system parameters.

Controller tuning is the process of adjusting control parameters to obtain an acceptable controller response, and it is typically accomplished via either a model-based or a simulation-based approach. *Model-based tuning* is an analytical technique that is primarily used to tune simple control systems and to analyze the mathematical approximations of complex control systems that were obtained through prior system knowledge or measurements. It involves developing a mathematical construct of a controller and its associated system. The controller is then designed and tuned to determine the control system parameters based upon specified performance criteria. The

model-based tuning process is illustrated in Figure 1.6. Model-based tuning becomes impractical as the underlying system's sophistication increases due to the corresponding mathematical model's additional complexity.

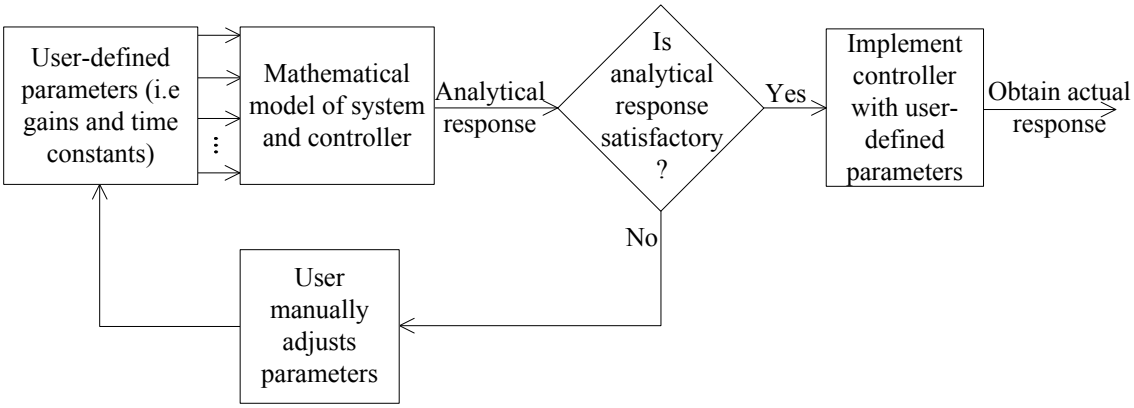

Figure 1.6: Model-based controller tuning

Simulation-based controller tuning uses simulation software to construct a controller model. Different controller parameters are simulated, and the results are then compared to specified performance criteria until an acceptable set of controller parameters are determined. The simulation-based tuning process is illustrated in Figure 1.7. This can be accomplished either by trial and error or else through exhaustive parameter testing. *Simulation-based optimization* is an extension of simulation-based modeling that employs software to optimize controller parameters based upon a user-defined objective function [**5**], [**6**].

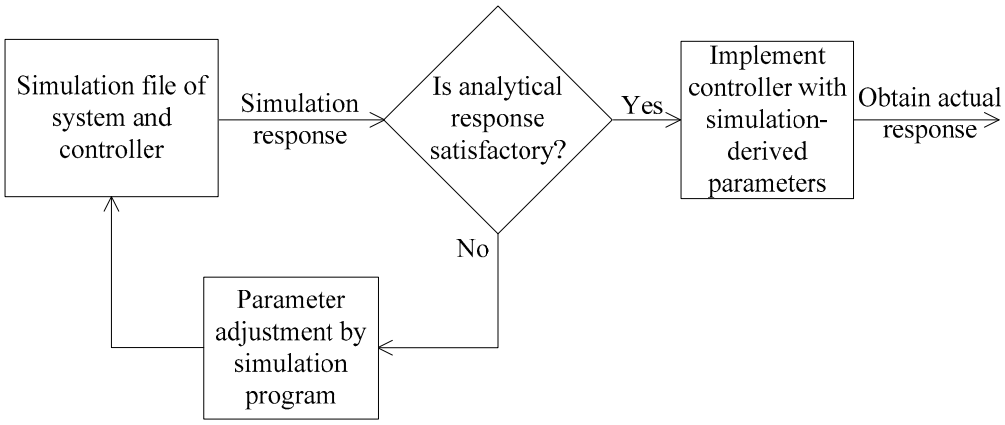

Figure 1.7: Simulation-based controller tuning

Both model-based and simulation-based controller tuning techniques are typically used in feedback control systems whose controller parameters are determined by their response to a predetermined input such as a step function. Both approaches suffer from the controller tuning's high dependence upon the properties being controlled and require precise models to create a well performing control system.

Set-point modulation (SPM) is an emerging control technique that circumvents these drawbacks. Rather than relying on access to the control variables, SPM is implemented as an outer control loop as shown in Figure 1.8, that modifies the control system's reference value, or *set-point*, based solely upon the system's output error and trajectory [**7**], [**8**], [**9**]. If the control system response sufficiently deviates from the set-point, the SPM control scheme modifies the set-point to reduce the output overshoot and settling time. This scheme therefore enhances system controllability without requiring direct access to the underlying control system [**10**]. Manipulating the set-point enables SPM to simultaneously reduce the settling time and improve the overshoot/undershoot. Additionally, a control scheme that manipulates its set-point based upon its output

properties may provide better performance than traditional non-SPM control schemes [**7**], [**11**].

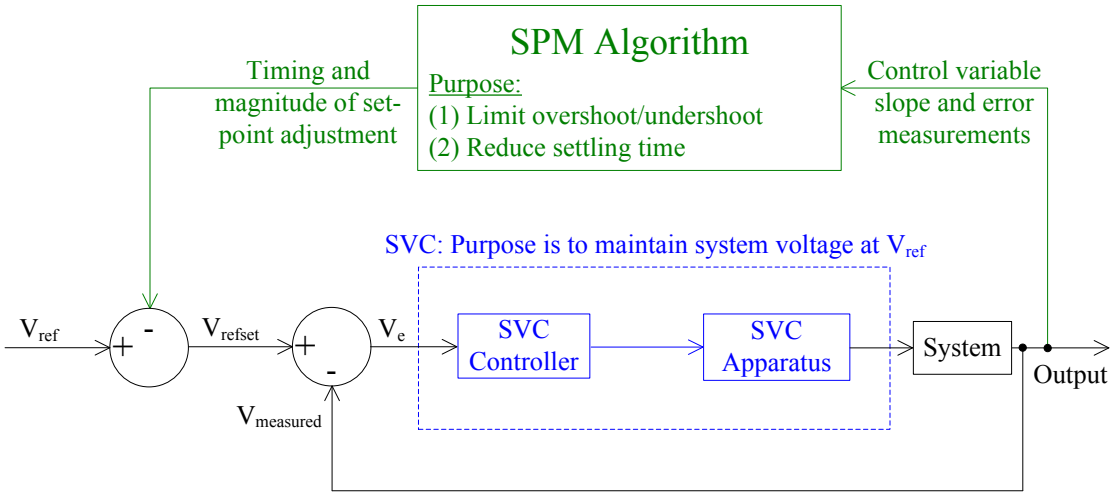

Figure 1.8: Set-point modulation diagram

1.3 Problem Definition

SPM algorithms have thus far been limited to adjusting set-points through a fixed scaling multiplier known as a *modulation index* [**9**]. Traditional SPM scales, or *modulates*, the set-point by a predetermined amount depending upon the control variable's error and slope. This thesis aims to further improve SPM performance by using fuzzy logic to determine a variable modulation index. A fuzzy logic-based SPM algorithm is applied to simulated SVC control systems in order to produce set-point adjustments that simultaneously limit the controlled variable's overshoot or undershoot while reducing its settling time. A comparison of traditional SPM and fuzzy-logic based SPM is shown in Figure 1.9. The fuzzy logic-based SPM algorithm is then applied to Manitoba Hydro's Ponton SVC control system in order to quantitatively evaluate its performance.

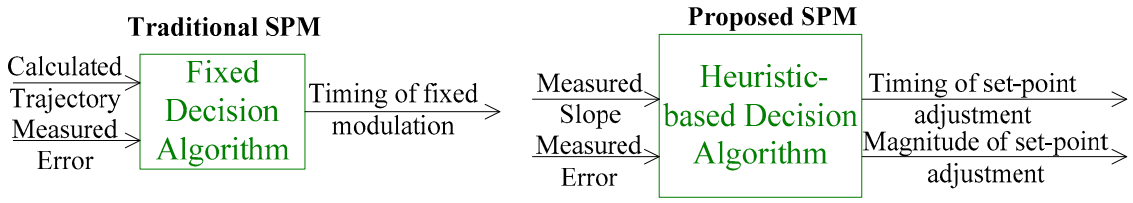

Figure 1.9: Different types of SPM

1.4 Motivation for Research

Modulating the control system's set-point with fuzzy SPM algorithms instead of sharply defined decision-making algorithms would further enhance SPM's existing performance superiority over traditional control schemes by increasing operational and decision-making flexibility. Implementing this SPM control scheme to SVC controllers in particular would therefore improve transmission line voltage overshoots and undershoots and reduce settling times. This in turn enables designers to devise more robust SVCs and allow utilities to more efficiently utilize the existing transmission infrastructure by operating the system closer to its theoretical and operational limits.

1.5 Thesis Organization

The design and implementation of an SVC fuzzy logic-based set-point modulation system requires an understanding of the underlying concepts of static var compensators, fuzzy logic, and set-point modulation.

Chapter two provides a general SVC background, including SVCs' benefits, their constituent devices, various topologies, and control system considerations.

Chapter three discusses fuzzy logic and its potential ability to replace more traditional control system methodologies.

Chapter four covers SPM in-depth, describes its compatibility with fuzzy logic-based algorithms, and applies a fuzzy logic-based SPM control scheme to a generalized representative second order system.

Chapter five analyzes the results obtained from applying fuzzy logic-based SPM control methods to Manitoba Hydro's Ponton SVC controller.

Chapter six summarizes this thesis' contributions and provides future work recommendations.

Chapter 2 Reactive Power and Static Var Compensators

A balanced steady state ac power system is characterized by three single phase alternating voltage waveforms that are electrically separated from each other by 120° phase shifts, as shown in Figure 2.1.

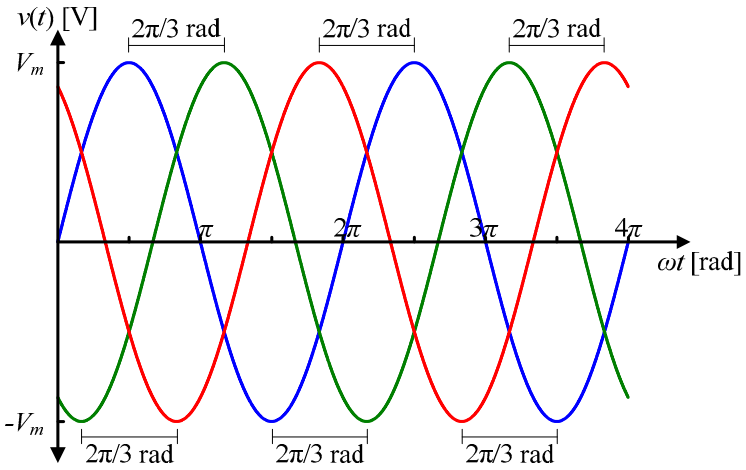

Figure 2.1: Three phase voltage waveforms

Voltage and current phasors are complex quantities, and the total *apparent power*, *S*, which is measured in Volt-Amperes [VA], can therefore be expressed as the vector sum of a real component, *P*, and an imaginary component, *Q*. The real power is also called *active power* and is measured in Watts [W], while imaginary power is referred to as *reactive power* and is measured in Volt-Amperes Reactive, or *Vars* [Var]. Reactive power is stored both everywhere along the transmission line and at the load. Active power that is not dissipated along the transmission line as heat is consumed by customers to produce work.

$$S = V_{rms} I_{rms}^{*} \qquad \text{[VA]} \qquad (2.1)$$

$$S = \mathrm{Re}\{S\} + j\,\mathrm{Im}\{S\} \qquad \text{[VA]} \qquad (2.2a)$$

$$S = P + jQ \qquad \text{[VA]} \qquad (2.2b)$$

Steady state transmission line and load characteristics can be modeled as complex impedances or admittances arising from a combination of resistances, inductances and capacitances. These complex impedances produce a phase shift, θ, between the voltage and current waveforms.

$$S = V_{rms} I_{rms} \cos\theta + jV_{rms} I_{rms} \sin\theta \qquad \text{[VA]} \qquad (2.2c)$$

where

$$\theta = \tan^{-1}\left[\frac{\text{Im}\{S\}}{\text{Re}\{S\}}\right] = \frac{Q}{P} \qquad \text{[rad]} \qquad (2.3)$$

The relationships between these power components are shown in Figure 2.2.

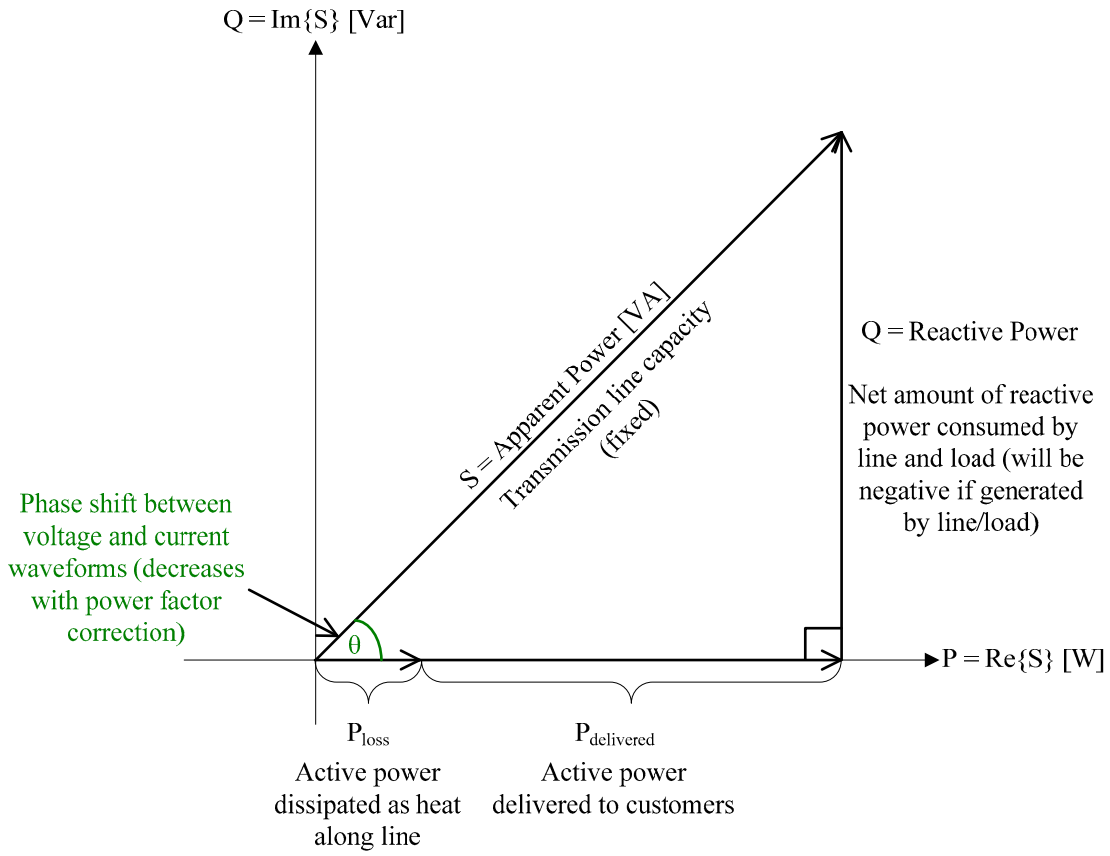

Figure 2.2: Apparent power triangle

Because the transmission line's apparent power capacity is fixed, *power factor correction* is employed to minimize the reactive power consumed and therefore maximize the amount of real power that can be transmitted. Power factor correction reduces the net reactive power by introducing inductive or capacitive elements to the system in order to bring θ, and therefore the imaginary portion of the impedance and the reactive power, as close to zero as possible as depicted in Figure 2.3, thereby reducing the phase angle between the voltage and current waveforms.

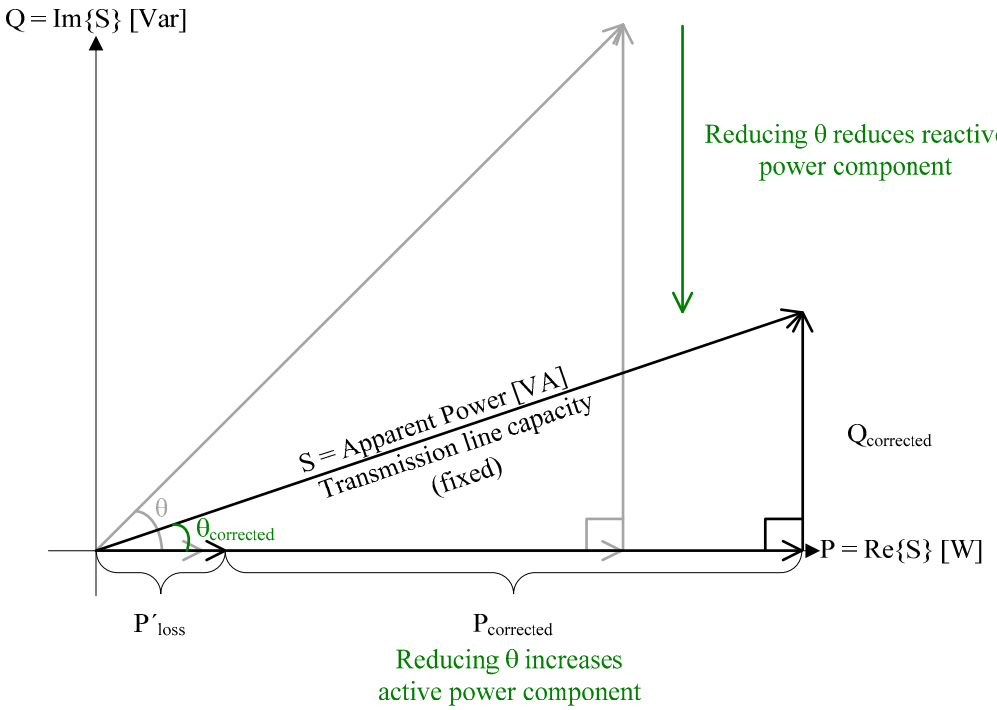

Figure 2.3: Apparent power triangle illustrating power factor correction

$$pf = \cos(\theta) = \cos\left[\tan^{-1}\left(\frac{Q}{P}\right)\right] \tag{2.4}$$

Substituting the complex form of Ohm's law

$$I = YV \qquad \text{[A]} \tag{2.5}$$

into equation (2.1) yields:

$$S = V_{rms}^2 Y^* = V_{rms}^2 \left(G - jB\right) \qquad \text{[VA]} \qquad (2.6)$$

where the *conductance*, G, and the *susceptance, B*, are both measured in Siemans [S]. The real and reactive power can therefore be expressed as

$$P = \mathrm{Re}\{S\} = V_{rms}^2 G \qquad \text{[W]} \qquad (2.7a)$$

$$Q = \mathrm{Im}\{S\} = -V_{rms}^2 B \qquad \text{[Var]} \qquad (2.7b)$$

where inductor and capacitor admittances are modeled as

$$Y_{ind} = G_{ind} + jB_{ind} \qquad G_{ind} = 0 \qquad B_{ind} = \frac{-1}{\omega L} \qquad \text{[S]} \qquad (2.8a)$$

$$Y_{cap} = G_{cap} + jB_{cap} \qquad G_{cap} = 0 \qquad B_{cap} = \omega C \qquad \text{[S]} \qquad (2.8b)$$

and the apparent power characteristics are therefore described by

$$S_{ind} = P_{ind} + jQ_{ind} \text{ [VA]} \qquad P_{ind} = 0 \text{ [W]} \qquad Q_{ind} = \frac{V_{rms}^2}{\omega L} \qquad \text{[Var]} \qquad (2.9a)$$

$$S_{cap} = P_{cap} + jQ_{cap} \text{ [VA]} \qquad P_{ind} = 0 \text{ [W]} \qquad Q_{cap} = -V_{rms}^2 \omega C \qquad \text{[Var]} \qquad (2.9b)$$

Inductors are said to *absorb reactive power* because a positive quantity of reactive power flows into an inductor. Conversely, capacitors are said to *generate* or *inject reactive power* because a negative quantity of reactive power flows into a capacitor. Connecting inductors and capacitors to the power system alters the system's susceptance and therefore the amount of reactive power generated or absorbed.

While fixed elements can be deliberately added to control system voltages, controllable reactive power devices may be required to control the system within a narrow range of voltages. A *Static Var Compensator* (SVC) is an example of a controllable device that provides reactive power compensation under either steady state

or transient system conditions. It accomplishes this by connecting a continually varying susceptance to either absorb or generate various amounts of reactive power depending upon system requirements. By providing reactive power compensation, an SVC can rapidly regulate or control the power system's terminal voltage [**12**], [**13**] while maintaining synchronism. Utilities employ SVCs in order to:

- correct phase imbalances [**14**], [**15**]
- improve the power factor of loads [**13**], [**14**]
- improve the system's steady state transmission capacity and transient stability [**16**], [**17**], [**18**]
- dampen power oscillations [**18**], [**19**], [**20**], [**21**] and subsynchronous oscillations [**13**]
- reduce voltage flicker caused by load fluctuations [**12**], [**13**]
- improve HVDC terminal performance [**13**]
- support system voltages [**18**]

Practical SVCs consist of various combinations of standard devices depending upon design objectives, size restrictions, and installation costs.

2.1 SVC Apparatus

2.1.1 Anti-parallel Thyristor Pair

A *thyristor* is a circuit element that acts as a diode by only allowing unidirectional current conduction. However, unlike a diode, a thyristor will not conduct even when forward biased unless a *gate pulse signal* is also provided to enable it. An *anti-parallel thyristor* arrangement functions as a fully controllable bidirectional switch that enables current conduction during both of the supply voltage's positive and negative half-cycles. Thyristors can begin to conduct, or *fire*, at any point while the thyristor is forward biased and will continue conducting until the current flowing through the thyristor reverses direction. Varying the timing of the thyristor's firing therefore controls the amount of

voltage in the system, as depicted in Figure 2.4 for a resistive load. This provides a controllable way to insert and remove devices from the power system, which enables reactive power manipulation, according to equation (2.7b).

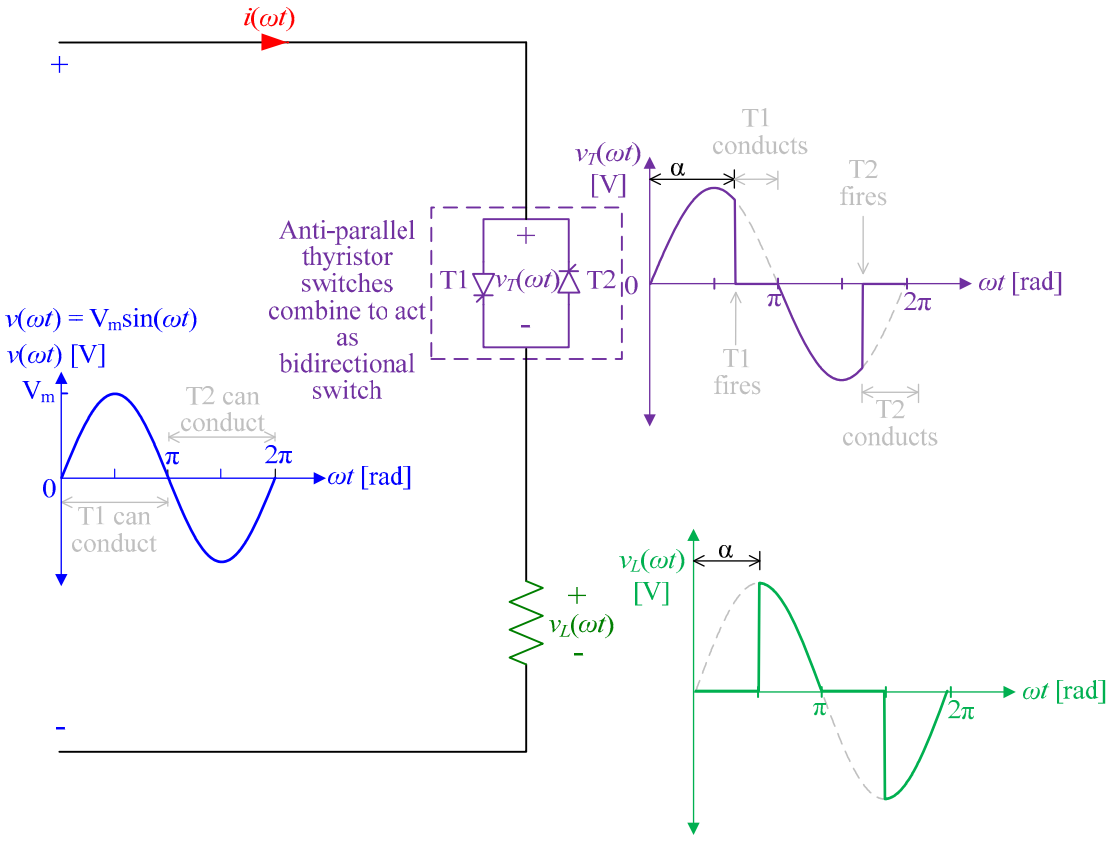

Figure 2.4: Anti-parallel thyristor and associated waveforms

The timing of the thyristor firing is referenced in terms of radians and is referred to as the *thyristor firing angle*, α. Figure 2.5 illustrates the voltage waveform generated by the anti-parallel thyristor pair for various values of α.

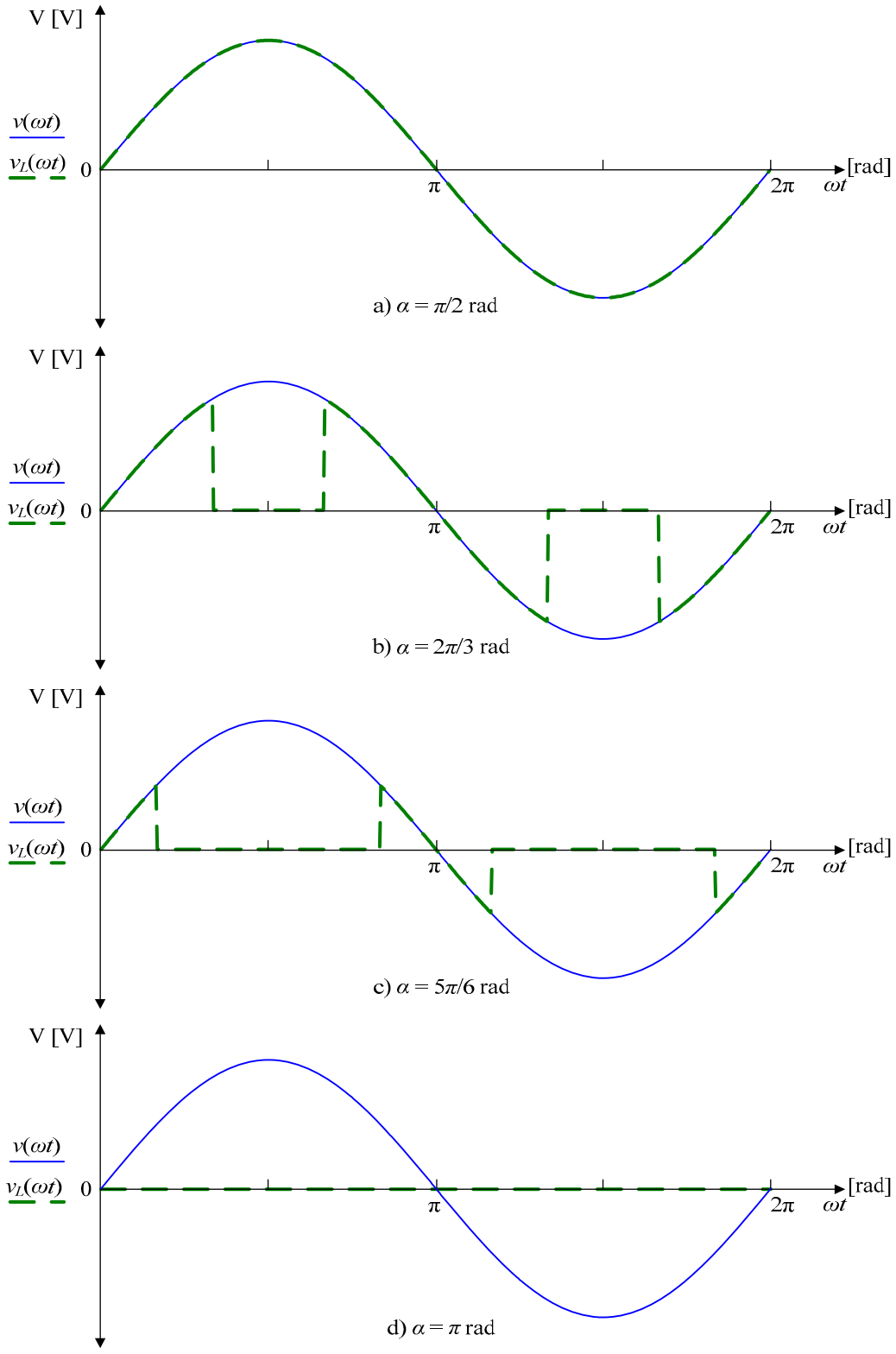

Figure 2.5: Voltage produced by anti-parallel thyristor pair for different thyristor firing angles

2.1.2 Thyristor Controlled Reactor

A *Thyristor Controlled Reactor (TCR)* is the fundamental SVC building block and comprises an inductor, or *reactor*, in series with an anti-parallel thyristor pair as shown in Figure 2.6. The anti-parallel thyristors enable the reactor to be inserted into the power system for a fraction of the power system's fundamental period. The reactor's inclusion introduces a phase shift between the supply voltage and the fundamental current waveform through the inductor.

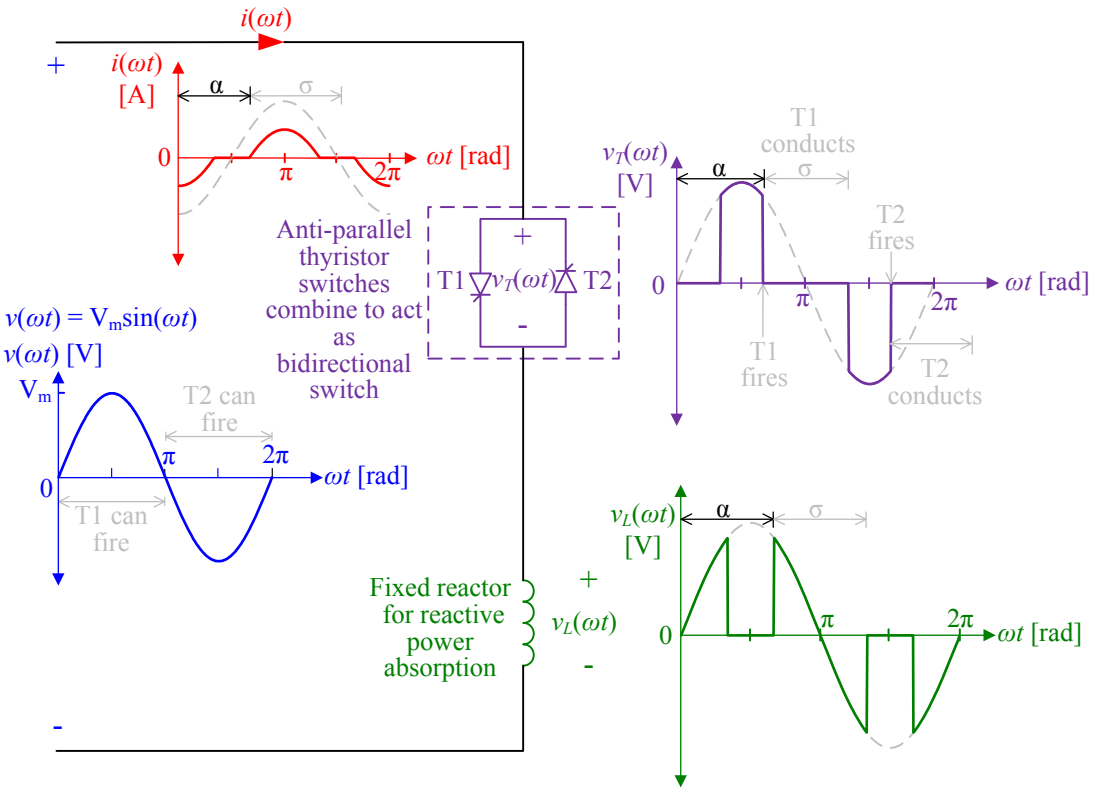

Figure 2.6: Single-phase TCR schematic and associated waveforms

The TCR's *current conduction interval*, σ, which describes the angular interval over which a specific thyristor conducts and is varied by controlling the thyristor firing angle, α, as measured from the zero crossing of the voltage $v(t)$ applied across the TCR

terminals[1]. The current conduction interval is defined in terms of a thyristor's firing angle by[2]:

$$\sigma = 2(\pi - \alpha), \quad \frac{\pi}{2} \le \alpha \le \pi \qquad \text{[rad]} \qquad (2.10)$$

Varying the firing angle produces a current waveform with a controllable fundamental component, where $\alpha = \pi/2$ causes the anti-parallel thyristors to act as a short circuit that enables full current conduction and $\alpha = \pi$ causes the anti-parallel thyristors to act as an open circuit that blocks all current conduction. A firing angle of $\alpha < \pi/2$ creates an asymmetrical TCR current, which in turn produces a current waveform with overly high harmonic content and a dc bias, both of which are unacceptable in ac power networks [**2**]. A firing angle $\alpha > \pi$ is also impossible because the thyristors would be reverse-biased and therefore unable to conduct.

With an applied system voltage of $v(\omega t) = V_m \sin(\omega t)$, the instantaneous current $i(\omega t)$ produced is shown in equation (2.11) and illustrated in Figure 2.7.

$$i(\omega t) = \begin{cases} -V_m \dfrac{[\cos(\omega t) + \cos(\alpha)]}{\omega L}, & 0 \text{ rad} \le \omega t \le (\pi - \alpha) \text{ rad} \\ 0, & (\pi - \alpha) \text{ rad} \le \omega t \le \alpha \text{ rad} \\ -V_m \dfrac{[\cos(\omega t) - \cos(\alpha)]}{\omega L}, & \alpha \text{ rad} \le \omega t \le (2\pi - \alpha) \text{ rad} \\ 0, & (2\pi - \alpha) \text{ rad} \le \omega t \le (\pi + \alpha) \text{ rad} \\ -V_m \dfrac{[\cos(\omega t) + \cos(\alpha)]}{\omega L}, & (\pi + \alpha) \text{ rad} \le \omega t \le 2\pi \text{ rad} \end{cases} \qquad \text{[A]} \qquad (2.11)$$

[1] Some authors measure the firing angle from the supply voltage's peak V_m instead of its zero crossing. This phase shifts the expressions for the TCR's fundamental and the harmonic currents [**15**].

[2] Because the firing angle and current conduction interval can be defined in terms of each other, the firing angle will be used exclusively throughout the remainder of this thesis for consistency.

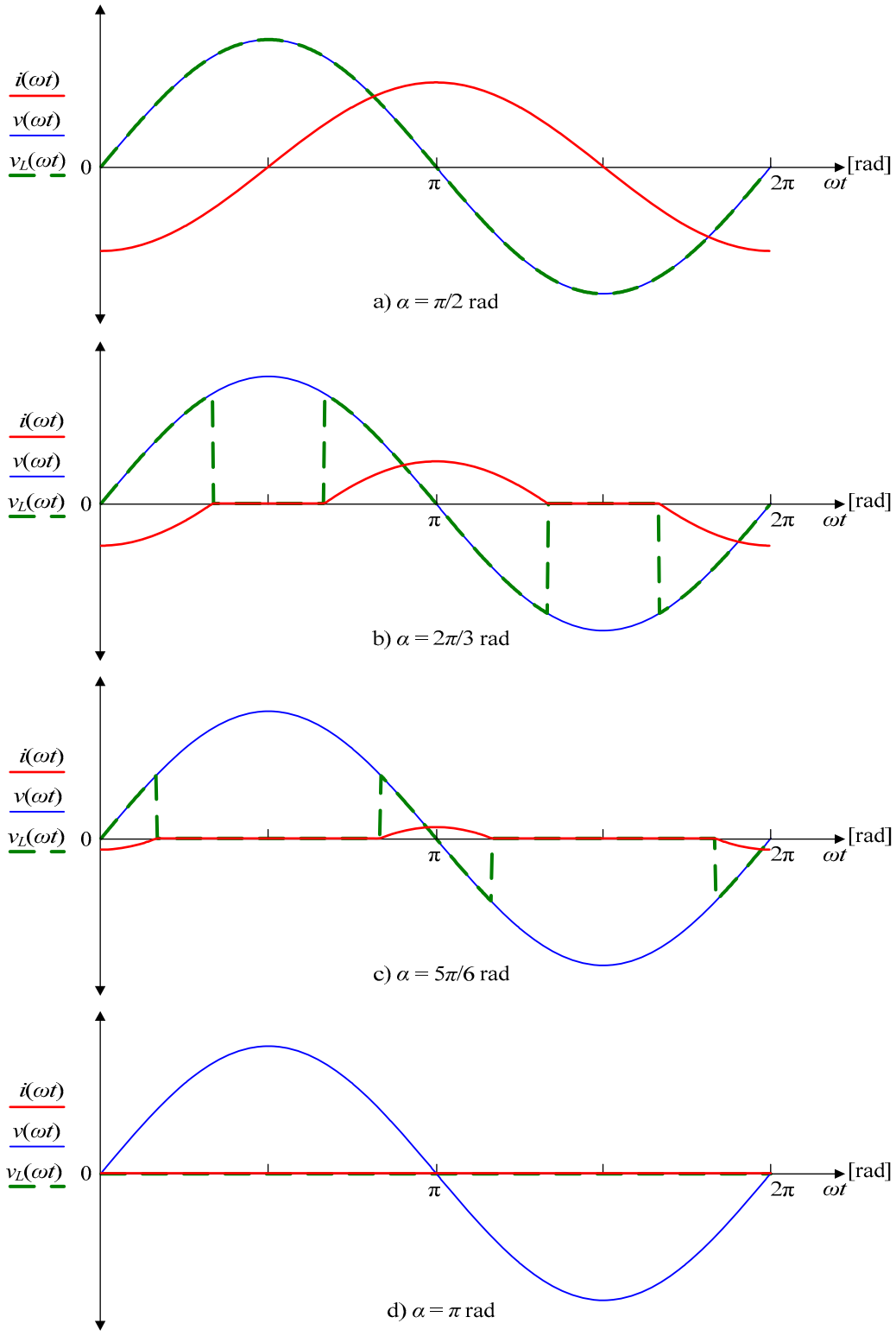

Figure 2.7: TCR current waveforms with varying firing angles

Applying Fourier analysis to equation (2.11) allows the amplitude of the current's fundamental component to be expressed as a function of the thyristor firing angle:

$$I_{1TCR}(\alpha) = V_m\left[\frac{2\pi - 2\alpha + \sin(2\alpha)}{\pi\omega L}\right], \quad \frac{\pi}{2}\,\text{rad} \le \alpha \le \pi\,\text{rad} \qquad \text{[A]} \qquad (2.12)$$

At the fundamental frequency, the TCR current can be interpreted as the product of a constant voltage, V_m, and a purely inductive susceptance, B_{1TCR}, whose magnitude varies as a function of the anti-parallel thyristors' selected firing angle:

$$I_{1TCR}(\alpha) = V_m B_{1TCR}(\alpha), \quad \frac{\pi}{2}\,\text{rad} \le \alpha \le \pi\,\text{rad} \qquad \text{[A]} \qquad (2.13a)$$

where

$$B_{1TCR}(\alpha) = -\left[\frac{2\pi - 2\alpha + \sin(2\alpha)}{\pi\omega L}\right], \quad \frac{\pi}{2}\,\text{rad} \le \alpha \le \pi\,\text{rad} \qquad \text{[S]} \qquad (2.13b)$$

From equation (2.7b), $Q_{TCR} = -V_{RMS}^2 B_{TCR}$, and the TCR circuit can therefore absorb a variable amount of reactive power depending upon the firing angle, α as shown in Figure 2.8.

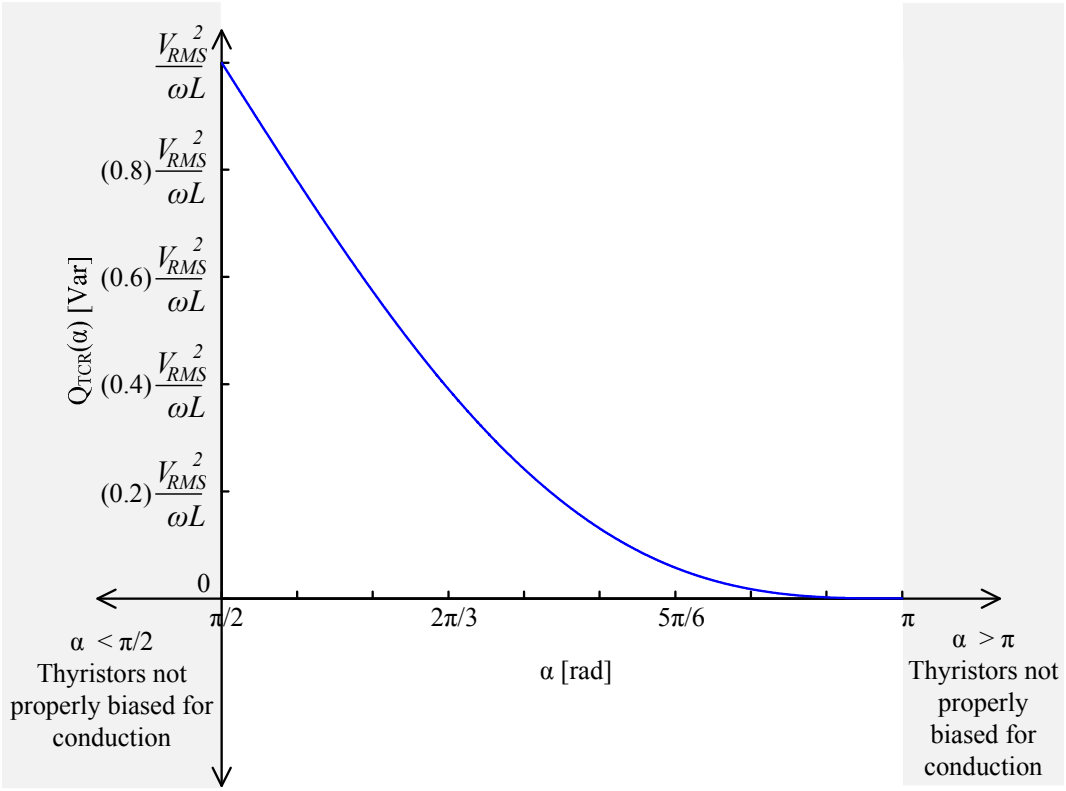

Figure 2.8: TCR reactive power vs. firing angle

The TCR's voltage-reactive power characteristic is illustrated in Figure 2.9. The TCR can maintain the system voltage by varying the thyristor firing angle and therefore the fundamental current's magnitude. If the system voltage exceeds the desired voltage, V_{ref}, the ensuing firing angle reduction will increase the TCR's reactive power absorption and reduce the voltage back to V_{ref}. Conversely, if the system voltage dips below V_{ref}, the TCR's firing angle will increase to absorb less reactive power and cause the voltage to rise back to V_{ref}.

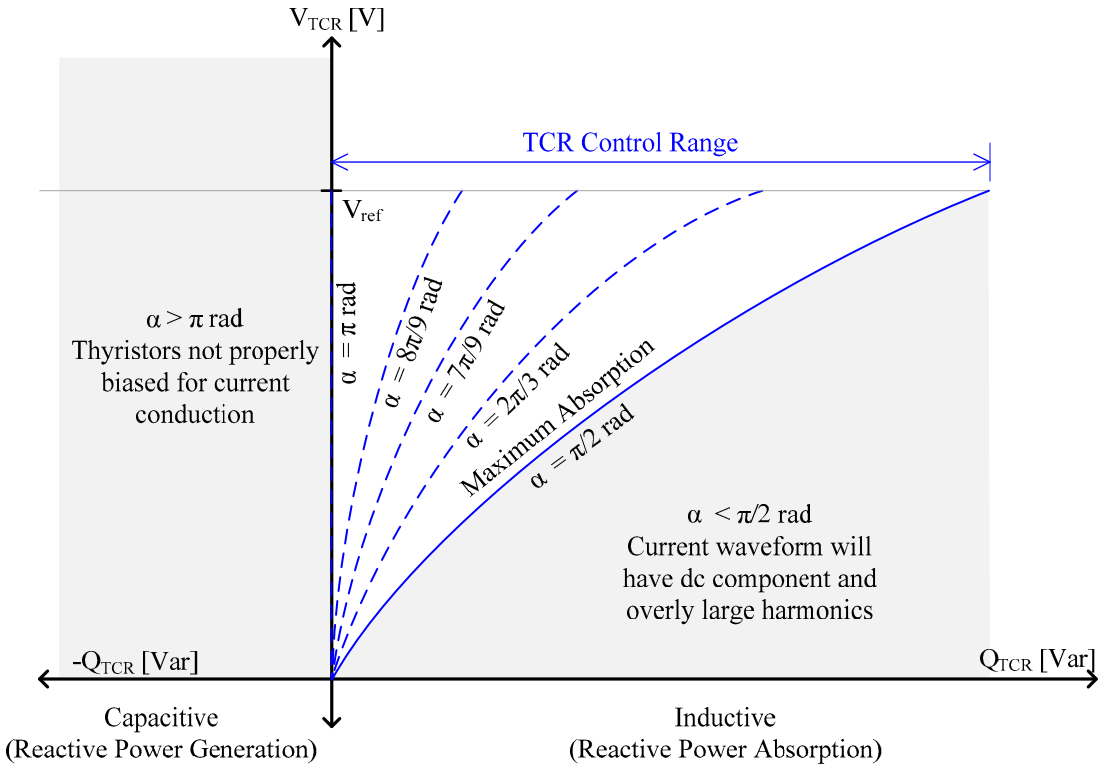

Figure 2.9: TCR's V-Q characteristic

The thyristor firing angle, α, affects the TCR-generated current harmonics as well as the fundamental. Applying Fourier analysis to equation (2.11) shows that the current amplitude, I_n, of the n^{th} order harmonic differs greatly depending upon α:

$$I_n = \frac{4}{\pi}\frac{V_m}{\omega L}\left[\frac{\sin\left(\alpha-\frac{\pi}{2}\right)\cos\left(n(\alpha-\frac{\pi}{2})\right)-n\cos\left(\alpha-\frac{\pi}{2}\right)\sin\left(n(\alpha-\frac{\pi}{2})\right)}{n\left(n^2-1\right)}\right],\ n\geq 3, n\ odd \qquad [A] \quad (2.14)$$

$$I_n = 0,\ n\ even$$

Harmonics of order *3n*, which are known as *triple-n harmonics*, are generated by the TCR but do not appear on the transmission system when three-phase TCRs are connected in a delta configuration, as is typically the case [**4**]. Figure 2.10 compares the harmonic current magnitudes as a percentage of the fundamental magnitude over the TCR's operational range.

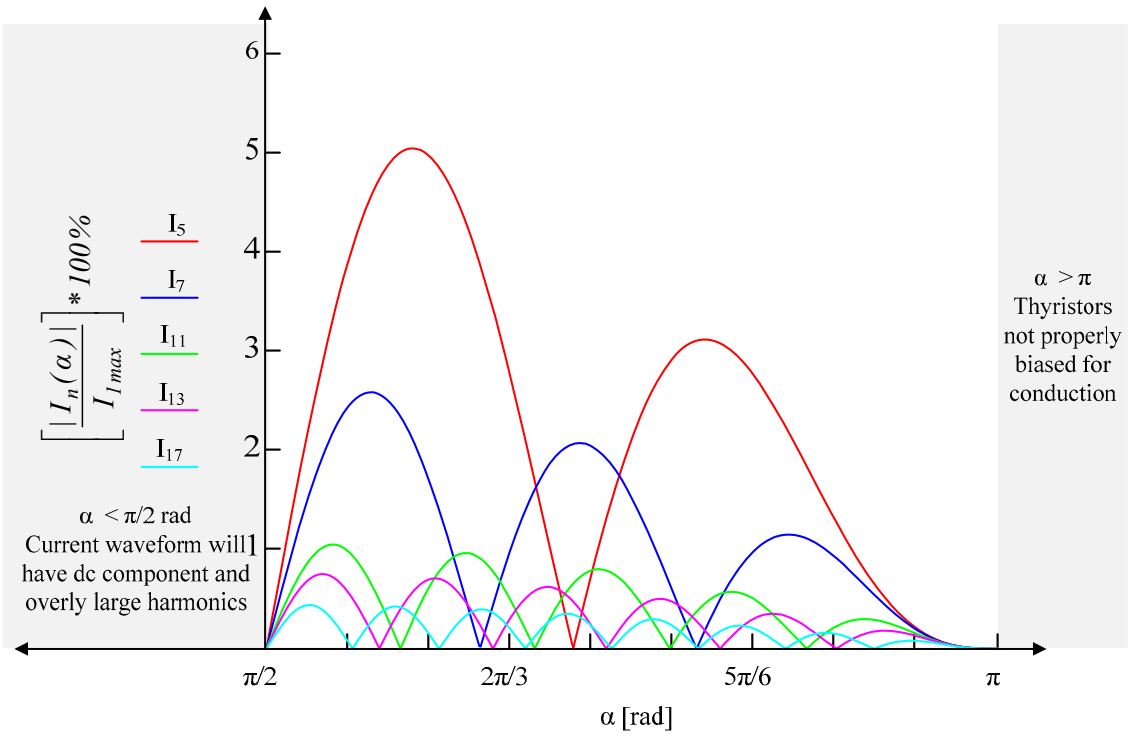

Figure 2.10: TCR harmonics as a percent of TCR fundamental current magnitude

Figure 2.11 illustrates the total harmonic current magnitude's variation as a percentage of the current fundamental's maximum value over the operational TCR range. A filter is usually connected to the TCR to provide a ground path for the 5th and higher order harmonics in order to minimize their effect on the power system [**18**]. Because all non-fundamental harmonics are either filtered or cancelled out, subsequent analysis can be limited to the TCR current's fundamental component.

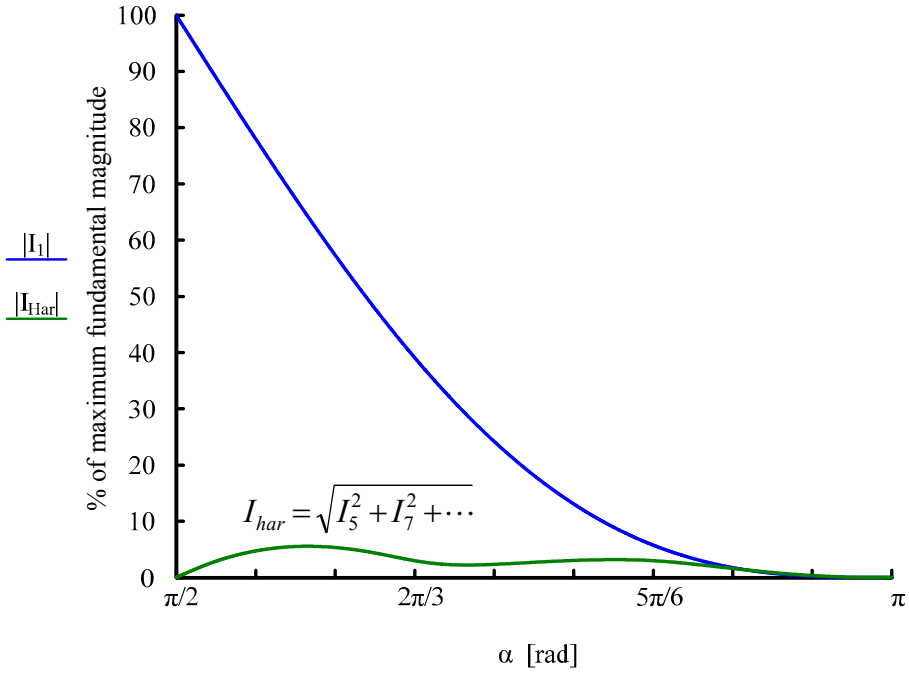

Figure 2.11: TCR fundamental current and total harmonic current

2.1.3 Fixed Capacitor-Thyristor Controlled Reactor (FC-TCR)

Although TCRs can only provide varying amounts of reactive power absorption, power systems usually require reactive power generation. A TCR is therefore rarely used on its own but is instead combined with fixed shunt capacitors to produce a continuously variable reactive power source. This configuration is called a *Fixed Capacitor-Thyristor Controlled Reactor* (*FC-TCR*), and is illustrated in Figure 2.12.

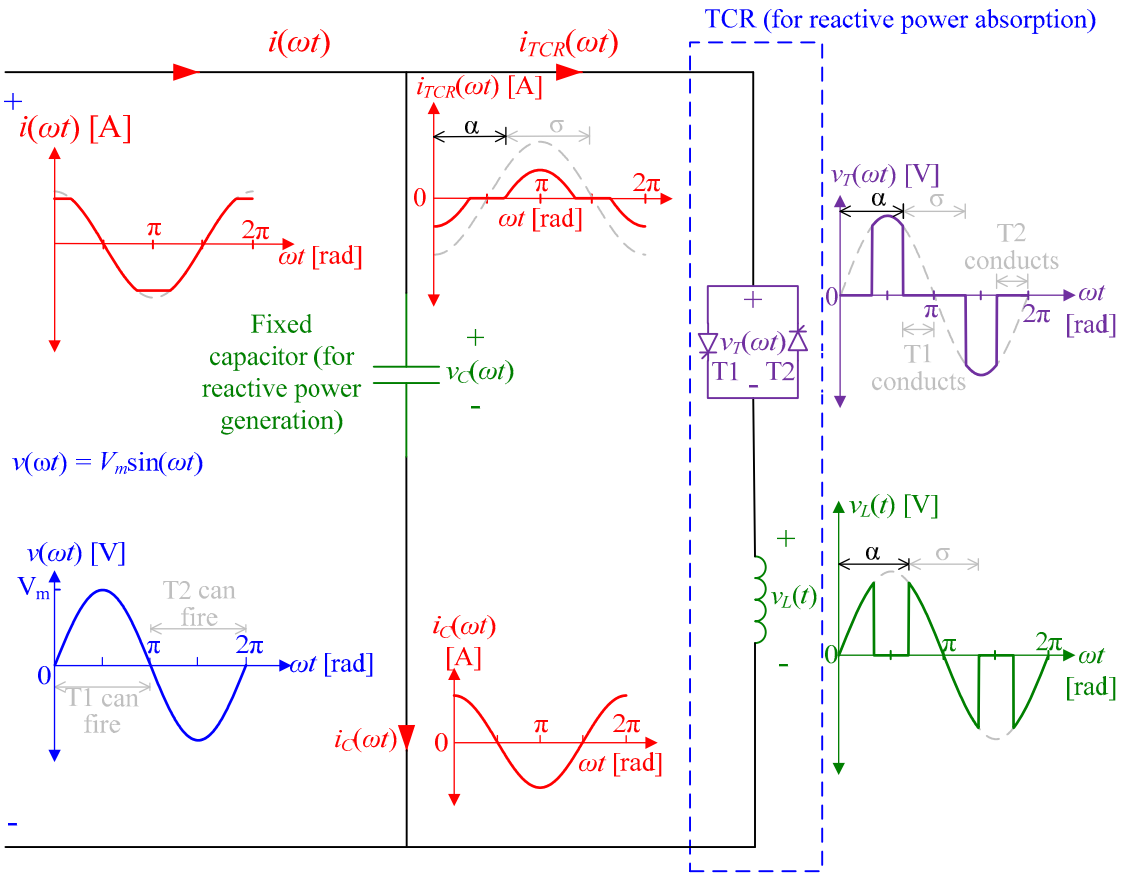

Figure 2.12: Single-phase fixed capacitor TCR (FC-TCR)

The capacitor bank is mathematically modeled by adding the fixed capacitor's susceptance to the TCR's fundamental susceptance. Combining (2.8b) and (2.13b) yields:

$$B_{1FC-TCR}(\alpha) = B_{FC} + B_{1TCR}(\alpha)$$
$$B_{1FC-TCR}(\alpha) = \omega C - \frac{2\pi - 2\alpha - \sin(2\alpha)}{\pi\omega L} \quad [S] \qquad (2.15)$$

By equation (2.6b), the FC-TCR's reactive power characteristic may be modeled as shown in equation (2.16), and depicted graphically in Figure 2.13

$$Q_{1FC-TCR}(\alpha) = Q_{FC} + Q_{1TCR}(\alpha)$$
$$Q_{1FC-TCR}(\alpha) = V_{rms}^2 B_{1FC-TCR}(\alpha)$$
$$Q_{1FC-TCR}(\alpha) = V_{rms}{}^2 \omega C - V_{rms}^2 \left[\frac{2\pi - 2\alpha - \sin(2\alpha)}{\pi\omega L}\right] \quad [Var] \qquad (2.16)$$

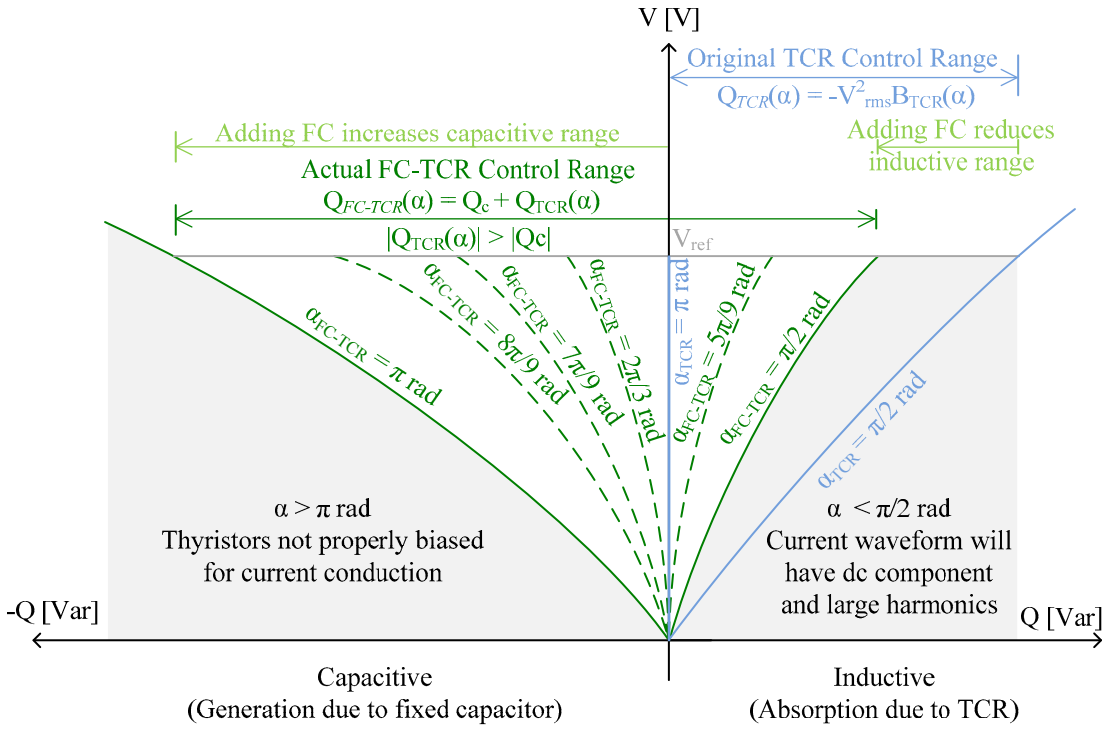

Figure 2.13: Single-phase FC-TCR's V-Q characteristic

This modified susceptance essentially biases the original TCR's voltage-reactive power characteristic towards the generation portion of the reactive power region, and the TCR's reactive power rating is therefore designed to be greater than its fixed capacitor reactive power rating to ensure its ability to operate in the inductive region when required. This enables the FC-TCR to either generate or absorb a net amount of reactive power depending upon system requirements.

Increasing the fixed capacitance term in equation (2.16) increases the reactive power generation. A system that requires a large amount of reactive power may therefore require an FC-TCR comprising multiple fixed shunt capacitors shown in Figure 2.14, which the SVC employs to generate a continuous range of reactive power shown in Figure 2.15. The mechanical switches shown in Figure 2.14 are required to place the fixed capacitors into and out of the system.

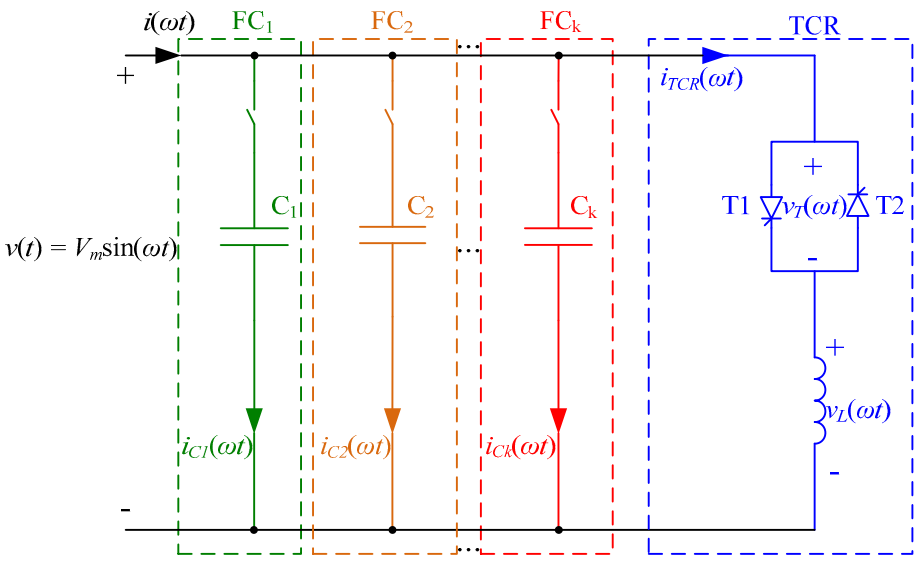

Figure 2.14: Single-phase FC-TCR with multiple fixed capacitors

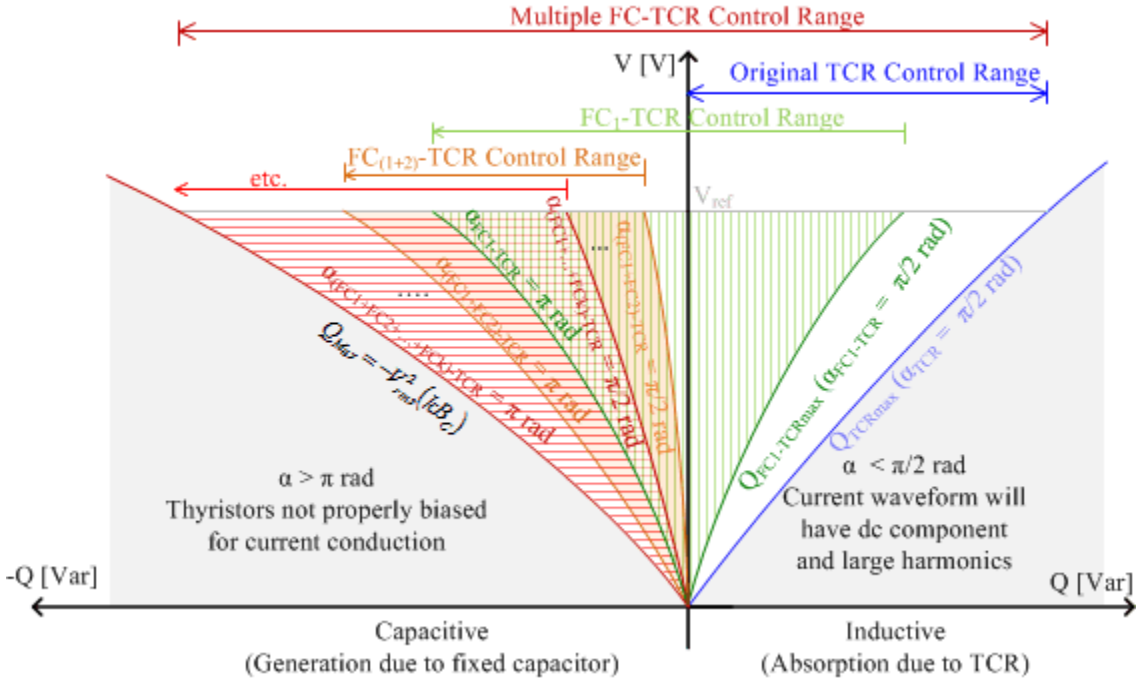

Figure 2.15: V-Q characteristic for FC-TCR with multiple fixed capacitors

2.1.4 Thyristor Switched Capacitor (TSC)

The power system exhibits transients whenever an FC-TCR's fixed capacitors connect to or disconnect from it because the capacitor voltage does not exactly match the system voltage at the time of connection. The *Thyristor Switched Capacitor* (*TSC*)

illustrated in Figure 2.16 provides a theoretical operational improvement by enabling a capacitive element to rapidly switch into and out of the power system in a transient-free manner under certain conditions. The TSC consists of a pair of anti-parallel thyristors series connected to a fixed capacitor and a series reactor known as a *current limiting reactor* (CLR).

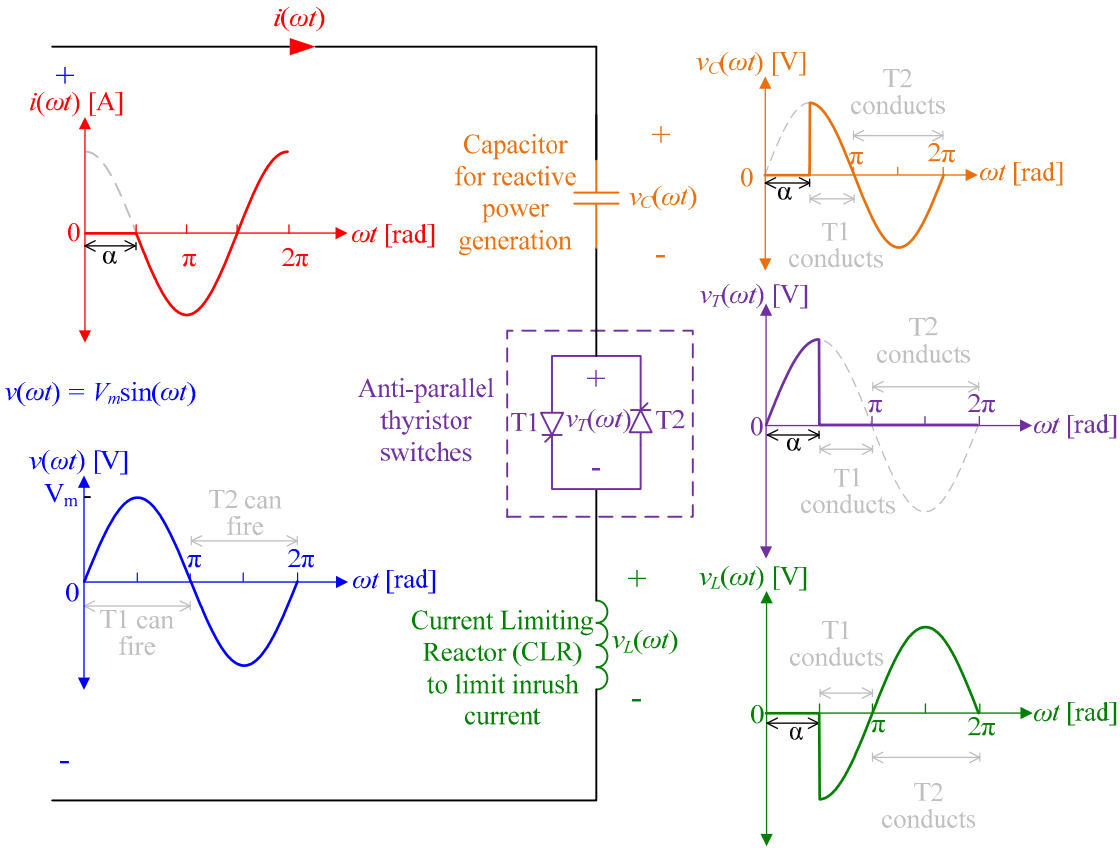

Figure 2.16: Single-phase TSC

The theoretical operational benefit introduced by the series capacitive element is offset by increased cost and additional design challenges. This is because placing the TSC into service is operationally equivalent to connecting a capacitor to a voltage source. Any difference between the capacitor's stored voltage and the voltage across the capacitor at the time of switching produces an *inrush current* whose magnitude or rate of

change in magnitude may damage the thyristors. Provisions are normally taken to both minimize the likelihood of inrush current and to reduce the severity of its occurance.

Because it is impossible to completely prevent current inrush, TSC designs require a CLR, whose inductance protects the thyristors by limiting the rate of change of current through the TSC branch to

$$\frac{di_L(t)}{dt} = \frac{v_L(t)}{L} \qquad \text{[A/s]} \qquad (2.17)$$

Despite the CLR's necessity, its inclusion risks producing oscillations in the TSC-generated current at the specific frequency for which the capacitor's impedance cancels the reactor impedance. This *resonant frequency*, ω_r, can be mathematically expressed in terms of the system's fundamental frequency, ω_0, as:

$$\omega_r = \frac{1}{\sqrt{LC}} = r\omega_0 \qquad \text{[rad/s]} \qquad (2.18)$$

where

$$r = \sqrt{\frac{|B_{ind}|}{|B_{cap}|}} \qquad (2.19)$$

Applying the Laplace transform to the TSC's governing second order differential equation produces the expression for the current, $i(t)$, that flows during the TSC's conduction. Assuming a system voltage of $v(t) = V_m\sin(\omega t)$ and a voltage $V_C(\omega t=\alpha)$ across the capacitor during the TSC's initial conduction, $i(t)$ can be expressed as the sum of a fundamental frequency component, i_{ac}, and a resonant frequency component caused by the presence of the fixed capacitor and series CLR [**22**]:

$$i(t) = i_{ac}\cos(\omega t) + \left[rB_c \left(V_c(\omega t)\big|_{\omega t=\alpha} - V_m \sin(\alpha)\frac{r^2}{r^2-1} \right) \sin\left(\omega_r t - \alpha\frac{\omega_r}{\omega} \right) + i_{ac}\cos(\alpha)\cos\left(\omega_r t - \alpha\frac{\omega_r}{\omega} \right) \right] \quad \text{[A]} \quad (2.20)$$

$$= \text{Fundamental Frequency Term} + \text{Resonant Frequency Term}$$

$$= f(\text{steady state response}) + f(\text{transient response})$$

where i_{ac} is the current amplitude of the TSC's circuit steady state response:

$$i_{ac} = V_m B_C \frac{r^2}{r^2-1} \quad \text{[A]} \quad (2.21)$$

The $r^2/(r^2\text{-}1)$ term is referred to as the *magnification factor* and is a function of the TSC's reactive element parameters. The TSC's resonant frequency is normally designed for a value that is between four and five times that of the fundamental frequency as shown in Figure 2.17 in order to provide a magnification factor sufficiently close to unity [**22**]. Tuning the TSC branch's resonant frequency to $\omega_r < 3\omega$ produces a magnification factor that is appreciably greater than one, thereby creating current magnitudes that may exceed the SVC's component ratings. Conversely, tuning the TSC branch's resonant frequency to $\omega_r > 5\omega$ produces unacceptably large transient current amplitudes.

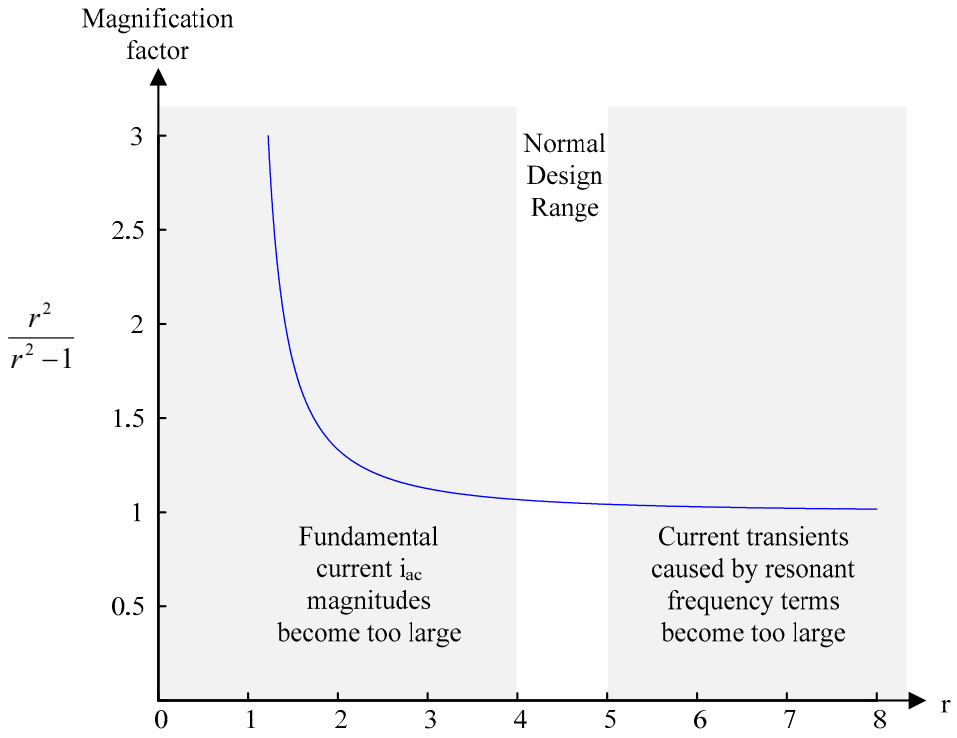

Figure 2.17: Magnification factor as a function of r

Although equation (2.20) appears to suggest that TSCs should employ very large reactors in order to reduce the current inrush to a negligible amount, three practical considerations limit the CLR size. First, increasing the inductor size also increases the time required for the voltage across the TSC to reach a steady state value. Moreover, the additional reactive power absorbed by the CLR offsets the TSC's intended purpose of injecting reactive power. Finally, equation (2.19) implies that increasing the reactor size would also necessitate increasing the capacitor size in order to keep the magnification factor within the desired range.

While CLRs limit the severity of current inrush, other techniques are simultaneously employed to reduce the likelihood of inrush occurring at all. Such techniques curtail or ideally eliminate the current transients resulting from the TSC's connection to the power

system and reduce the CLR's inclusion to merely a necessary precautionary protective design measure.

One method for eliminating possible transient currents involves timing the switching to minimize the resonant frequency term of equation (2.20). This can be theoretically accomplished by simultaneously satisfying the following conditions, neither of which is perfectly realizable in a practical system:

$$\cos(\omega t)\big|_{\omega t=\alpha} = 0 \Rightarrow \alpha = (2n+1)\left(\frac{\pi}{2}\right),\ \text{n} = 0,1,2,... \qquad \text{[rad]} \qquad (2.22a)$$

$$\therefore \sin(\alpha) = \pm 1$$

$$V_C(\omega t))\big|_{\omega t=\alpha} = \pm V_m \frac{r^2}{r^2 - 1} \qquad \text{[V]} \qquad (2.22b)$$

Since the system voltage is $v(t) = V_m \sin(\omega t)$, equation (2.22a) implies that the switch may only be permitted to close at the supply voltage waveform's positive or negative peak values, which corresponds to $\omega t = \pi/2$ or $\omega t = 3\pi/2$, respectively. Similarly, the TSC can only be removed from service at the point in every half-cycle at which $i(\omega t) = 0$. The TSC is removed from service by blocking the firing pulses to both thyristors in order to naturally extinguish the current at the subsequent zero crossing. Therefore, unlike the TCR, which operates for any firing angle in the range between $\pi/2 \leq \alpha \leq \pi$, a TSC acts as discrete device that can only enter service at $\alpha = \pi/2$ or $\alpha = 3\pi/2$ and be removed from service at $\alpha = \pi$ or $\alpha = 2\pi$.

While equation (2.22a) restricts the TSC's instant of switching, equation (2.22b) confines the capacitor charge to a specific value at that switching instant. Simultaneously satisfying both of these equations precludes inrush from occurring by ensuring that the

TSC is only inserted into the power system when the system and the capacitor voltages are identical.

It is impossible to physically realize either of the conditions dictated by equations (2.22a) and (2.22b). The former condition cannot be met in practice due to the impossibility of timing the exact switching instants, and the latter criterion cannot be met because the voltage across a practical capacitor slowly decays over time, as illustrated in Figure 2.18. The inability to meet either condition renders transients inevitable whenever the TSC switches into the transmission circuit, thereby requiring the CLR's inclusion in the TSC design in order to protect the power electronics. SVC designs therefore employ specialized switching schemes to further minimize the inevitable switching transients and better approach these ideal criteria [**22**].

An alternative technique exists to reduce or eliminate transient currents altogether without restricting the TSC's range of operation, but this method is rarely used in practice. A shunt-connected *charging circuit* that charges the capacitor when it is disconnected from the system can ensure that the voltage across the capacitor matches the system voltage at the instant of switching. Although a charging circuit would ideally be added to the TSC circuit to maintain the capacitor's charge at this level, such circuits are expensive to implement and are therefore rarely installed [**22**].

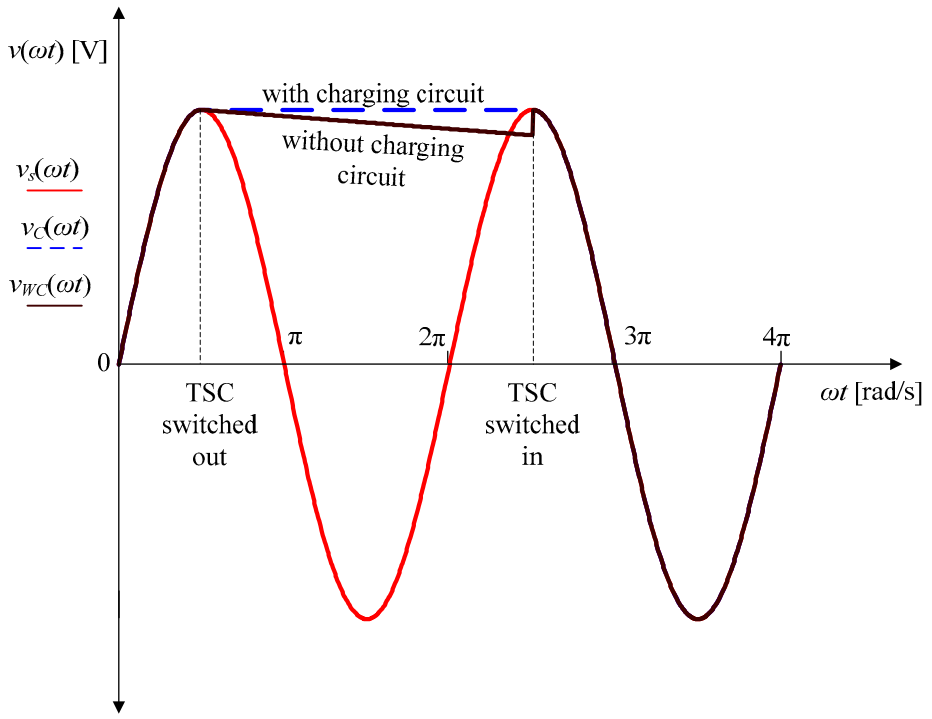

Figure 2.18: TSC voltage waveform

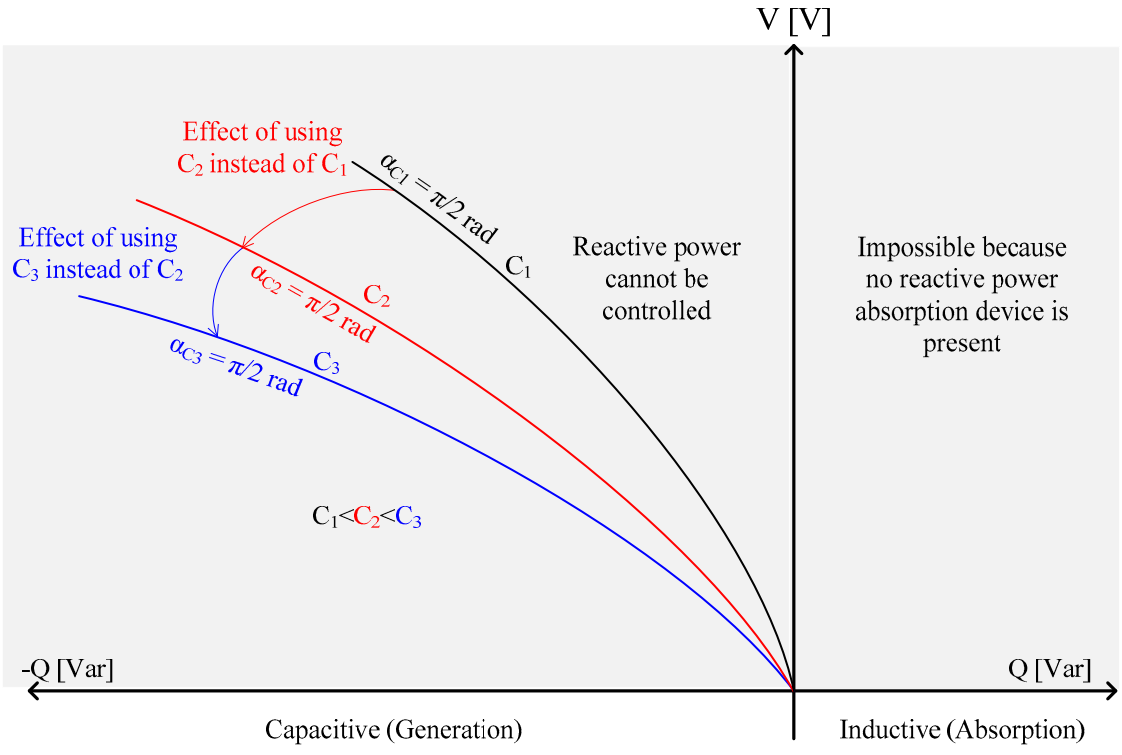

Figure 2.19: Effect of capacitor size on a single-phase TSC V-Q characteristic

More practical TSCs employ multiple capacitor branches, each of which can be independently switched into and out of operation. Although this resulting configuration continues to lack full reactive power control, it at least provides multiple discrete levels of reactive power. An SVC with k TSC branches will normally comprise k-1 branches of susceptance B_C and one branch of susceptance $B_C/2$ to enable finer control between branches A single line diagram of this configuration is shown in Figure 2.20. A voltage deadband is also employed to ensure that TSC branches do not continuously switch on and off while the voltage remains within the deadband as illustrated in Figure 2.21.

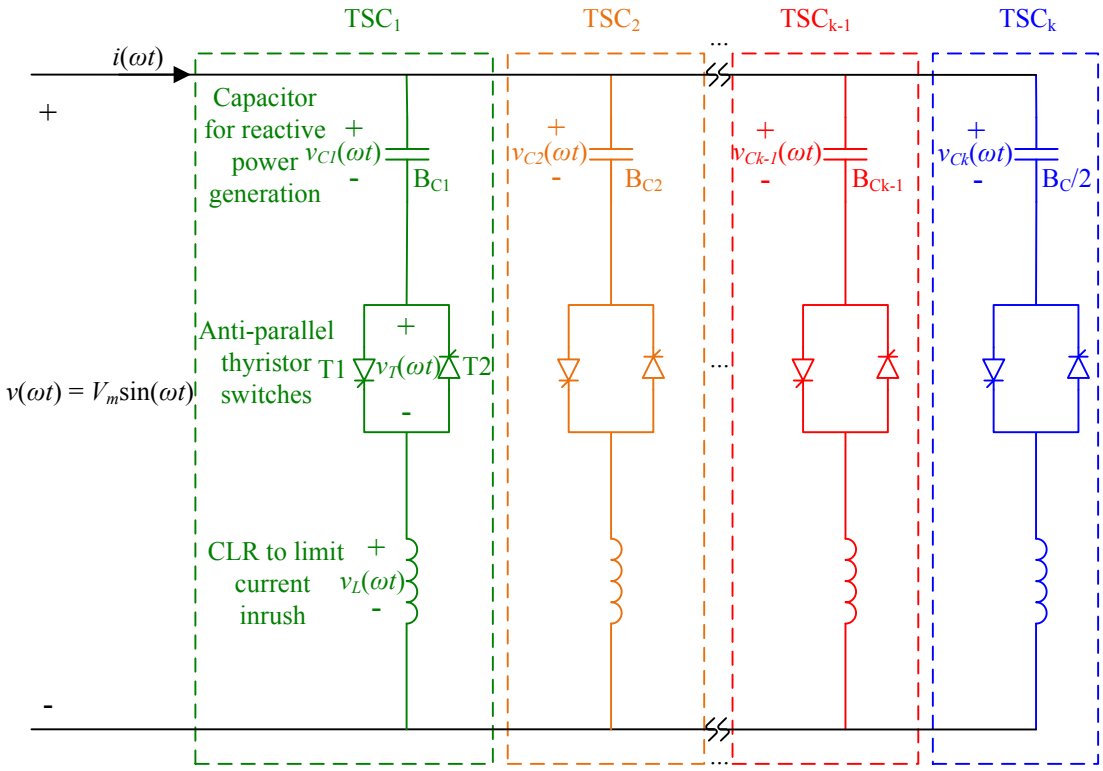

Figure 2.20: Multiple TSCs

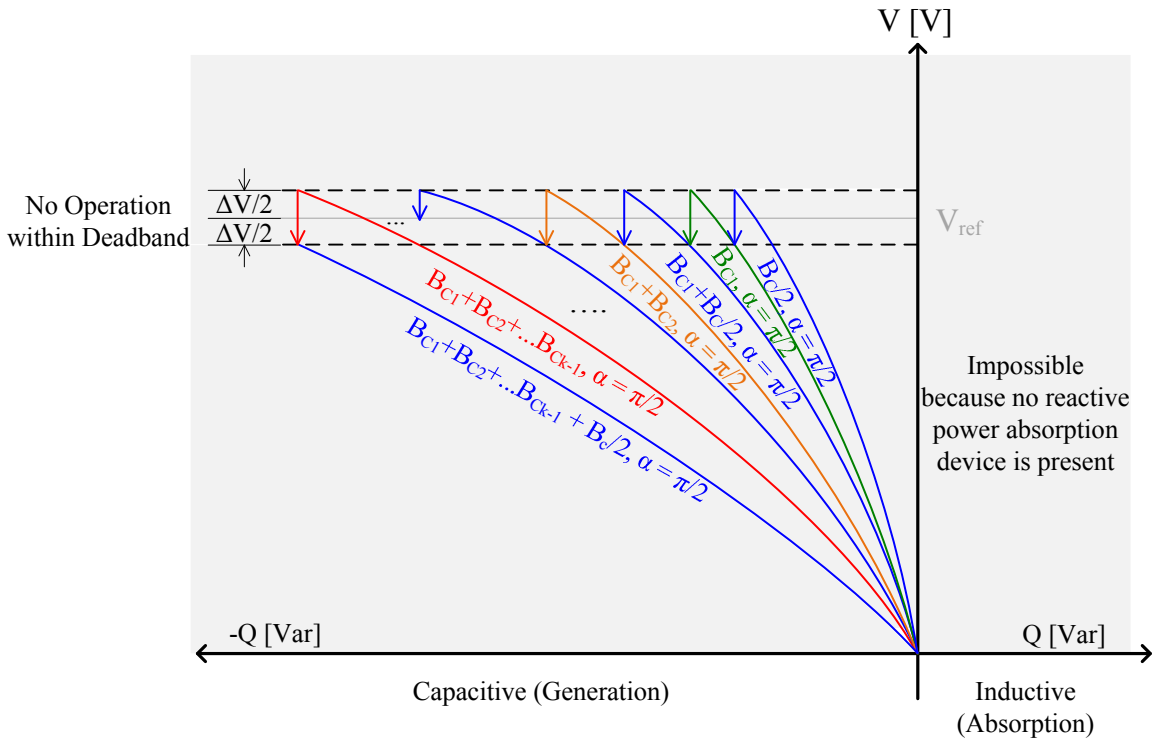

Figure 2.21: V-Q characteristic of *k* single-phase TSCs

2.1.5 Thyristor Switched Capacitor-Thyristor Controlled Reactor (TSC-TCR)

The TSC's advantage of reduced transient response is offset by their discrete operational characteristics, which limit their use in systems that require continuous reactive power control. Adding a TCR to the TSC provides sufficient controllability to produce a *Thyristor Switched Capacitor-Thyristor Controlled Reactor* (*TSC-TCR*) with a continuous V-Q characteristic. This arrangement is illustrated in Figure 2.22. Not only does the TSC-TCR have greater operational flexibility than a TSC, it also produces fewer steady state losses than an FC-TCR [**22**], [**23**].

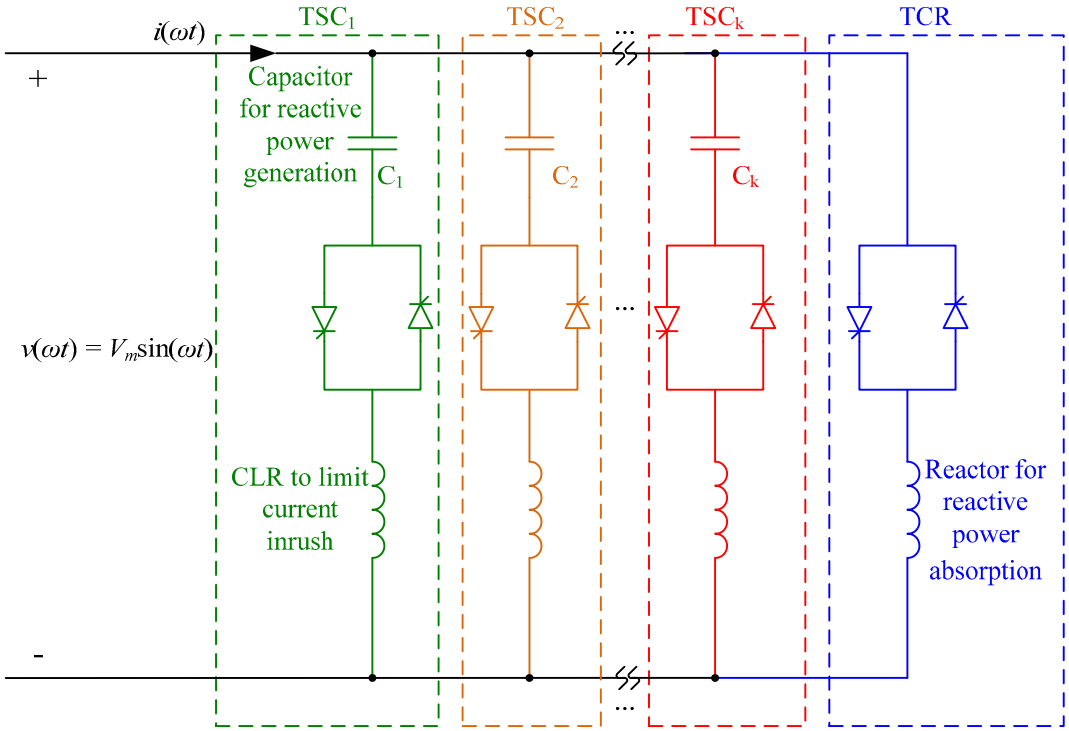

Figure 2.22: TSC-TCR

The TSC-TCR's reactor is typically sized with a slightly higher reactive power rating than an individual TSC component to provide the SVC with overlapping reactive power ranges over the discrete TSCs. This effectively creates a reactive power deadband and limits unnecessary switching. The TSC-TCR's V-Q characteristic is shown in Figure 2.23.

During large system disturbances, an FC-TCR behaves as a parallel LC branch that may resonate with the transmission system. In contrast, the TSC-TCR can remove itself from service sufficiently quickly to preclude it from resonating with the transmission system during or immediately after large disturbances [**22**].

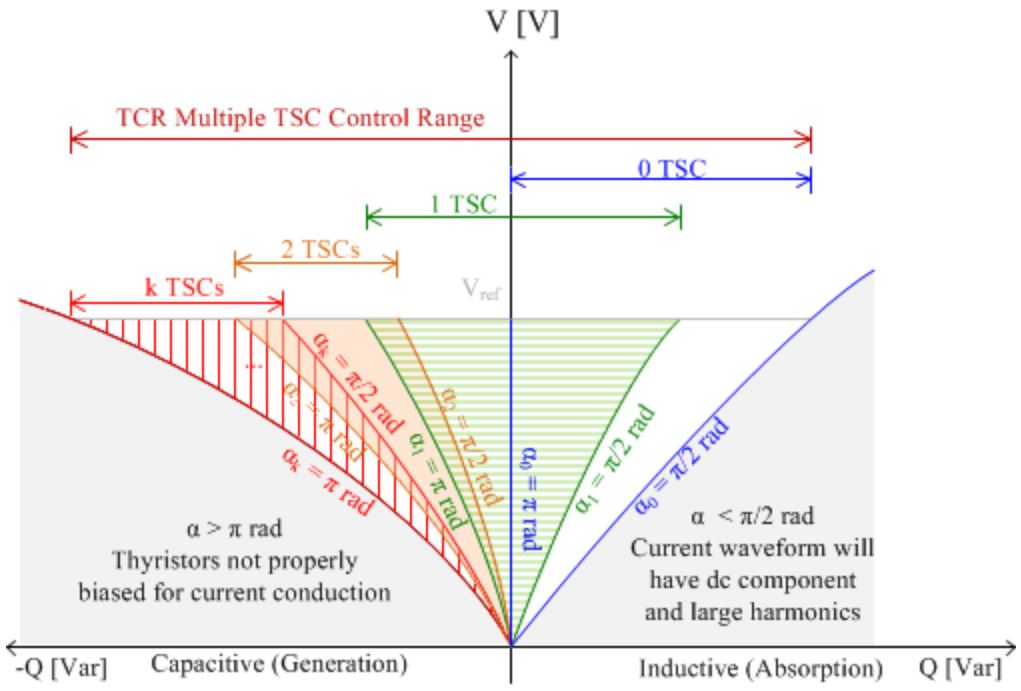

Figure 2.23: V-Q characteristic for a TCR multiple TSC arrangement

2.1.6 Practical Considerations

The idealized SVC configurations discussed thus far have ignored many design considerations required for practical implementation. For example, an SVC does not directly connect to the transmission system, but is rather connected through a step-down transformer whose windings behave as reactors that introduce additional susceptance to the idealized V-Q characteristics discussed [**22**]. An SVC can also employ filter banks that assist in steady state reactive power compensation in addition to filtering out unwanted current harmonics. This is accomplished by tuning LC filters so that the capacitors' reactive power generation is much larger than the inductors' reactive power absorption, thereby causing the filter to function like a capacitor connected to the SVC terminals [**17**]. This shifts the already discussed idealized V-Q characteristics towards the generation region of the V-Q characteristic.

2.2 SVC Control System

A practical SVC also requires a control system to effectively employ its constituent components. General SVC control systems typically consist of a measurement system, a voltage regulator, a gate pulse generator (GPG), and a synchronizing system as shown in Figure 2.24 [**22**]. Auxiliary control functionality is also sometimes included when required for cases such as power oscillation damping.

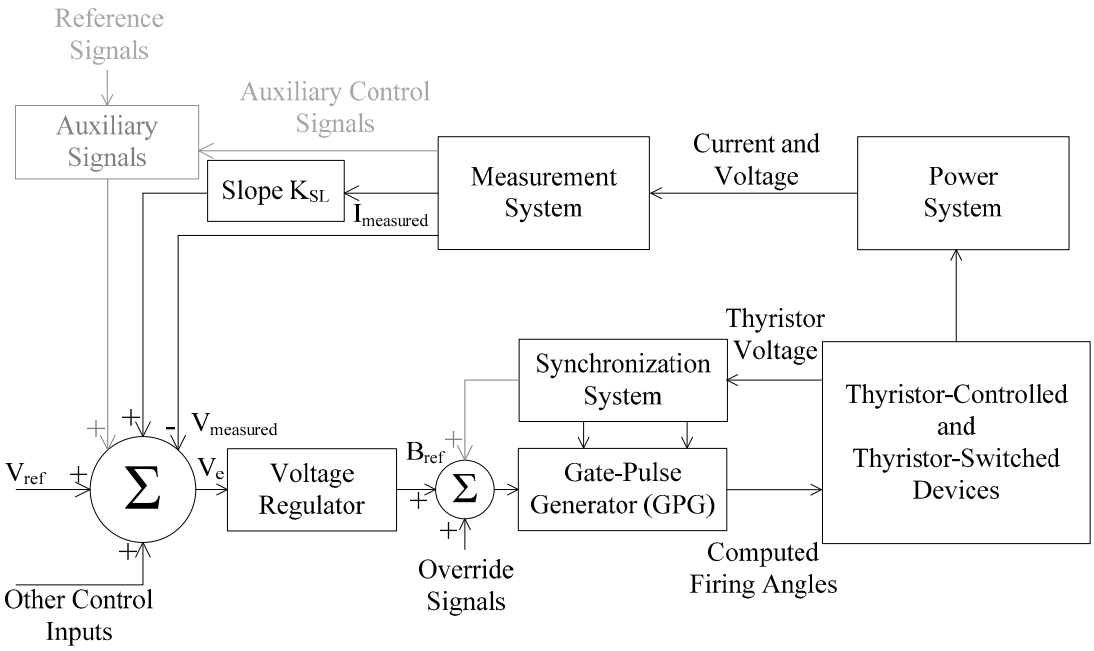

Figure 2.24: A typical SVC control block diagram

2.2.1 Measurement System

The measurement system provides the inputs that the control system requires to perform its desired operations. Some of these values are directly measured while others are derived from basic current and voltage measurements. The required measurement parameters depend upon the type of SVC control employed.

Table 2.1: Possible SVC system measurements

Voltages	Currents	Auxiliary Measurements
Individual Phases	Individual Phases	Individual Phase Reactive Power
3-phase RMS	3-phase RMS	Transmission Line Real Power Transmission Line Reactive Power
Positive and Negative Sequence	Transmission Line	Bus Angles Bus Frequency
Magnitude Squared		Synchronous Generator Angular Velocity

2.2.2 Synchronization System

The synchronization system generates reference signals that are synchronized to the system voltage's fundamental frequency. The *gate pulse generator* (GPG) uses these references to produce the SVC's TCR and TSC firing pulses, and although it typically uses a phase locked loop (PLL) to do so, other reference signals such as the thyristor voltages have also been used [**22**]. A model of of PLL for an SVC controller is depicted in Figure 2.25.

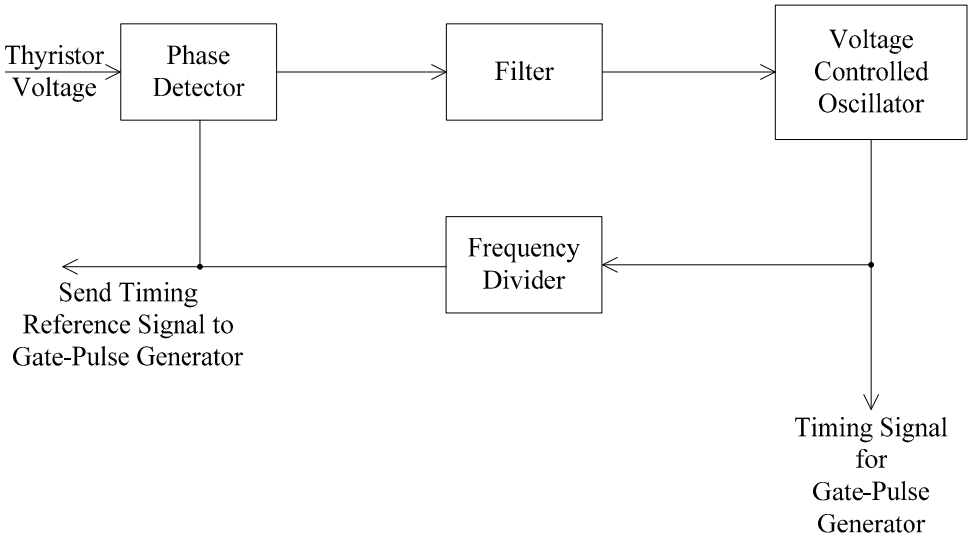

Figure 2.25: PLL model for SVC controller

Irrespective of the method employed, all synchronization systems must minimize the generation of non-characteristic harmonics while accurately tracking the system's phase and frequency. They must also remain insensitive to events such as supply voltage

distortions and severe system disturbances, and they must rapidly resynchronize upon fault clearing in order to maintain system reliability [**22**].

2.2.3 Voltage Regulator

The SVC voltage regulator uses the voltage error, V_e, to produce the reference susceptance value, B_{ref}, required to obtain the desired SVC bus voltage.

A slope, or *droop*, of K_{SL} is typically included in the SVC voltage-current characteristics as shown in Figure 2.26 [**22**]. This droop reduces the SVC's reactive power rating, prevents the SVC from reaching its reactive power limits too frequently, and facilitates reactive power sharing between multiple parallel compensators. Droop is implemented by multiplying the measured SVC current by the droop value K_{SL} when SVC current measurements can be reliably obtained. If SVC current measurements are unattainable, the SVC voltage is assumed to be near unity, thereby producing a reference susceptance that is approximately equal to the SVC current. Typical K_{SL} values lie between 3-5%, but they can sometimes range as wide as 1-10% [**22**].

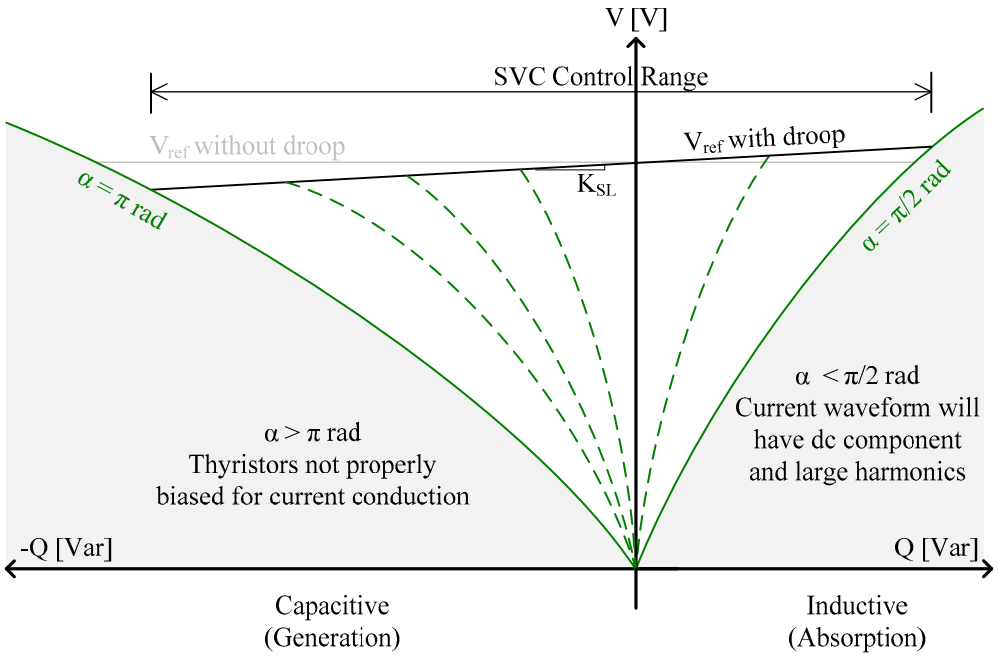

Figure 2.26: SVC V-Q characteristic with droop

2.2.4 Gate-Pulse Generator

The gate-pulse generator (GPG) receives a reference susceptance signal from the voltage regulator and translates this into firing pulses that the SVC thyristor devices use to generate the required susceptance. In SVCs consisting of only a TCR and fixed capacitors, the GPG calculates the susceptance needed by the TCR to cancel the excess capacitance. In SVCs comprising a TCR, fixed capacitors and a TSC, the GPG must also determine the number of TSCs to be switched in order to meet the reactive power requirements, calculate the corresponding TCR firing angles to realize this susceptance, and then determine the TSC connection sequence that ensures minimal transient capacitive switching [**24**].

The GPG accomplishes its tasks by first dividing the required susceptance, B_C, by the susceptance of a single TSC. This value, k_C, is rounded up to the next largest integer value to ensure that sufficient capacitive susceptance exists in the circuit. The required

inductive susceptance is computed by taking the difference between $k_C B_C$ and B_{ref}. The GPG then calculates the required TCR firing angle to realize this susceptance. Switching transients are minimized by employing the methodology outlined in [**22**] and illustrated in Figure 2.27.

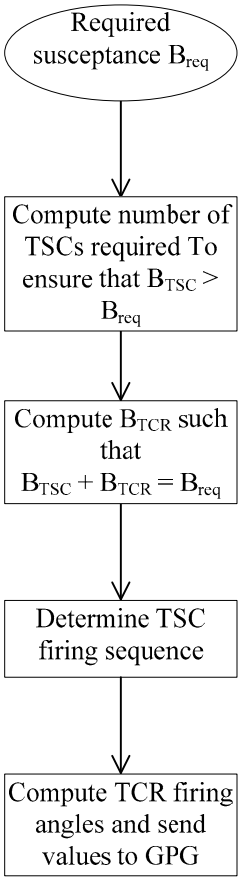

Figure 2.27: Gate-Pulse Generator Flowchart

The fundamental SVC system principles that have been briefly introduced in this chapter can be better optimized for operational performance by employing more complex control algorithms. Chapter three provides an overview of the fuzzy logic and fuzzy inference systems that can be utilized in order to do so.

Chapter 3 Fuzzy Logic

This chapter introduces fuzzy logic, its basic operators, and its applicability to decision making processes.

In set theory, an *element* is the label assigned to an abstract object, and a *set* is an arbitrarily defined grouping of possible elements. Traditional set theory requires that each element be rigidly categorized as either completely belonging to a set or entirely excluded from it. For example, a car can be classified as an element within the set of motorized vehicles and excluded from the set of Latin American coffee beans.

Traditional set theory's classification method suffices for elements that have well-defined properties, but it becomes more problematic when applied to context sensitive classifications. For example, a particular car whose speed cannot physically exceed 200 km/h could have this property mathematically described by a set whose elements contain all possible speeds between 0 km/h and 200 km/h. To categorize these speeds, traditional set theory requires defining a threshold speed such as 100 km/h as a boundary above which all speeds would be considered *fast* and below which all speeds would be considered *slow*. However, the negligible practical distinction between 99.999 km/h and 100.001 km/h makes it intuitively inconsistent to classify such speeds differently.

Fuzzy logic is a more generalized form of set theory that is better suited to mathematically describe a system's qualitative properties [**23**], [**25**], [**26**]. It does so by employing a class of objects called *fuzzy sets* whose elements may have varying degrees of membership. This degree of membership is usually determined by a *membership function* (MF) that maps an element to a value between zero and one.

In fuzzy set theory, a fuzzy element for the above car example would be defined as possible car speeds, x km/h. A membership function $\mu_{fast}(x)$ would then be defined to create a continuous grade of membership that relates speeds with the term *fast*.

3.1 Fundamental of Fuzzy Logic

3.1.1 Membership Functions

An element x has a degree of membership y in a fuzzy set that is defined by a membership function $y=\mu(x)$, where y lies on the interval [0, 1] and is said to be the *fuzzified* value of x.

Consider again the definition of "fast", which could be defined by a simple membership function such as equation (3.1) and depicted in Figure 3.2.

$$y = \mu_{fast}(x) = 0.005x, \quad 0 \text{ km/h} \le x \le 200 \text{ km/h} \tag{3.1}$$

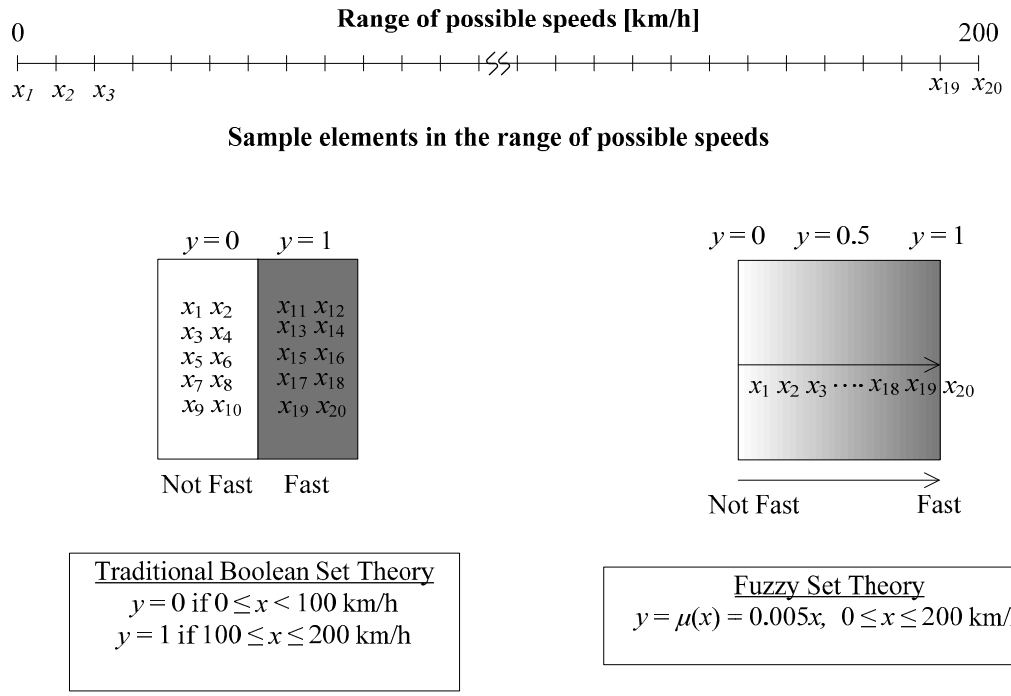

Figure 3.1: A comparison of traditional set theory and fuzzy set theory

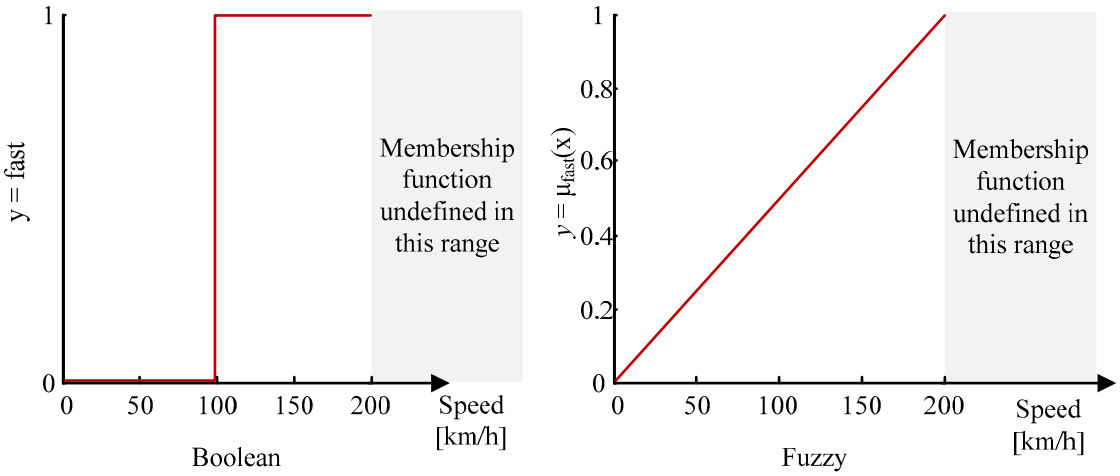

Figure 3.2: A possible membership function for fast speeds

Although the above example fuzzifies a car's speed in an elementary way, membership functions can be as simple or as complicated as an application requires. For example, defining speeds between 0 and 50 km/h to be even remotely *fast* when considering driving speeds along the Trans-Canada Highway would be inappropriate. In this instance, it would be preferable to define any speed below 50 km/h as having a membership value of zero in the set of *fast* speeds and to assign a unity membership value to all speeds above 150 km/h. The membership function between these two extremes could smoothly transition from "not at all fast" to "fast" to reflect the intuitive notion that the degree of membership to the set of *fast* speeds increases proportionately with increasing car speeds. Such a membership function is expressed mathematically in Equation (3.2) and is illustrated in Figure 3.3. Using this membership function, a 70 km/h speed is given a value of 0.2, indicating a "slightly fast" speed. Conversely, a 140 km/h speed is assigned a value of 0.9, indicating a speed that is quite a bit more fast than slow.

$$y = \mu_{fast}(x) = \begin{cases} 0, & 0\ \text{km/hr} \le x \le 50\ \text{km/hr} \\ 0.01(x-50), & 50\ \text{km/hr} < x < 150\ \text{km/hr} \\ 1, & 150\ \text{km/hr} \le x \le 200\ \text{km/hr} \end{cases} \quad (3.2)$$

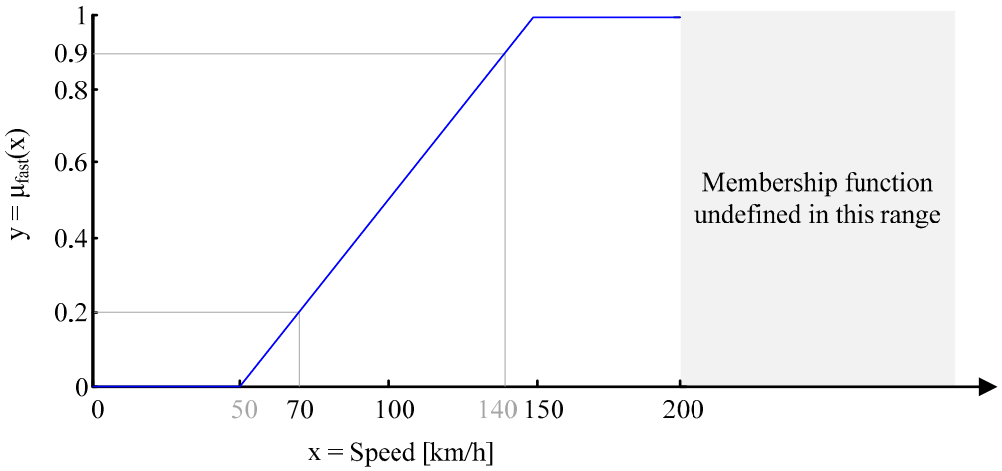

Figure 3.3: Membership function for determining fast speed

3.1.2 Fuzzy Operators

Just as arithmetic operators such as addition and multiplication combine and manipulate numbers, *fuzzy operators* are used to combine and manipulate fuzzified elements. The *intersection* (AND, ∩), *union* (OR, ∪), *negation* (NOT, ¬), and *implication* (IF-THEN, $\Rightarrow$) operators are the four fundamental traditional logic operators that form the foundation of Boolean logic and traditional set theory. The underlying concepts conveyed by the first three of these operators can be extended into the fuzzy domain with varying degrees of ease. For such cases, fuzzy logic becomes a superset of traditional Boolean logic, and fuzzy operators reduce to traditional set theory operators when specific elements within a fuzzy set have the traditional Boolean membership values of

either zero or one. The following sets A and B as shown in Figure 3.4 will be used to compare and contrast Boolean and fuzzy operators.

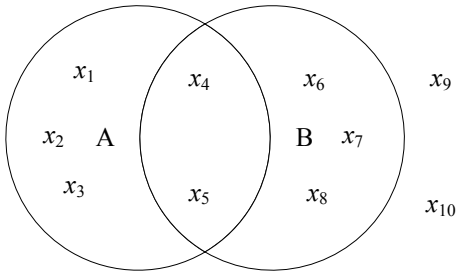

$$\{x_1, x_2, x_3, x_4, x_5\} \in A$$
$$\{x_4, x_5, x_6, x_7, x_8\} \in B$$

Figure 3.4: Illustrative sets

3.1.2.1 Intersection

The *intersection* of two sets A and B is mathematically described by the expression below and illustrated in Figure 3.5.

$$A \cap B = \{x | x \in A \text{ and } x \in B\}$$

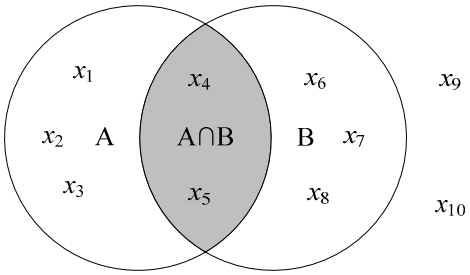

Figure 3.5: Venn diagram of the intersection of two sets in traditional set theory

Under Boolean logic, any element that belongs to both set A and set B is a member of the intersection set and assigned a value of 1, whereas any element that belongs exclusively to either set A or set B, or that belongs to neither set A nor set B, is excluded from this set and assigned a value of 0. The elements x_4 and x_5 in Figure 3.5 belong to both sets A and B and therefore belong to the intersection of the two sets. The intersection of the two sets of Figure 3.5 is shown in Table 3.1.

Table 3.1: Boolean intersection truth table

Element	A	B	A∩B
x_1	1	0	0
x_2	1	0	0
x_3	1	0	0
x_4	1	1	1
x_5	1	1	1
x_6	0	1	0
x_7	0	1	0
x_8	0	1	0
x_9	0	0	0
x_{10}	0	0	0

Many methods exist for extending this Boolean intersection operator into the fuzzy domain [**26**], but this thesis restricts the fuzzy intersection operator to the minimum value of two quantities. This *minimum operator*, Min(A,B), maintains the traditional set theory boundary conditions while enabling its extension to the membership values between 0 and 1 that are typically encountered in fuzzy logic. The highlighted entries in Table 3.2 indicate the minimum operator's reduction to the Boolean logic intersection when the memberships to a fuzzy set are Boolean values.

Table 3.2: Minimum operator for fuzzy and Boolean logic values

Fuzzy Operator

A	B	Min(A,B)
0	0	0
0	0.33	0
0	0.66	0
0	1	0
0.33	0	0
0.33	0.33	0.33
0.33	0.66	0.33
0.33	1	0.33
0.66	0	0
0.66	0.33	0.33
0.66	0.66	0.66
0.66	1	0.66
1	0	0
1	0.33	0.33
1	0.66	0.66
1	1	1

Boolean Operator

A	B	A∩B
0	0	0
0	1	0
1	0	0
1	1	1

3.1.2.2 Union

The *union* operator in traditional set theory can be described mathematically by the below expression and illustrated in Figure 3.6.

$$A \cup B = \{x | x \in A \text{ or } x \in B\}$$

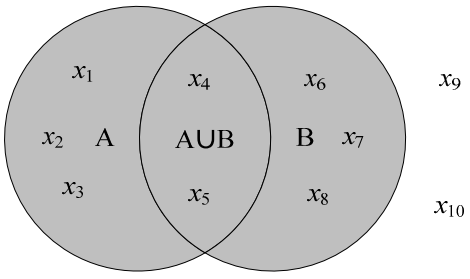

Figure 3.6: Venn diagram of the union of two sets in traditional set theory

Under Boolean logic, any element that belongs to either set *A* or set *B*, or to both set *A* and set *B*, is a member of the union set and assigned a value of 1, whereas any element

that belongs to neither set *A* nor set *B* is not a member of this set and assigned a value of 0. The Boolean union operator can be described in Table 3.3.

Table 3.3: Boolean union truth table

Element	A	B	A ∪ B
x_1	1	0	1
x_2	1	0	1
x_3	1	0	1
x_4	1	1	1
x_5	1	1	1
x_6	0	1	1
x_7	0	1	1
x_8	0	1	1
x_9	0	0	0
x_{10}	0	0	0

As with the fuzzy intersection operator, many fuzzy union definitions can be employed [**26**]. However, this thesis applies the *maximum operator*, Max(*A*,*B*) when discussing the fuzzy union operator in order to maintain traditional logic and still permit varying degrees of membership. Table 3.4 illustrates the maximum operator for membership values that lie between 0 and 1.

Table 3.4: Maximum operator for fuzzy and Boolean logic values

Fuzzy Operator

A	B	Max(A,B)
0	0	0
0	0.33	0.33
0	0.66	0.66
0	1	1
0.33	0	0.33
0.33	0.33	0.33
0.33	0.66	0.66
0.33	1	1
0.66	0	0.66
0.66	0.33	0.66
0.66	0.66	0.66
0.66	1	1
1	0	1
1	0.33	1
1	0.66	1
1	1	1

Boolean Operator

A	B	A ∪ B
0	0	0
0	1	1
1	0	1
1	1	1

3.1.2.3 *Complement*

The *complement* in traditional set theory can be mathematically described by the expression below and illustrated in Figure 3.7.

$$\neg A = \{x | x \notin A\}$$

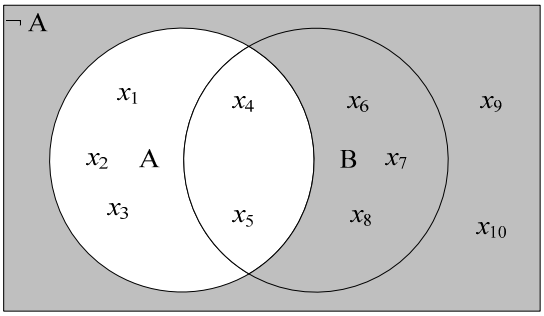

Figure 3.7: Venn diagram of the complement of a set in traditional set theory

Under Boolean logic, any element that does not belong set A is a member of the complement of A and assigned a value of 1, whereas any element that belongs to set A is

not a member of the complement of A and is assigned a value of 0. Boolean logic expresses the complement operator as shown in Table 3.5.

Table 3.5: Boolean complement truth table

Element	A	¬A
x_1	1	0
x_2	1	0
x_3	1	0
x_4	1	0
x_5	1	0
x_6	0	1
x_7	0	1
x_8	0	1
x_9	0	1
x_{10}	0	1

The fuzzy complement operator can be defined as 1-$\mu(x)$ where $\mu(x)$ is the membership value of the fuzzy set. This definition maintains the traditional logic operator while extending its meaning into the fuzzy domain, and it is normally the only definition used. Table 3.6 provides illustrative values of sample complement operations on fuzzy logic values.

Table 3.6: Complement operator for fuzzy and Boolean logic values

Fuzzy Operator

A	1-A
0	1
0.25	0.75
0.5	0.5
0.75	0.25
1	0

Boolean Operator

A	¬A
0	1
1	0

3.1.2.4 Implication

Implication in traditional set theory is also known as a *conditional sentence*. Implications are of the form *"if* P*, then* Q*"* and can be mathematically represented as

$$P \Rightarrow Q$$

where P is the *antecedent*, or *premise*, and Q is the *consequent*, or *conclusion*. Implications can also have multiple premises of the form "If P and R, then Q". Boolean logic expresses the implication operator as shown in Table 3.7.

Table 3.7: Boolean implication truth table

P	**Q**	**P ⇒ Q**
0	0	1
0	1	1
1	0	0
1	1	1

Unlike previous operators discussed, the fuzzy implication operator does not reduce to the traditional set theory implication. Because the fuzzified values of the premises, which are known as *partial premises*, may assume any value over the range [0, 1], fuzzy logic requires a more complex implication operator than Boolean logic, whose element values are limited to either 0 or 1. The existence of partial premises implies the impossibility of drawing a fixed conclusion. Instead, partial premises are combined into a single fuzzified premise, which then combines with an entire *conclusion set* to yield a set representing the conclusion. Several techniques for implementing the fuzzy implication exist, with the two most commonly used methods being the *minimum* and *product* functions. This thesis arbitrarily uses the minimum method first introduced by Mamdani [**27**].

Fuzzy logic applies *if-then* rules to relate fuzzy sets to each other. If A and B are fuzzy sets represented by linguistic variables, then fuzzy logic applies an *if-then* rule of the form:

If x *is* A, *then* y *is* B.

For example, a driver who encounters a stop sign may apply an if-then rule illustrated in Figure 3.8.

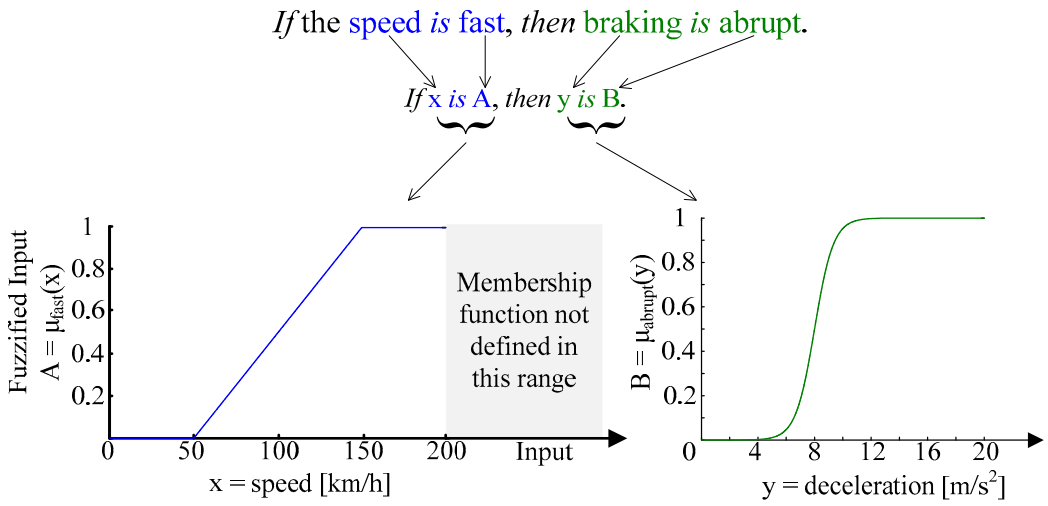

Figure 3.8: Single premise fuzzy if-then rule

where *speed* is the input x to the if-then rule, *braking* is the output y, and A and B are fuzzy sets corresponding to *fast* and *abrupt*, respectively.

In this example, a driver's speed maps to a fuzzified input value of between 0 and 1 depending upon the degree to which the speed input is considered *fast*. The conclusion "braking is abrupt" is the assignment of the entire fuzzy set *abrupt* to the output braking.

A fuzzy if-then statement can also have multiple premises, such as:

If x_1 *is* A_1 and x_2 is A_2, *then* y *is* B.

This type of statement is illustrated in Figure 3.9.

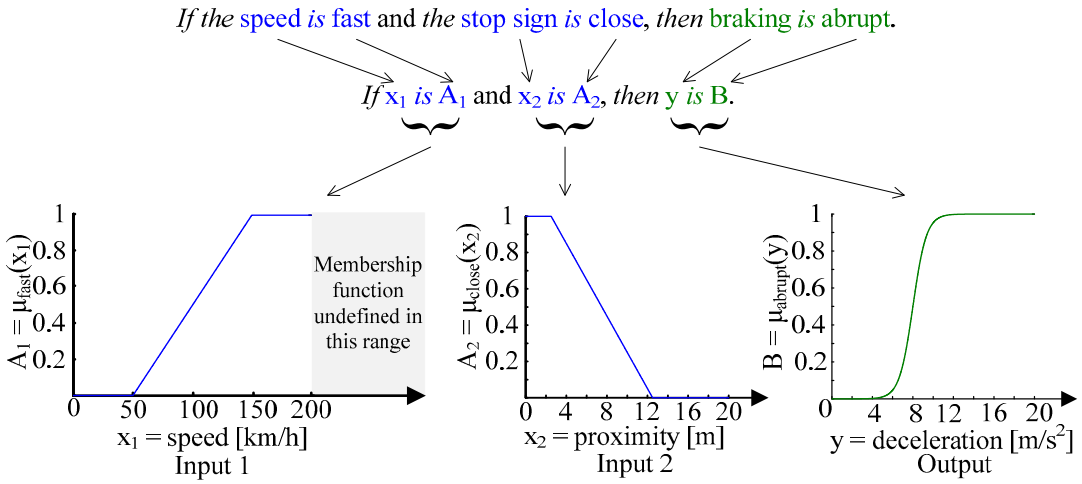

Figure 3.9: Multiple premise fuzzy if-then rule

The multiple premises are combined to produce a single value representing the entire premise. This value can then be used to draw a conclusion or inputted into a fuzzy inference process. The output of a fuzzy if-then rule is itself a fuzzy set whose membership function represents the qualities of the conclusion.

For example, motorists driving at 100 km/h who sees a stop sign 4.5 meters away and utilizing the minimum implication method results in the braking conclusion set shown in Figure 3.10.

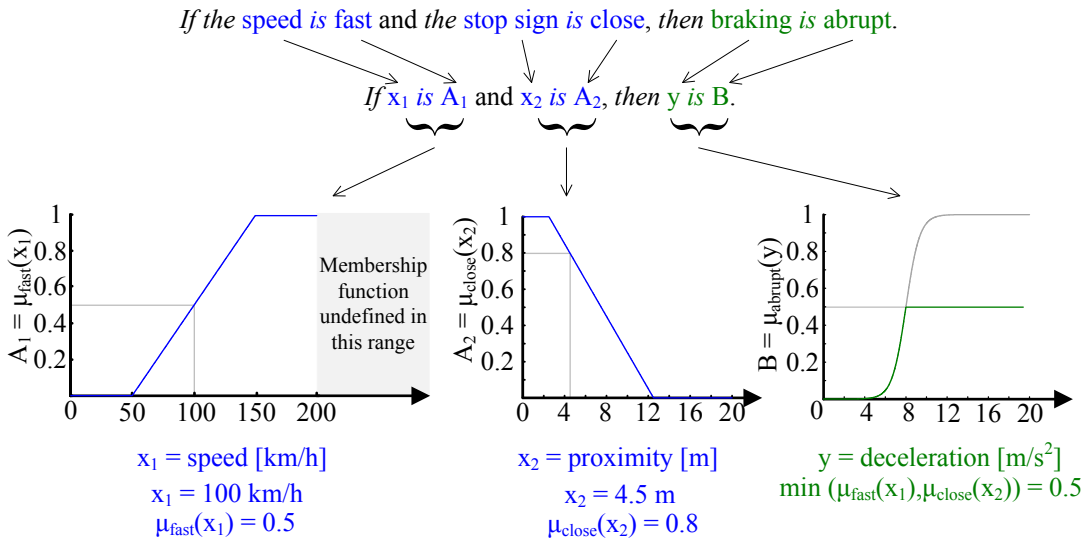

Figure 3.10: Multiple premise fuzzy if-then rule calculation

3.2 Fuzzy Inference Systems

Fuzzy inference is the process of applying fuzzy logic to a set of inputs in order to produce a set of outputs. A *fuzzy inference system* (FIS) is the construct that makes use of fuzzy inference and is depicted in Figure 3.11.

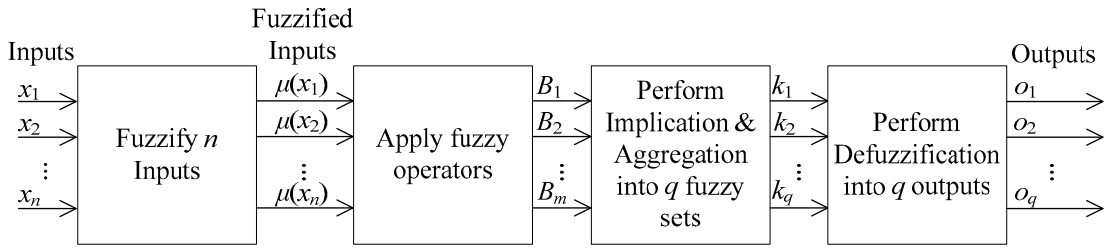

Figure 3.11: Block diagram of the generalized fuzzy inference process

The fuzzy inference process can be illustrated through an example involving the evaluation of a diving competition. The two criteria used for scoring such a competition are the dive's degree of difficulty and the flawlessness of its execution. This type of example precludes the use of Boolean logic, which can only judge the dive as poor or excellent without allowing for intermediate classifications. This methodology is shown in Figure 3.12 and the rules used are shown in Table 3.8.

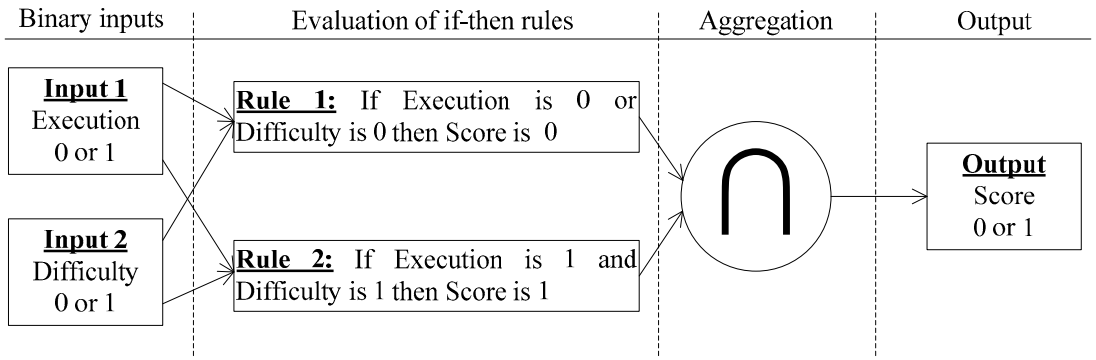

Figure 3.12: Employing Boolean logic to score a dive produces absurd results

Table 3.8: Boolean rules for diving example

Input 2: Difficulty \ Input 1: Execution	Poor	Excellent
Low	0	0
High	0	1

In contrast to the above Boolean system, a fuzzy system can assign scores along a continuum between very poor and very good. Both inputs may be evaluated on a scale of 0 to 10, where 0 is assigned to a very poor dive and 10 denotes a very good dive. The FIS uses each of the input values to determine the final score is shown in Figure 3.13, and the rules are shown in tabular form in Table 3.9.

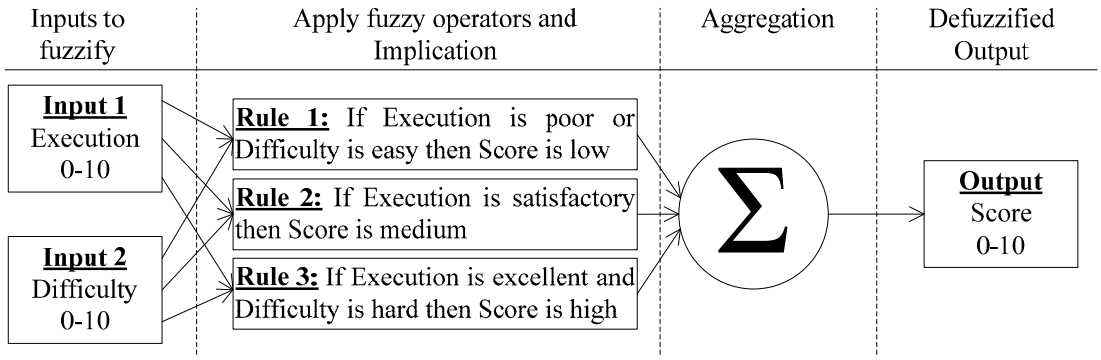

Figure 3.13: FIS diving example using fuzzy logic

Table 3.9: Fuzzy rules for diving example

Input 2: Difficulty \ Input 1: Execution	Poor	Satisfactory	Excellent
Easy	Low	Low/Medium	Low
Average	Low	Medium	
Hard	Low	Medium	High

3.2.1 Step One: Fuzzification

The FIS begins by determining each input's degree of membership in each of the problem's fuzzy sets. This is determined by first ranking the dive's qualitative descriptions between 0 and 10 and then applying the membership functions to each of these rankings to fuzzify the inputs between 0 and 1. In this case, the input values for execution and difficulty are each ranked from 0 to 10 and then mapped to the interval between 0 and 1 using membership functions. Each of the three rules that are applied in this example requires that each input be resolved into fuzzy sets corresponding to the qualitative descriptions:

- difficulty is easy
- difficulty is average
- difficulty is hard
- execution is poor
- execution is satisfactory
- execution is excellent

The shape of the membership functions shown in Figure 3.14 and 3.15 were chosen to reflect how these qualitative descriptors are perceived. The diving judges could select different membership functions depending upon their view as to what constitutes *easy*, *average*, *hard*, *poor*, *satisfactory*, and *excellent*.

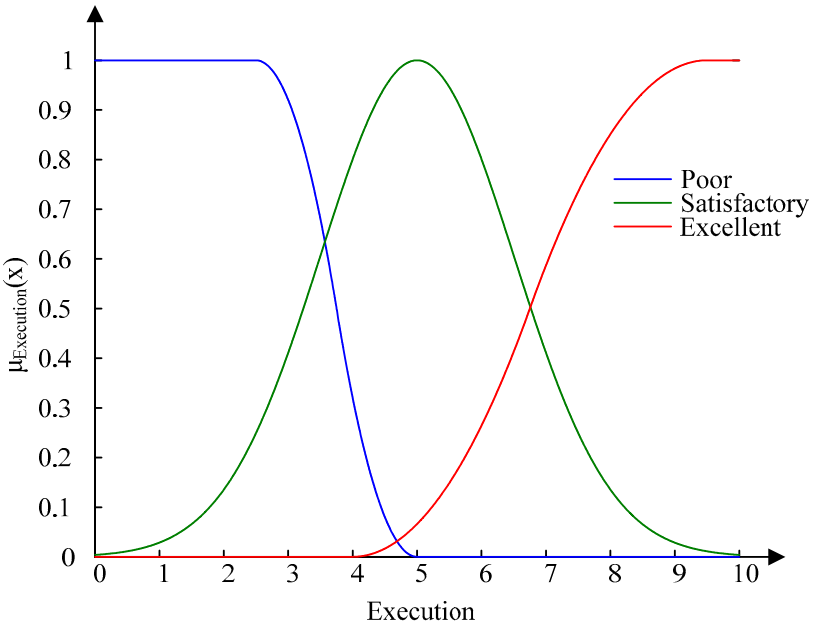

Figure 3.14: Execution membership functions

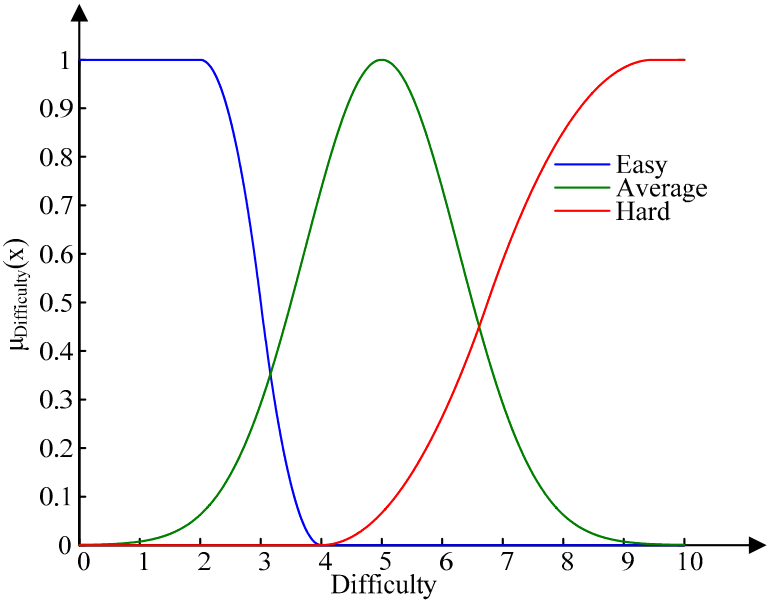

Figure 3.15: Difficulty membership functions

For example, a dive with an execution rating of 8 and a difficulty rating of 3 would produce the following fuzzified values shown in Figure 3.16.

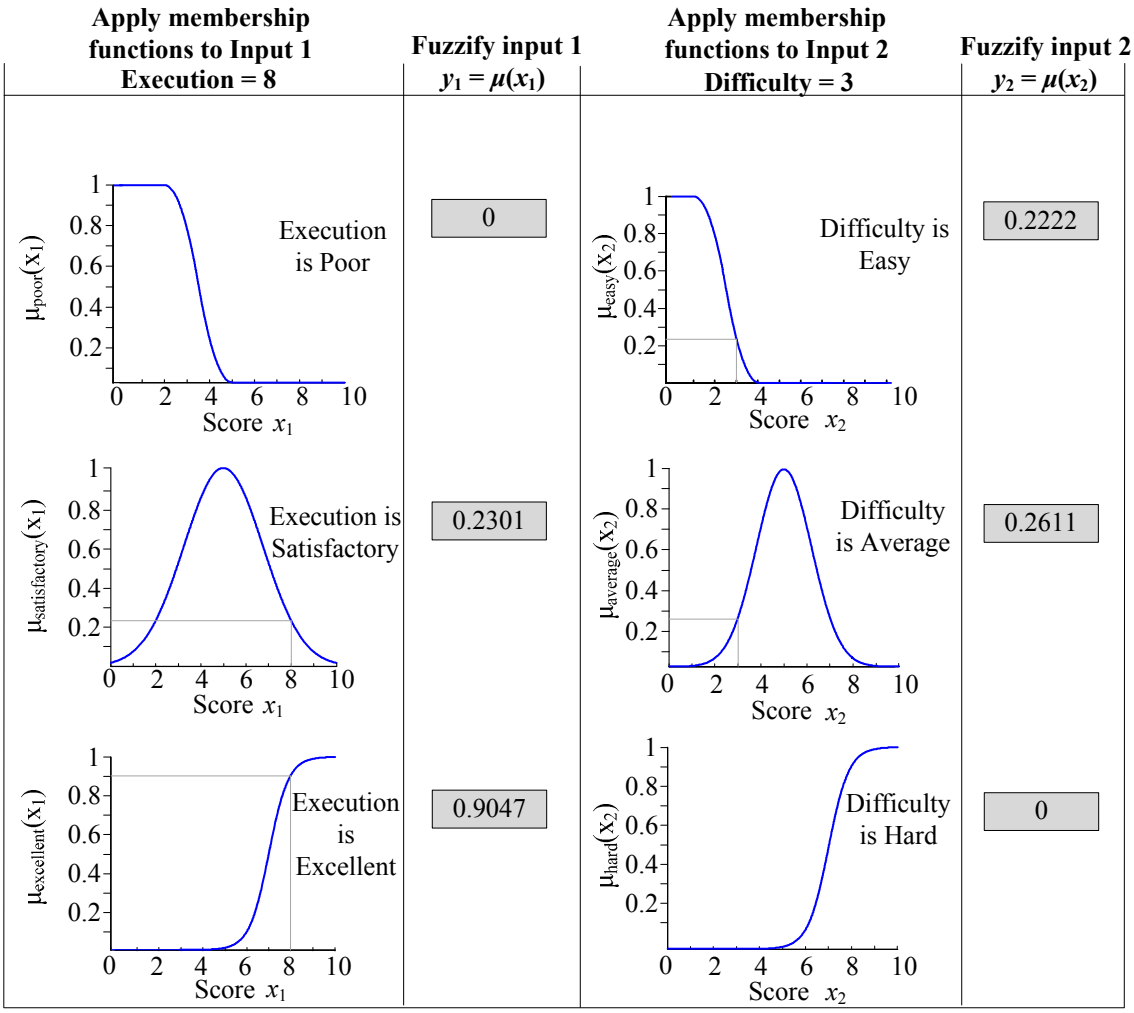

Figure 3.16: Step 1 involves fuzzifying execution and difficulty inputs

3.2.2 Step Two: Application of Fuzzy Operators

Once the inputs have all been fuzzified by their respective membership functions, rules with multiple premises can be evaluated. When the premise has multiple parts, the corresponding fuzzy operators linking each partial premise are applied such that a single value can be assigned to the entire premise.

Figure 3.17 illustrates the use of fuzzy operators: OR, or *maximum*, AND, or *minimum*, and a rule without a fuzzy operator. Because the OR function is applied to the multiple-premised Rule 1 that "If Execution is poor or Difficulty is easy, then the Score is

low", the maximum fuzzy value obtained from "Execution is poor" and "Difficulty is easy" is used as the fuzzy value of the entire premise. Conversely, because the AND function is applied to the multi-premised Rule 3, "If Execution is excellent and Difficulty is hard, then the Score is high", the minimum value obtained from "Execution is excellent" and "Difficulty is hard" is used as the fuzzy value of the entire premise. Finally, because Rule 2 lacks multiple premises, the fuzzy value of the premise is simply the fuzzy value of "Execution is satisfactory".

If a particular dive's execution is rated an 8 and the difficulty of the dive is graded as 3, these inputs are fuzzified using the appropriate membership functions (the *poor* membership function for execution and the *easy* membership function for difficulty) to obtain membership values of 0 and 0.2222 respectively. The fuzzy OR operator selects the maximum of the two values, or 0.2222. This completes the fuzzification of this particular rule. The results of applying fuzzy operators are summarized in Figure 3.17.

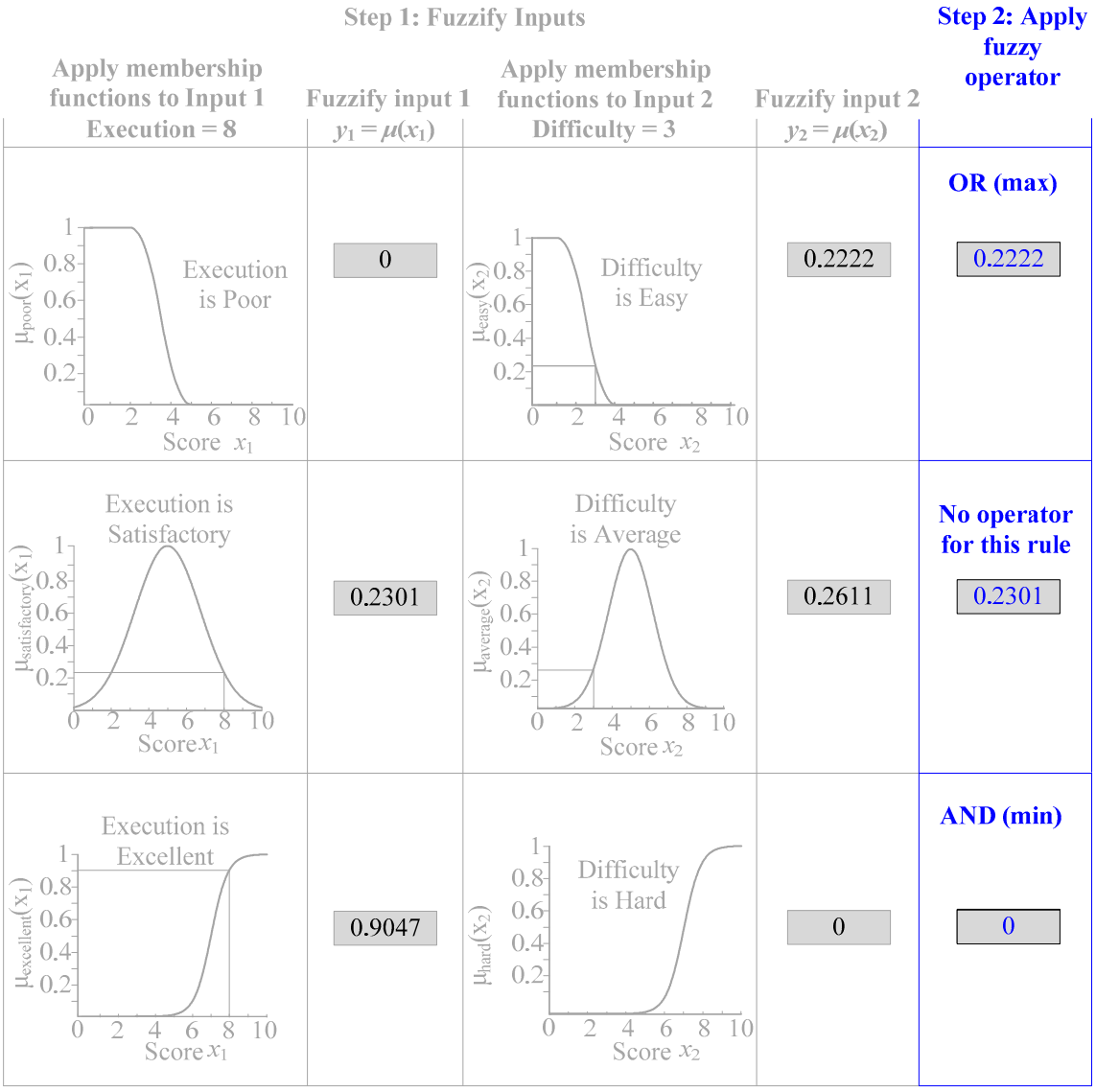

Figure 3.17: Step 2 evaluates fuzzified inputs by applying fuzzy operators

3.2.3 Step Three: Implication

Once the fuzzy operators combine all of the premise's components into a single value, the FIS performs the implication step to translate each rule's premise into a conclusion. This process combines the premise's single value with the consequent's membership function. The curves in Figure 3.18 illustrate the consequent's membership functions, which in this example correspond to the scoring of a dive. As with the

membership functions describing difficulty and execution, the membership function shapes are constructed at the user's discretion and can assume any form.

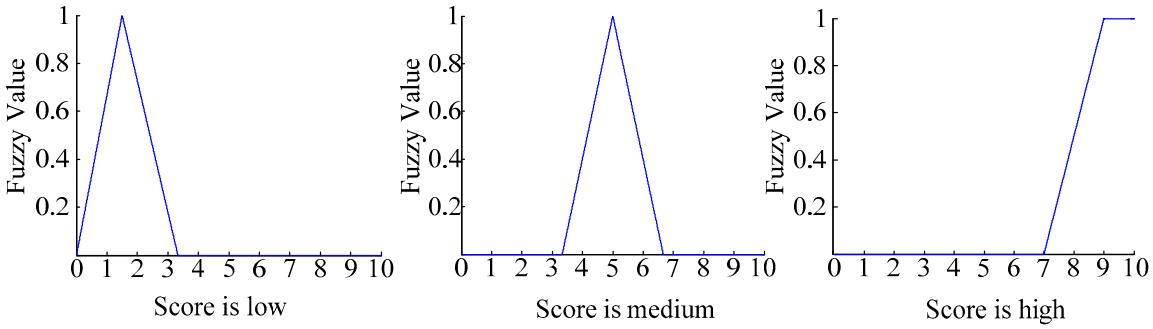

Figure 3.18: Scoring membership functions

This combination is performed for each FIS rule. In Rule 1, for example, the implication process combines the result of the premise 0.2222 with the membership function representing the consequent of Rule 1, which in this case is "Score is low". The membership function representing this consequent is in Figure 3.19.

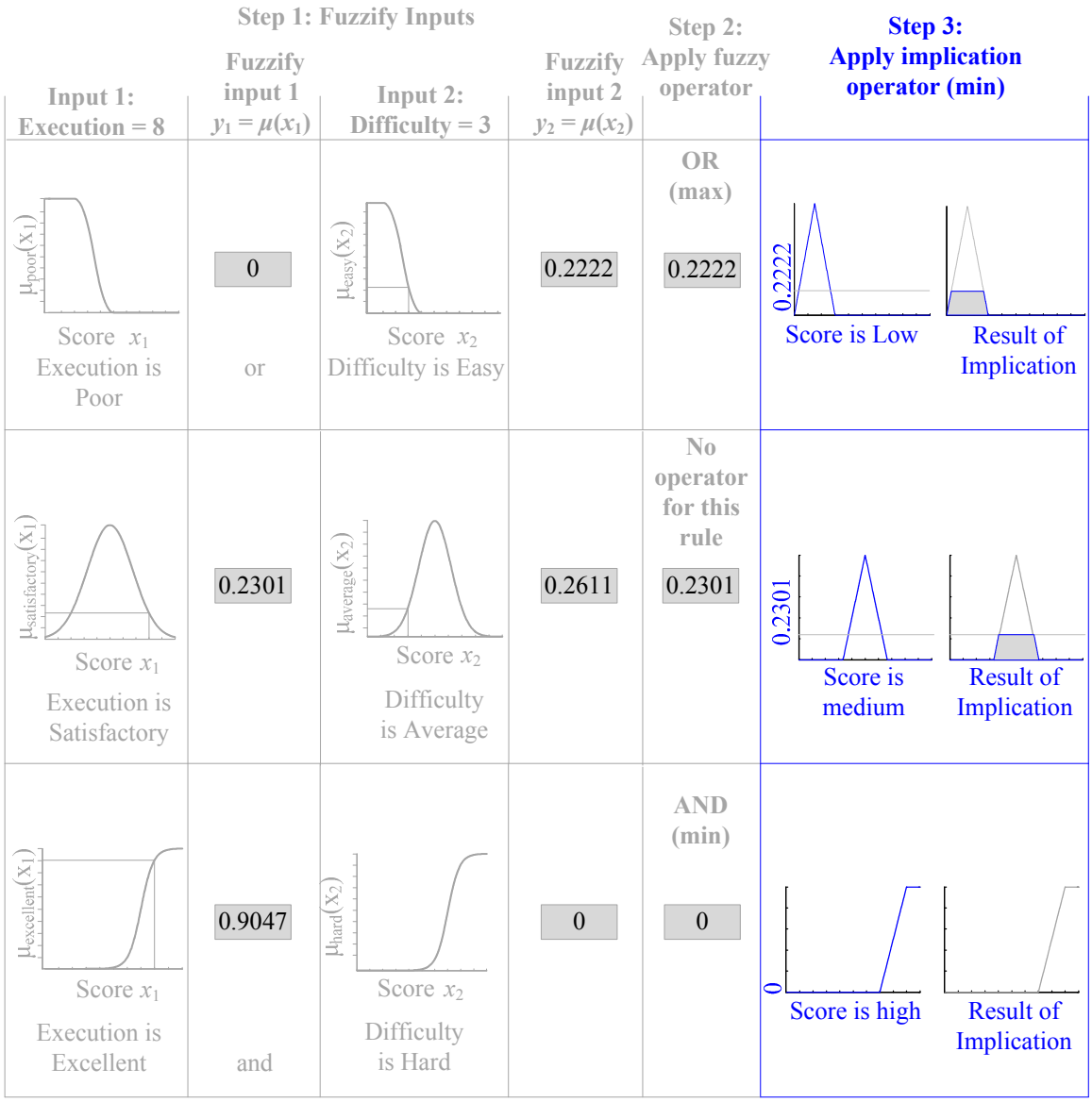

Figure 3.19: Application of the implication

3.2.4 Step Four: Aggregation

The *aggregation* procedure combines all of the fuzzy sets produced by the implication process into a single fuzzy conclusion set. Each output variable is aggregated once to produce a single fuzzy set for each output variable. This thesis uses the *maximum aggregation* method. Figure 3.20 illustrates how the aggregation method combines the

results of each rule to produce a resultant fuzzy conclusion set. Figure 3.21 shows the result of aggregation with its corresponding numerical boundaries.

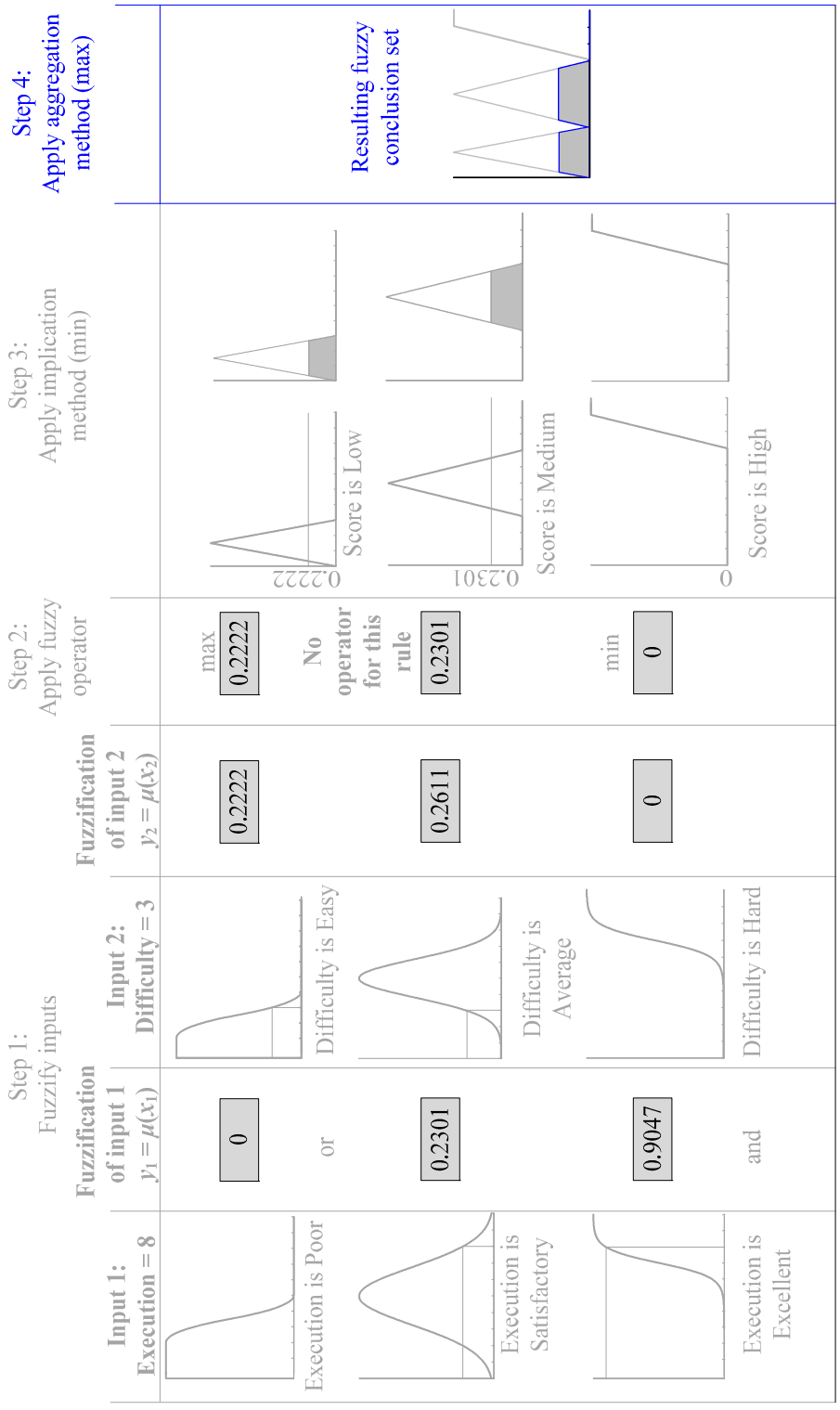

Figure 3.20: Aggregation of all of the rules

3.2.5 Step 5: Defuzzification

Upon aggregation, the conclusion set is *defuzzified* into a single output value. Several methods can be used to defuzzify the set, but this thesis employs the *centroid defuzzification method* due to its widespread use in fuzzy logic applications and its ease of implementation [**28**]. The object's centroid can be calculated by:

$$\text{centroid} = \int_a^b xf(x)dx \tag{3.3}$$

The integration limits a and b are defined by the centroid's boundaries, which typically correspond to the defuzzified output's minimum and maximum values.

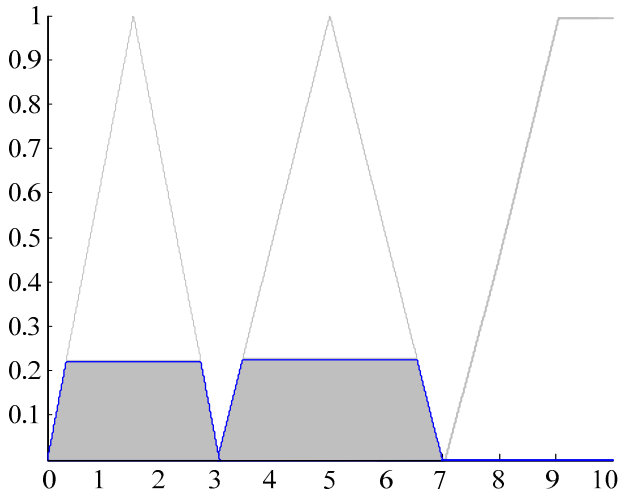

Figure 3.21: Defuzzification for diving example

Defuzzification produces the diver's final score based upon the inputs classifying the dive's difficulty and execution. Using equation (3.3) to defuzzify the diving example conclusion set produces

$$\text{defuzzified output} = \int_{0}^{0.3333} x\left(\frac{2}{3}x\right)dx + \int_{0.3333}^{2.6667} x(0.2222)dx + \int_{2.6667}^{3} x\left(-\frac{2}{3}x+2\right)dx + \int_{3}^{3.4444} x\left(\frac{1}{2}x-\frac{3}{2}\right)dx + \int_{3.4444}^{6.5556} x(0.2222)dx + \int_{6.5556}^{7} x\left(-\frac{1}{2}x+\frac{7}{2}\right)dx + \int_{7}^{10} 0dx \quad (3.3)$$

$$\text{defuzzified output} = 3.53$$

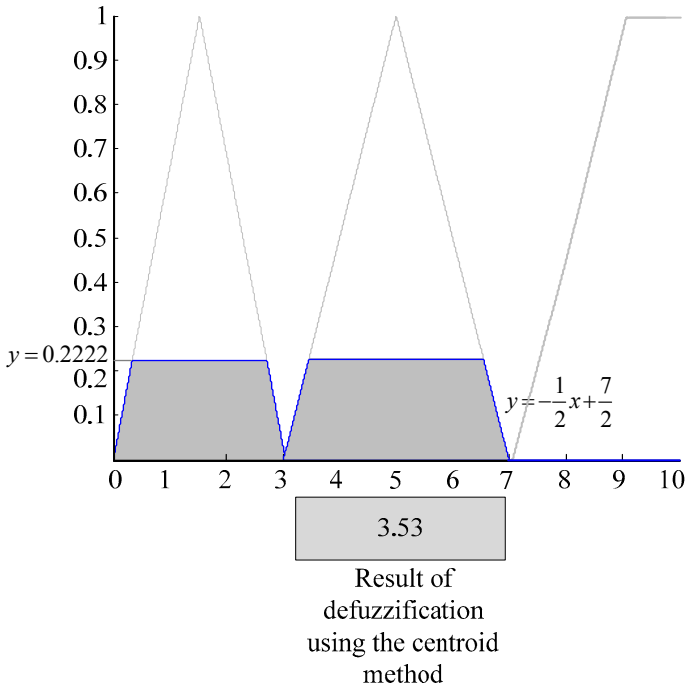

Figure 3.22: Defuzzification calculation for diving example

Fuzzy logic's applicability to systems that rely upon qualitative evaluations makes it useful for a wide range of applications spanning multiple disciplines. The intuitive explanations discussed in this chapter have illustrated the procedure for applying a FIS to simple decision making process. The next chapter introduces set-point modulation (SPM) and combines fuzzy logic with SPM to produce a decision-making control scheme that improves a generic second order system's performance.

Chapter 4 Set-Point Modulation

In discussing the reactive power characteristic's impact on real power transmission and voltage profiles, Chapter two limited its treatment to *steady state operational limits*. These regulatory and procedural limits restrict the transmission line's minimum and maximum terminal voltages for stability reasons and include other constraints such as the maximum amount of power that can flow on transmission lines without violating thermal limits. The power system is generally operated close to its steady state operational limits in order to maximize utilization of the existing infrastructure. This causes equipment ratings or regulatory restrictions to be temporarily exceeded during uncontrolled events such as fault-induced transients.

The power system includes many controllable devices to mitigate such violations. One approach involves improving the performance of traditional set-point tracking controllers such as typical Proportional-Integral-Derivative (PID) controllers shown in Figure 4.1. Such control improvements include simulation-based optimization of typical set-point tracking systems and online PID controller gain adjustments [**29**].

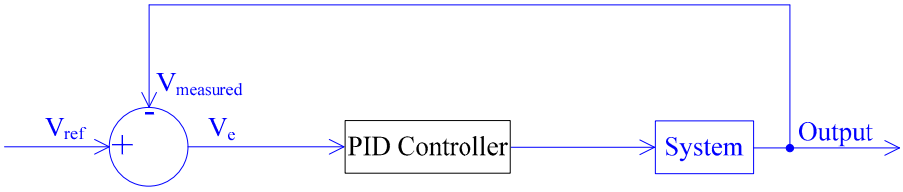

Figure 4.1: PID controller block diagram without SPM

An alternative approach enhances the power system's dynamic performance by manipulating the traditional control systems' *set-points*, or reference values, in real time. This method is generically referred to as *set-point modulation* (SPM) and is depicted in

Figure 4.2. Several SPM methods have been devised to improve overshoot/undershoot performance while simultaneously decreasing settling time of the system variable being controlled [**7**], [**9**].

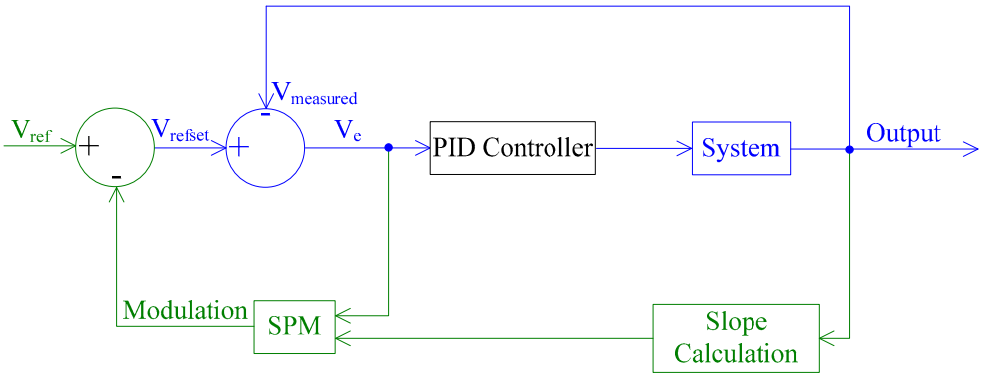

Figure 4.2: PID controller block diagrams with SPM

4.1 Feedforward Posicast Control

A second order system's *transfer function*, $G(s)$, with unity dc gain can be described in terms of its *damping ratio,* ζ, which is a unitless value that describes how second order system oscillations decay over time, and its *natural frequency* of oscillations, ω_n:

$$G(s) = \frac{\omega_n^2}{s^2 + 2\zeta\omega_n s + \omega_n^2} \tag{4.1}$$

The response, $y(t)$, of the transfer function $G(s)$ to a unit step change, $u(t)$, can be calculated as shown in equation (4.2) and shown graphically in Figure 4.3.

$$y(t) = 1 - \frac{e^{-\zeta\omega_n t}}{\sqrt{1-\zeta^2}}\sin(\omega_d t + \psi) \tag{4.2}$$

where the *damped frequency*, ω_d, and the phase shift, ψ, can be expressed as the following functions of ζ and ω_n:

$$\omega_d = \omega_n\sqrt{1-\zeta^2} \qquad \text{[rad/s]} \tag{4.3a}$$

$$\psi = \tan^{-1}\left(\frac{\sqrt{1-\zeta^2}}{\zeta}\right) \quad \text{[rad]} \qquad (4.3b)$$

A system characterized by $\zeta < 1$ is *underdamped* and will exhibit an overshoot, M_p. The underdamped transfer function, $G(s)$, has poles at

$$s_{1,2} = \sigma + j\omega = -\zeta\omega_n \pm j\omega_n\sqrt{1-\zeta^2} = -\zeta\omega_n \pm j\omega_d \qquad (4.4)$$

The peak value of the system response will be

$$y_{peak} = 1 + M_p \qquad (4.5)$$

where

$$M_p = e^{\frac{-\zeta\pi}{\sqrt{1-\zeta^2}}} \qquad (4.6)$$

The oscillation period of the response, T_d, which denotes the time between successive response peaks, is

$$T_d = 2t_p = \frac{2\pi}{\omega_d} = \frac{2\pi}{\omega_n\sqrt{1-\zeta^2}} \qquad (4.7)$$

where t_p is the length of time required for the response to attain its peak value.

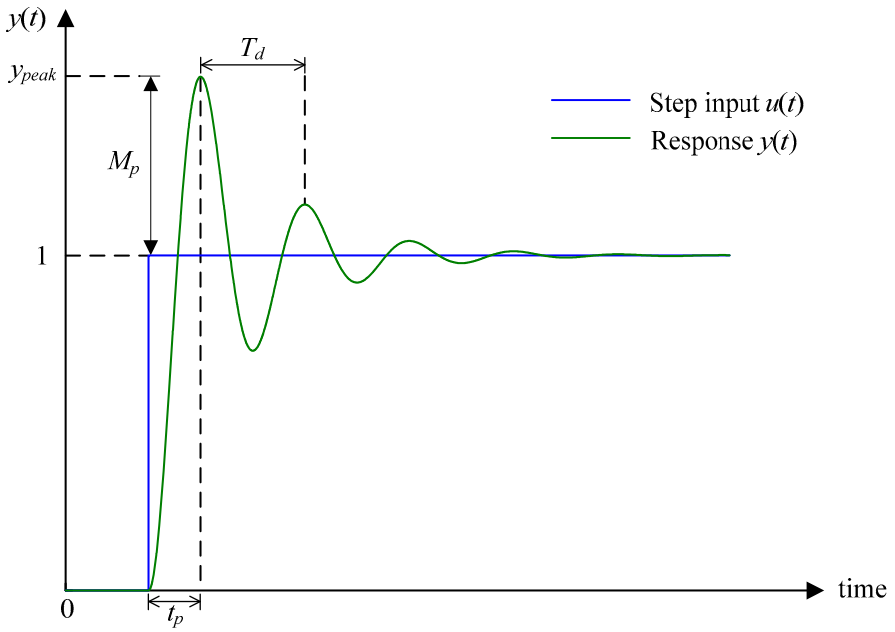

Figure 4.3: Underdamped second-order system response

The concept of improving transient behavior via set-point manipulation was first published in 1957 as *Posicast control* [7]. This predefined *feedforward control* methodology acts independently of the controller output and can completely eliminate a second order system's overshoot or undershoot response to an input step change in the system. It does so by employing the control method shown in Figure 4.4 to divide the input step into two parts that are separated by a fixed time delay, t_p.

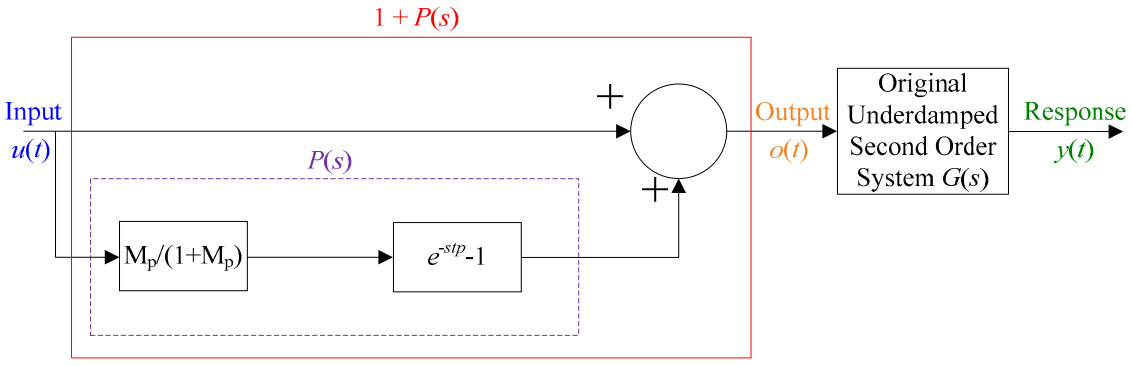

Figure 4.4: Half-cycle Posicast block diagram

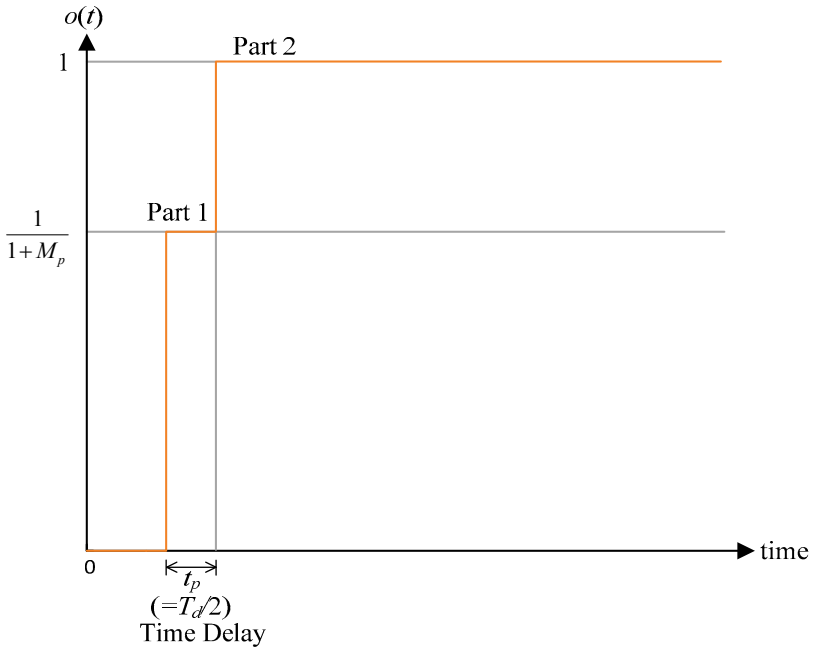

Figure 4.5: Posicast command

The first part scales the step change, $u(t)$, in such a way as to cause the response's peak value to reach the desired final output value of unity, as shown in Figure 4.5. The second part of the input, which is time-delayed by t_p, fixes this response to this desired value instead of oscillating about it. This second part's magnitude is devised such that the oscillations produced by the second step completely cancel those produced by the initial step. The resulting output attains its final value in half of the natural response period, T_d, and exhibits neither overshoot nor undershoot. Figure 4.6 illustrates the Posicast technique.

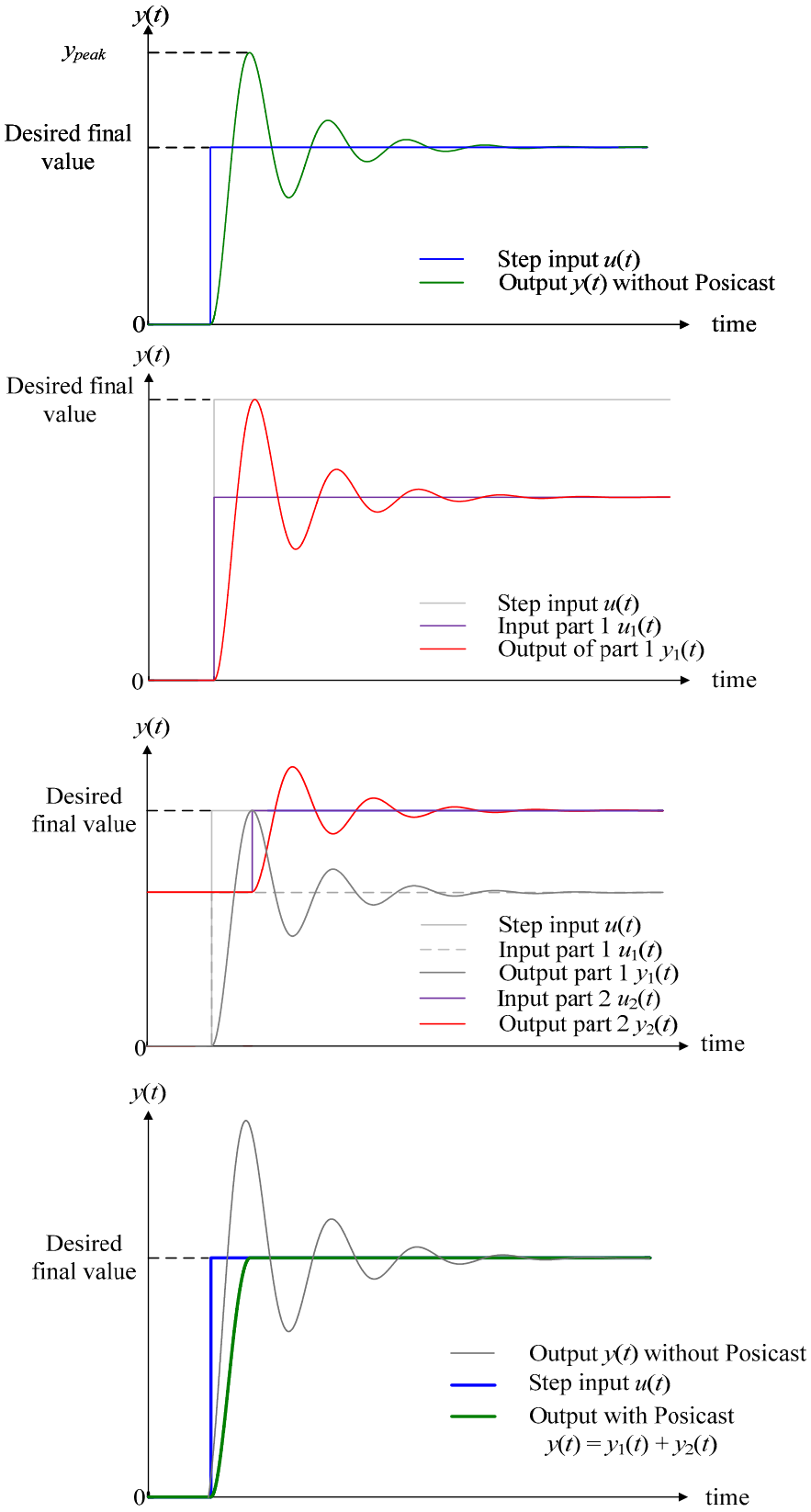

Figure 4.6: Application of Posicast control to eliminate overshoot

The feedforward Posicast method transfer function

$$1+P(s)=1+\frac{M_p}{1+M_p}\left(e^{-st_p}-1\right) \tag{4.8}$$

has roots of the form $s=\sigma+j\omega$, where

$$\sigma=\frac{2}{T_d}\ln(\delta)=-\zeta\omega_n \quad \text{[rad/s]} \tag{4.9a}$$

$$\omega=\frac{2\pi}{T_d}(2n+1)=\omega_n\sqrt{1-\zeta^2}\,(2n+1),\ n\in Z \quad \text{[rad/s]} \tag{4.9b}$$

From the Laplace domain perspective, Posicast is an *all-zero filter*, meaning that its transfer function has both no poles and an infinite set of zeros at odd multiples of ω_n as depicted in Figure 4.7.

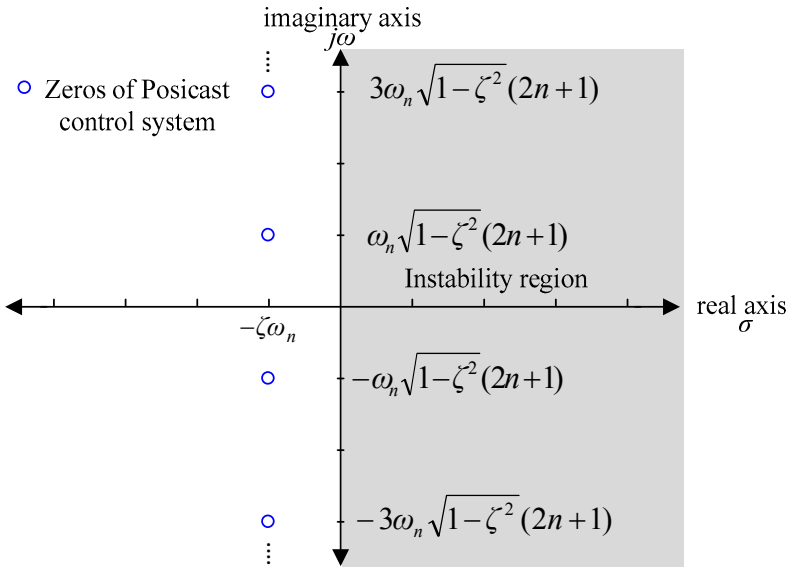

Figure 4.7: Pole-zero plot of the generalized Posicast transfer function

Feedforward Posicast control in underdamped second order systems will therefore introduce zeros that cancel the second order system's poles, which in turn eliminates any overshoot in the output response as shown in Figure 4.8. Posicast control can also be used

to cancel the dominant poles of higher order systems, although some overshoot or undershoot will remain in such cases [**30**].

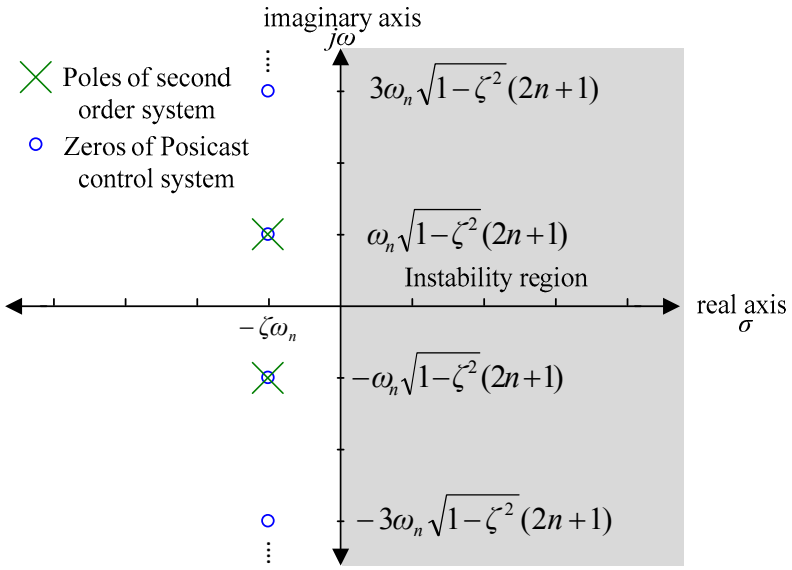

Figure 4.8: Pole-zero plot of Posicast cancelling out poles of second order system

To better understand feedforward Posicast's application to ideal second order systems, consider a second order system with $\omega_n = \sqrt{26}$, and $\zeta = 1/\sqrt{26}$. From equation (4.1), this produces a transfer function with two poles at $s = -1 \pm j5$ as shown in Figure 4.9.

$$G_0(s) = \frac{26}{s^2 + 2s + 26} \tag{4.10}$$

The Posicast parameters can be computed using equations (4.6) and (4.7)

$$M_p = e^{\frac{-\zeta\pi}{\sqrt{1-\zeta^2}}} = e^{\frac{-\frac{\pi}{\sqrt{26}}}{\sqrt{1-\left(\frac{1}{\sqrt{26}}\right)^2}}} = e^{\frac{-\pi}{5}} \tag{4.11}$$

and

$$T_d = \frac{2\pi}{\omega_n\sqrt{1-\zeta^2}} = \frac{2\pi}{\sqrt{26}\sqrt{1-\left(\frac{1}{\sqrt{26}}\right)^2}} = \frac{2\pi}{5} \tag{4.12}$$

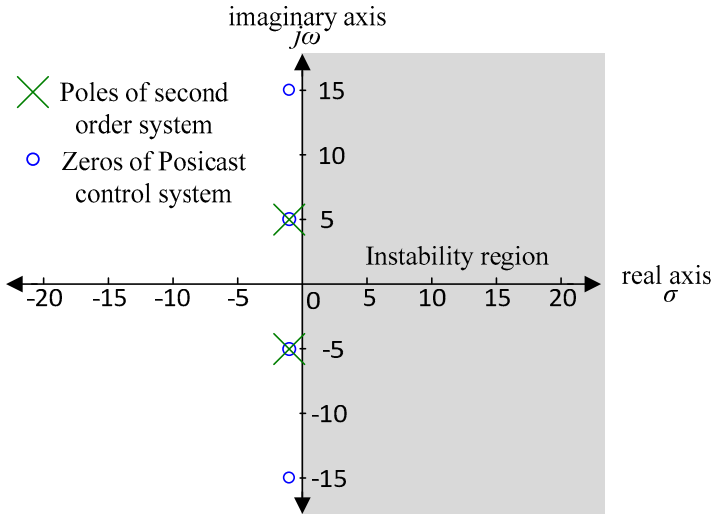

Figure 4.9: Pole-zero plot of example second order system

Substituting these values into equations (4.8) and (4.9) and applying feedforward Posicast control to the second order system yields a feedforward control system whose response exhibits no overshoot and settles immediately to the desired set-point, as shown in Figure 4.10b.

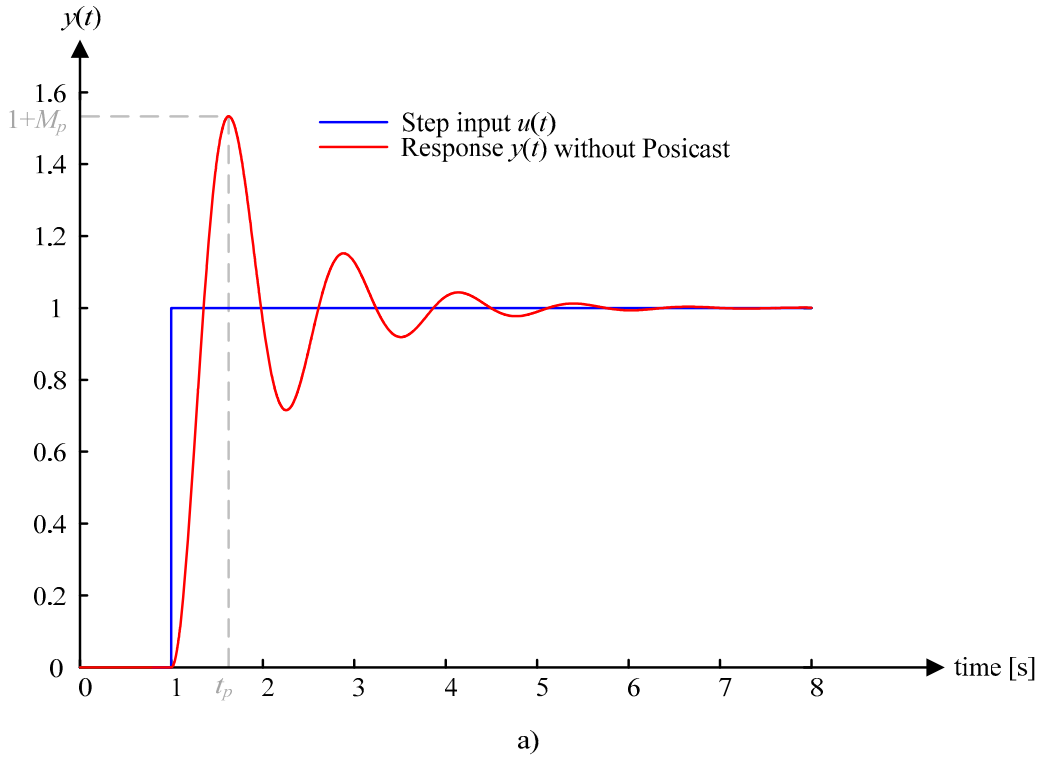

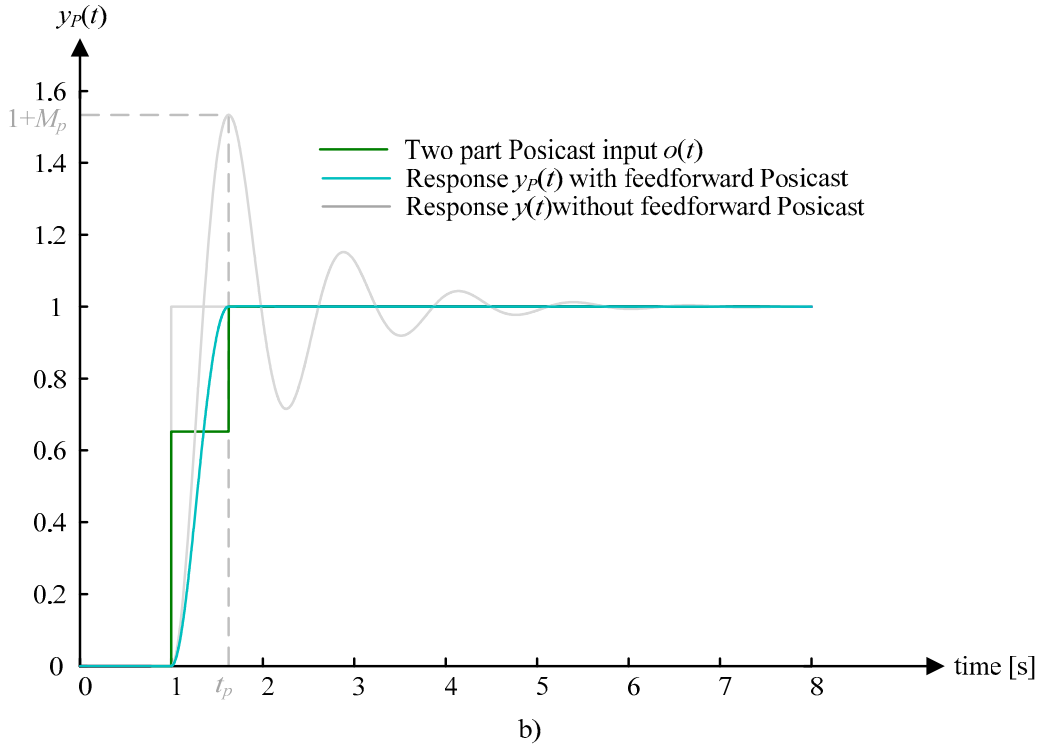

Figure 4.10: Second-order system response with and without Posicast

4.2 Feedback Posicast Control

The feedforward Posicast control suffers from the drawback of requiring advance knowledge of the precise location of a second order system's poles, or a highly accurate knowledge of a higher order system's dominant poles. Attempts have been made to reduce this sensitivity by decomposing the step change into multiple steps [**7**]. This extends feedforward Posicast by using multiple transitions to achieve faster than half-cycle response time [**8**].

Posicast control implementation has also recently been utilized within the feedback control structure illustrated in block diagram form in Figure 4.11 [**30**]. The resulting system is less sensitive to traditional Posicast parameters and yields better performance than traditional Posicast control when applied either to higher order systems with multiple sets of lightly damped poles or to systems with unmodeled lightly damped poles [**30**].

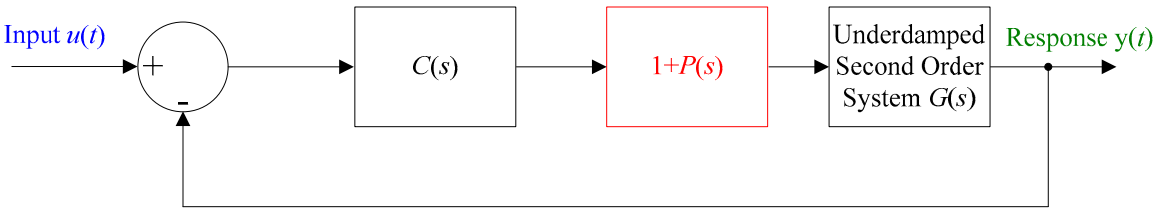

Figure 4.11: Feedback Posicast control

The feedback Posicast method can be illustrated by considering a lightly damped system with transfer function

$$G_1(s) = G_0(s)\frac{101}{s^2+2s+101} = \frac{26}{(s^2+2s+26)}\frac{101}{(s^2+2s+101)} \qquad (4.13)$$

The transfer function $G_1(s)$ has sets of poles located at s = -1 $\pm j5$ at s = -1 $\pm j10$. The first set represents the system's known poles while the latter set represents unmodeled lightly damped poles.

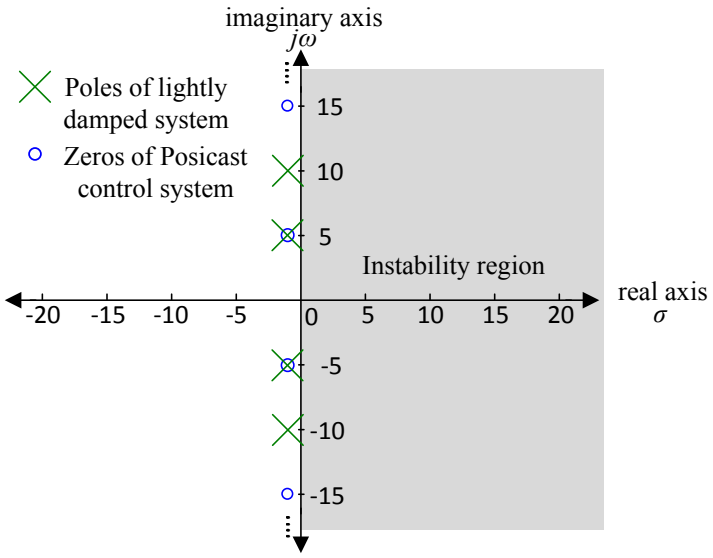

Figure 4.12: Pole-zero plot of lightly damped system with Posicast

The Posicast portion of the control method would be designed for $G_0(s)$ in order to eliminate the lower frequency poles. Feedback Posicast control also requires a *compensator* to lessen the effect of a mismatch between the actual system and the Posicast compensation. A compensator $C(s)$ can be a simple integrator of the form

$$C(s) = \frac{K}{s} \tag{4.14}$$

This type of compensator is chosen because it not only reduces sensitivity to mismatch, but it additionally ensures zero steady state error to constant reference commands and reduces high frequency gain. Figure 4.13 shows the transfer function $G_1(s)$ response to a unit step change using the feedforward and feedback Posicast methods for an integrator gain of $K = 1.1$.

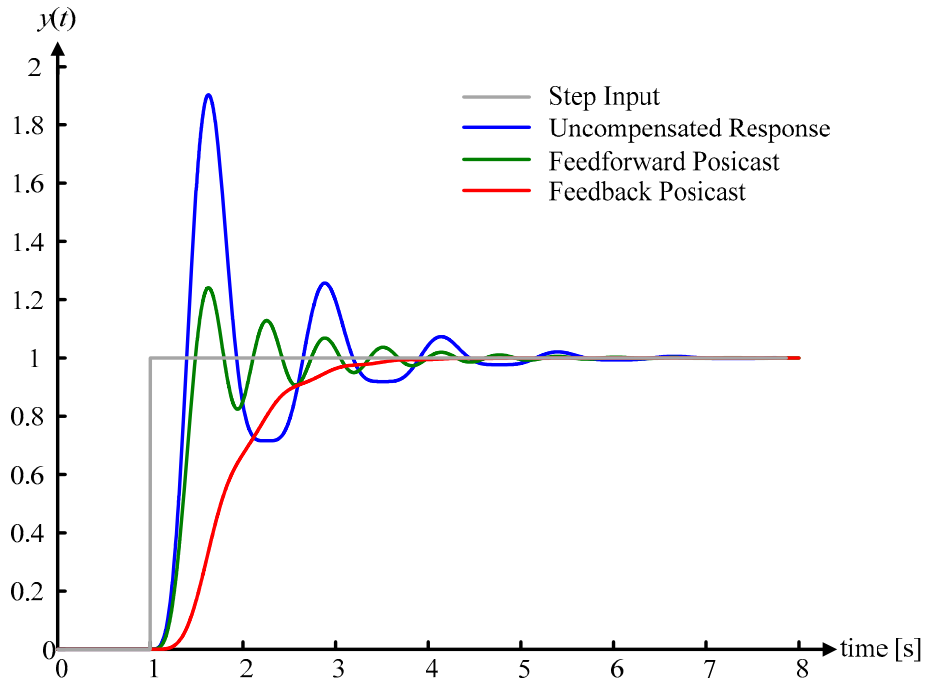

Figure 4.13: Comparison between feedforward and feedback Posicast control

The feedback Posicast control's overshoot performance is superior to that of the feedforward Posicast, which is quite sensitive to the additional underdamped poles in $G_1(s)$.

As with feedforward Posicast, feedback Posicast compensators also suffer from the significant drawback of requiring that the system model be both static and known to a high degree of accuracy. This method can also be classified as an *offline* set-point modulation method because the set-point itself is provided to the controlled system in stages and remains invariant to the Posicast control system. The remaining portions of this chapter discuss *online* SPM schemes, which directly manipulate the set-point provided to a system.

4.3 Set-Point Automatic Adjustment (SPAA)

The *Set-Point Automatic Adjustment* (SPAA) SPM technique was first proposed and implemented for mitigating large disturbances that occur when starting Distributed Energy Resources. The SPAA method can be used for second order systems or for systems where a second-order model is valid [**9**]. This method calculates intermediate set-points, which are denoted as *sp*, such that a set-point change will not exceed a specified maximum value, $y_{\max}$. These calculations employ equation (4.6) to compute the overshoot that would occur by applying a step change between two points sp_1 and sp_{final}. If the response variable's computed overshoot exceeds a specified maximum value $y_{\max}$, then intermediate set-points are computed such that the set-point changes will not violate $y_{\max}$. Once the calculated overshoot does not violate $y_{\max}$, then no further intermediate set-points are required, and the transition from sp_1 to sp_{final} can be applied without modification. This procedure is illustrated in Figure 4.14.

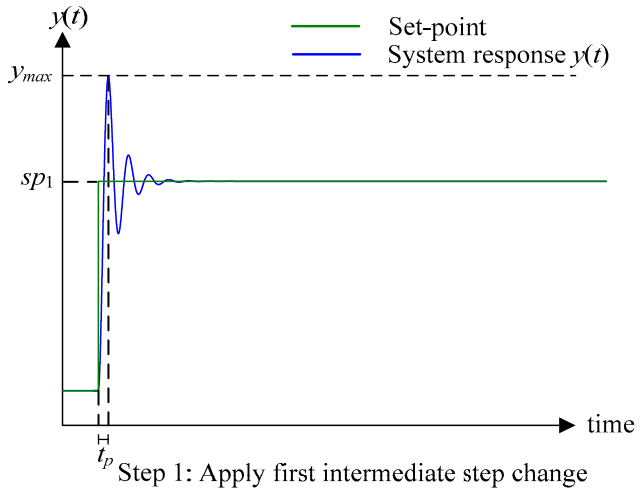

Step 1: Apply first intermediate step change sp_1 such that response does not violate y_{max}

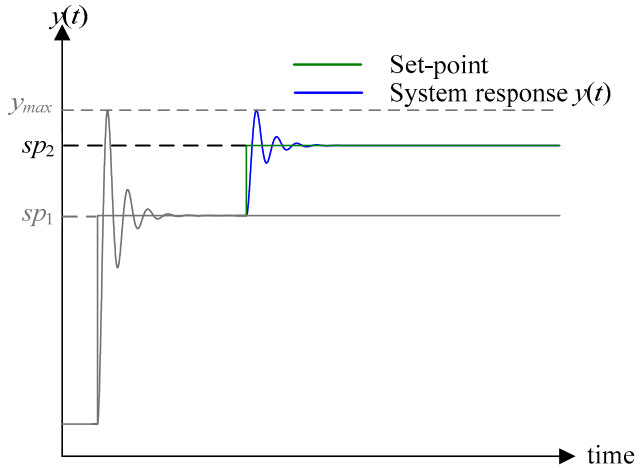

Step 2: Apply second intermediate step change sp_2 such that response does not violate y_{max}

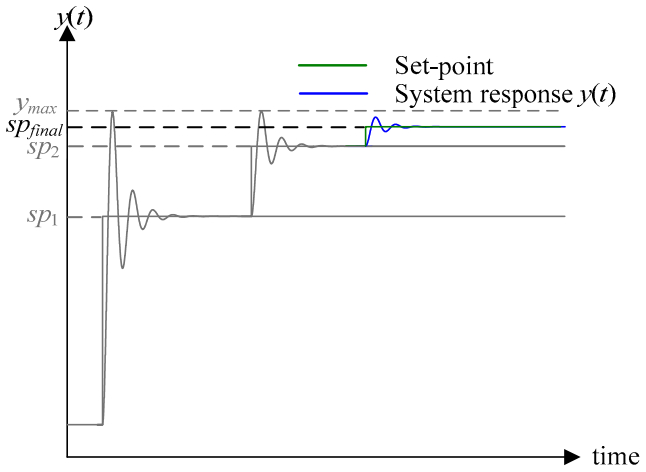

Step 3: Apply final step change sp_{final} such that response attains desired final value without ever violating y_{max}

Figure 4.14: Intermediate set-points and associated second order system response

The time evolution of an underdamped response variable corresponding to a step change from sp_1 to sp_{final} is

$$s(t) = sp_1 + (sp_{final} - sp_1)y(t) \tag{4.15}$$

Therefore the peak value of the response would be

$$s_{peak} = sp_1 + (sp_{final} - sp_1)y_{peak} \tag{4.16}$$

No intermediate set-points are required if $s_{\text{peak}} < y_{\max}$. However, if $s_{\text{peak}} > y_{\max}$, an intermediate set-point sp_2 ($sp_1 < sp_2 < sp_{2final} < y_{\max}$) will be calculated such that $s_{\text{peak}} \leq y_{\max}$. Combining equations (4.5), (4.6) and (4.16) results in equation (4.17), which is used for calculating intermediate set-points.

$$sp_2 = \frac{y_{\max} + M_p sp_1}{1 + M_p} \tag{4.17}$$

Several intermediate set-points may be required to achieve an acceptable response depending upon how restrictive $y_{\max}$ is with respect to the change being applied to the system. Figure 4.15 shows a flowchart of the SPAA technique.

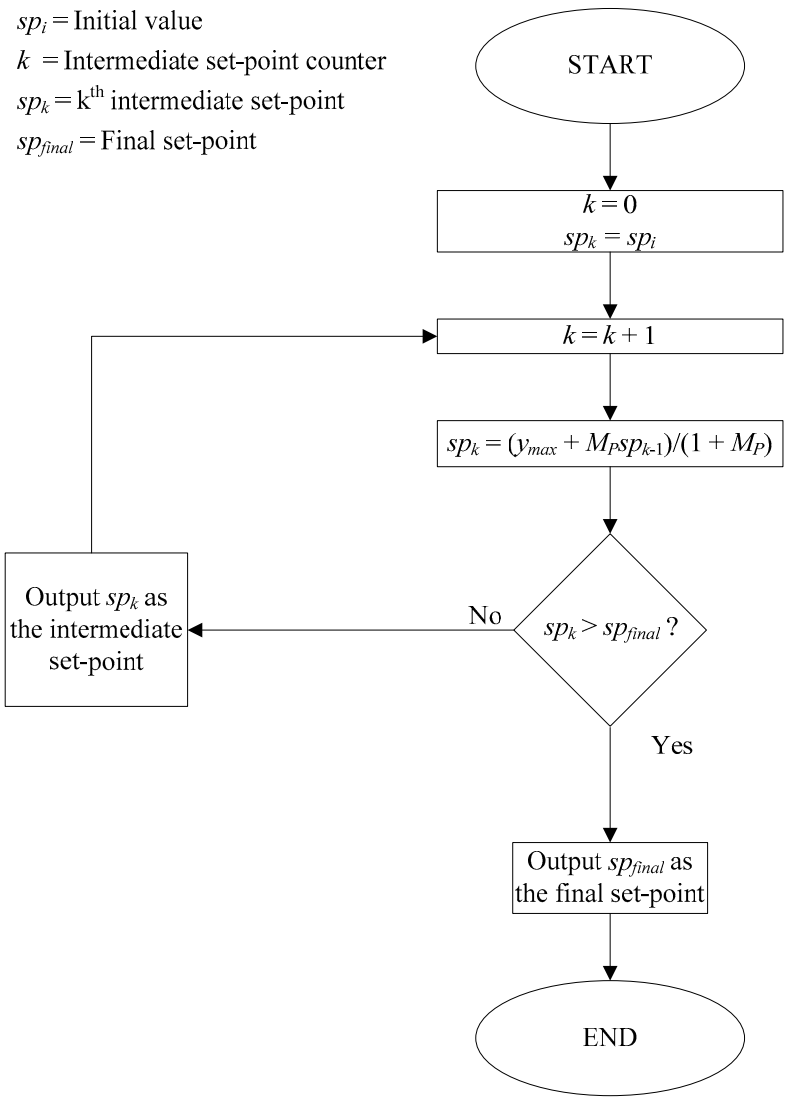

Figure 4.15: SPAA flowchart

To illustrate the series of intermediate set-point calculations, consider a second order transfer function of the form expressed in equation (4.1) with a damping ratio of ζ = 0.2155 and a natural frequency of ω_n = 82 rad/s:

$$G(s) = \frac{(82)^2}{s^2 + 2(0.2155)(82)s + (82)^2} = \frac{6724}{s^2 + 35.342s + 6724}$$

If it is desirable to change the set-point from 0.9 to 1.09 pu and the predetermined steady state limits are y_{min} = 0.9 pu and y_{max} = 1.1 pu, which are chosen by the user of the algorithm, equation (4.17) and the method shown in Figure 4.15 can be used to devise the set-points shown in Table 4.1.

Table 4.1: Calculated set-points using SPAA

Iteration	Set-point
0	0.900
1	1.033
2	1.078
3	1.090

Figure 4.16 shows the second order system's response to these set-point changes.

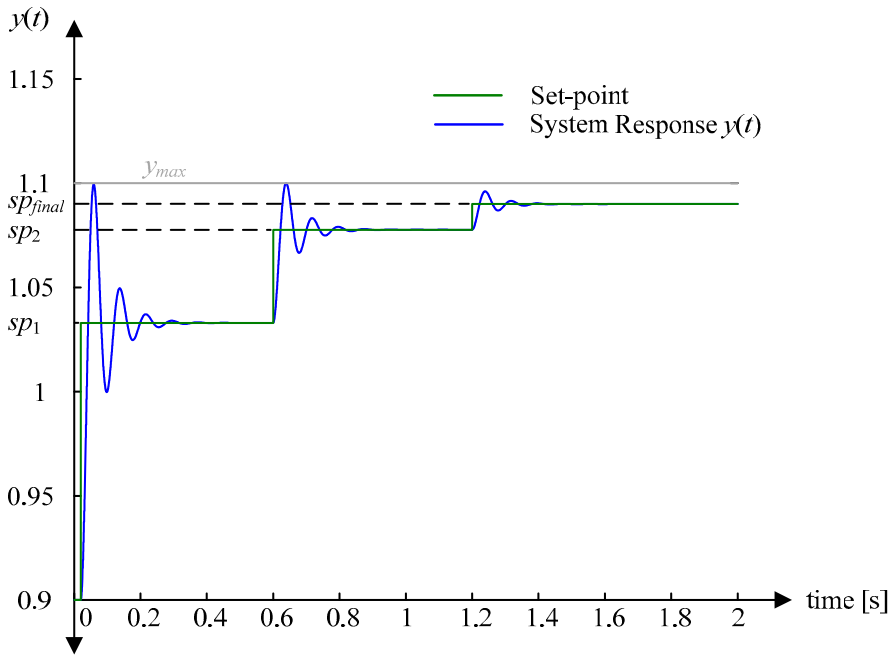

Figure 4.16: Application of SPAA to a second order system

This method shows that calculating intermediate set-points and applying them sequentially prevents violations from occurring for any system that can be modeled as a second order system.

4.4 Set-Point Automatic Adjustment-Correction Enabled (SPAACE)

The primary drawback to the SPAA method is that it requires an accurate second order system model before its intermediate set-points can be calculated. In contrast, the Set-Point Automatic Adjustment-Correction Enabled (SPAACE) method only requires limits of operation such as maximum allowable values instead of also requiring advanced knowledge of system parameters.

The SPAACE technique was originally primarily intended for microgrid applications [**9**]. By monitoring the controller output's response and modifying the control system's set-point when necessary to improve controller performance, SPAACE can respond to a wide variety of perturbations such as load fluctuations, electrical system faults, and other system disturbances.

Both predictive and non-predictive SPAACE methods exist [**10**]. In either case, the set-point is scaled by a fixed percentage of its original value. The response variable is the only monitored quantity of the non-predictive algorithm, and the set-point is adjusted to maintain the response variable within predefined limits as soon as the output crosses a predetermined threshold. The prediction-enabled SPAACE algorithm monitors both the response variable's actual response and the trend of the response, and it uses an extrapolation algorithm to project the response variables' trajectory. If a criterion violation is expected, SPAACE manipulates the set-point to either prevent its occurrence or to reduce the length of time of the violation [**9**]. As this is accomplished by choosing appropriate sampling and trajectory projection intervals, designers require sufficient understanding of the system to determine appropriate sampling times and the trajectory projection interval.

Consider again an underdamped second order system with $\zeta = 0.5169$, $\omega_n = 82$ rad/s, which has a transfer function of the form:

$$G(s) = \frac{6724}{s^2 + 84.7716s + 6724}$$

This example assumes a modulation index of $m = 0.2$ and the response variable's minimum and maximum permissible values of $y_{min} = 0.9$ pu and $y_{max} = 1.10$ pu, respectively. Figure 4.17 illustrates the application of SPAACE without prediction for a step change $u(t)$ applied from 0.9 pu to 1.09 pu at time $t = 0$. Once the response variable crosses the y_{max} threshold of 1.10 pu, the algorithm modifies the set-point from 1.09 pu to 0.872 pu at $t = 0.033$ s. In doing so, the algorithm forcibly reduces the response and produces less overshoot. Once the response variable lies within permissible limits, the set-point reverts to its original value.

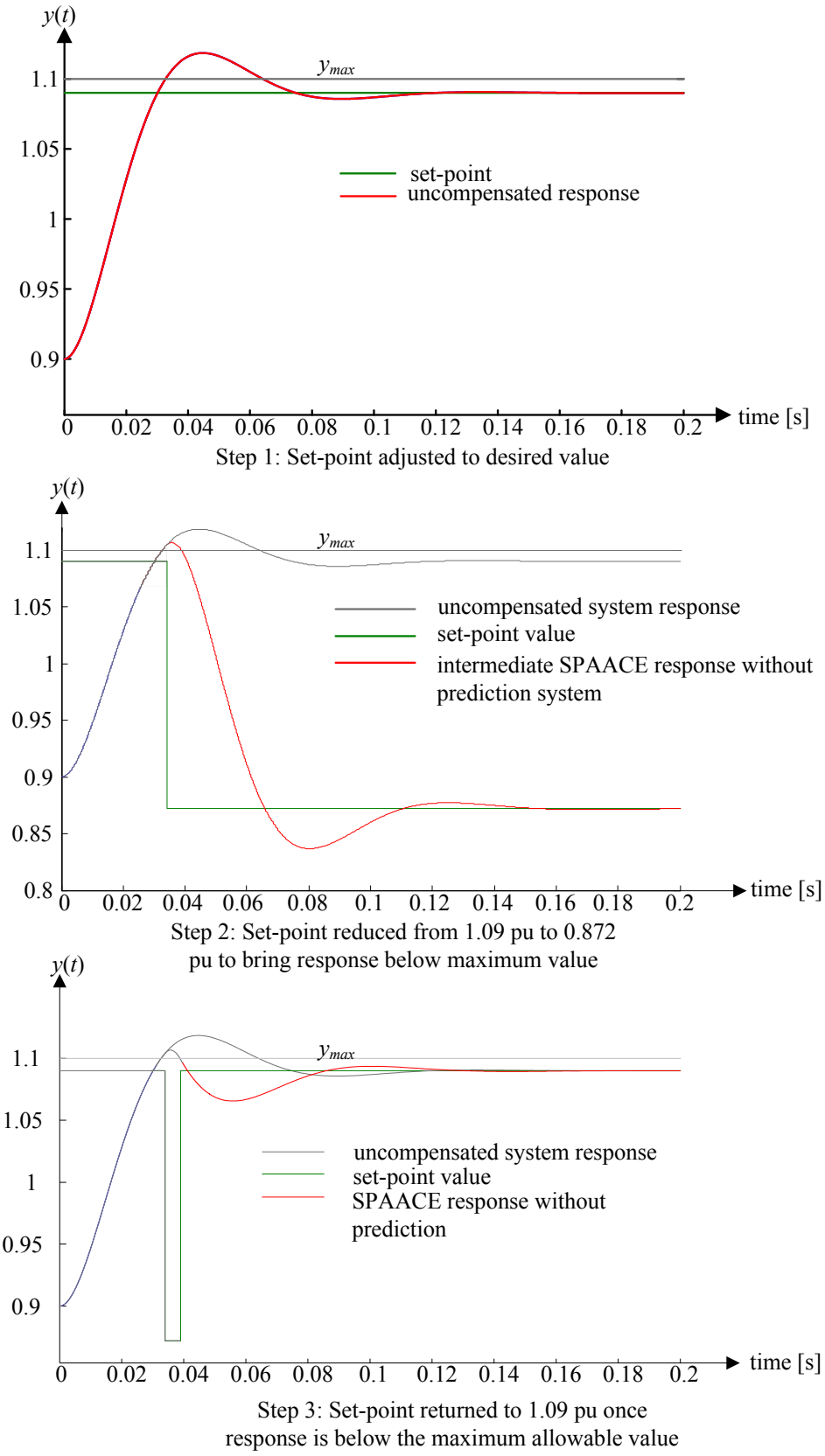

Figure 4.17: SPAACE example without prediction

Figure 4.18 shows the prediction-based SPAACE algorithm applied to the same underdamped second order system described above. The predictive algorithm monitors the response variable's trend and projects its trajectory to anticipate when the unaltered set-point response variable will violate the maximum threshold. As a result, the algorithm alters the set-point at $t = 0.03$ s, which is earlier than the case where SPAACE without prediction was used. The set-point then reverts to its original value at $t = 0.032$ s in order to force the response variable to more closely track the desired value. Not only does prediction-based SPAACE cause the response variable to attain its final value faster with less overshoot, but it also does so while remaining completely within the limits prescribed by the problem.

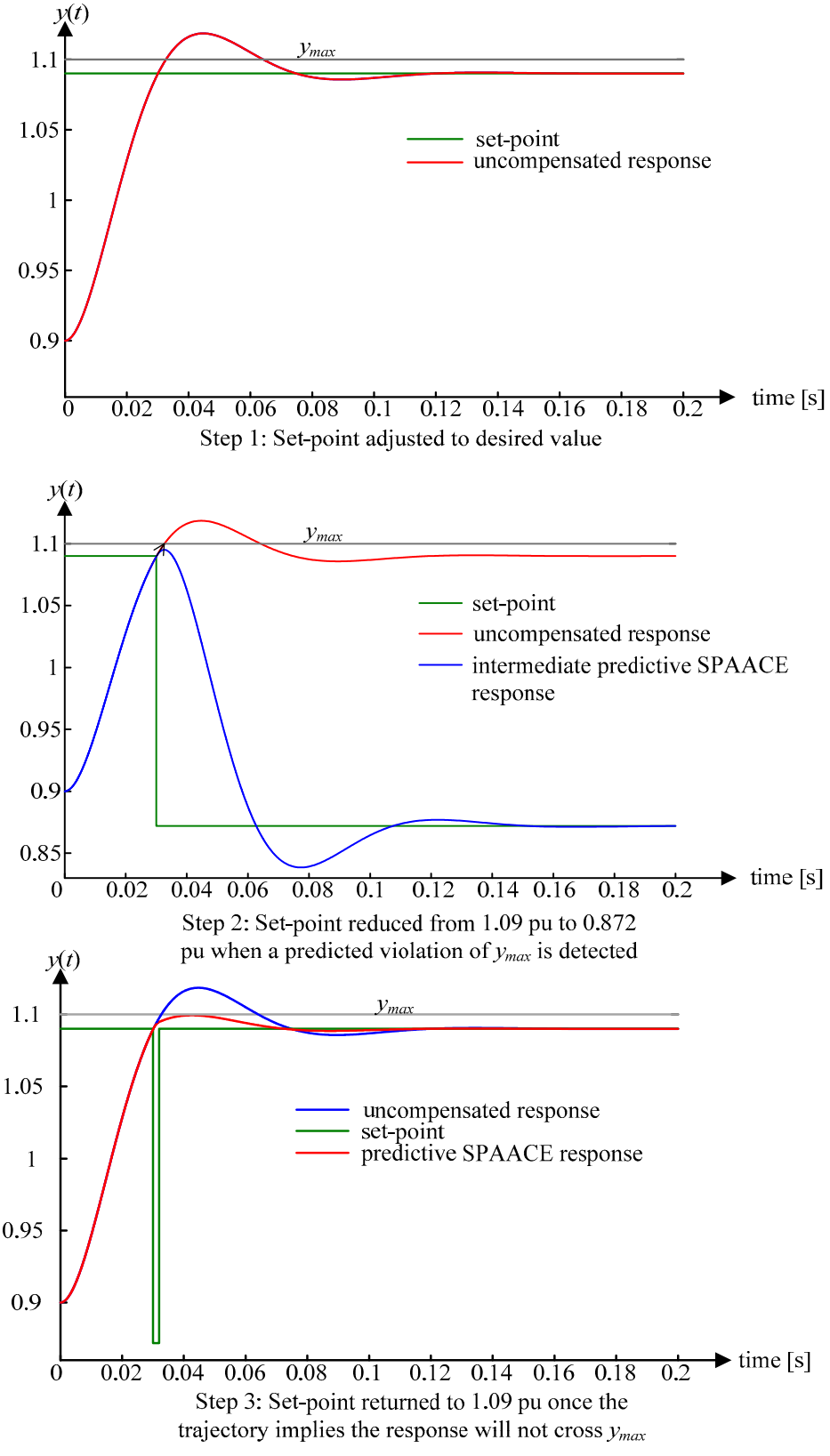

Figure 4.18: Prediction-based SPAACE example

4.5 Set-Point Modulation with Fuzzy Logic

This thesis introduces fuzzy logic to set-point modulation as an alternative to the previously described SPM algorithms. This was accomplished utilizing the MATLAB/Simulink software package. The control system response's slope and error measurements are inputted into a fuzzy inference system (FIS) that determines not only when to modify the set-point, but also to determine the scaling (*modulation*) of the system's set-point in order to improve the system response.

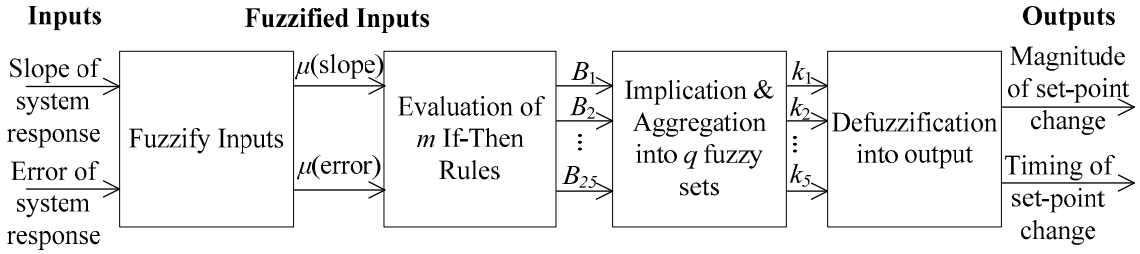

Figure 4.19: Fuzzy process for SPM

Figures 4.20 and 4.21 show the FIS membership functions used for the slope and error functions. The horizontal axis is not shown because it is modified depending upon the compensated system's characteristics.

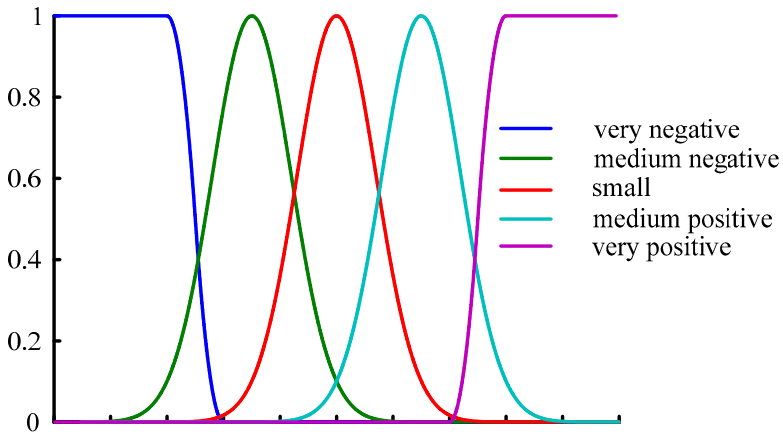

Figure 4.20: Membership functions for the slope input to the FIS

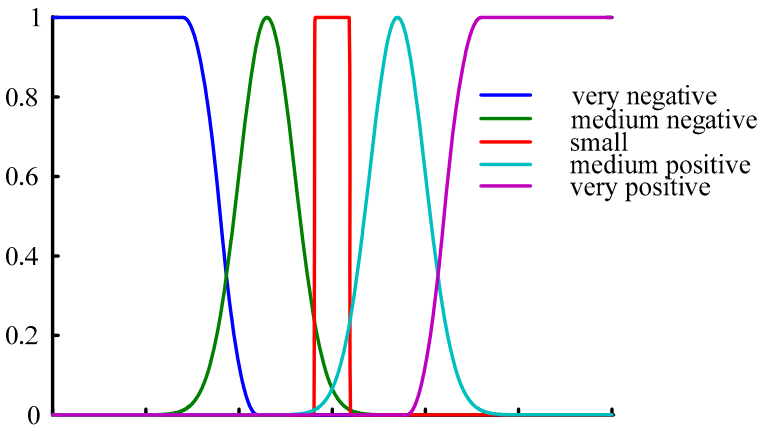

Figure 4.21: Membership functions for the error input to the FIS

These fuzzified inputs are then combined using the twenty-five if-then rules summarized in table 4.2.

Table 4.2: Rules for fuzzy logic SPM

Slope \ Error	Very Negative	Medium Negative	Small	Medium Positive	Very Positive
Very Negative	None	Medium Positive	Very Positive	Very Positive	Very Positive
Medium Negative	Medium Negative	None	Very Positive	Very Positive	Very Positive
Small	Very Negative	Medium Negative	None	Medium Positive	Very Positive
Medium Positive	Very Negative	Very Negative	Very Negative	None	Medium Positive
Very Positive	Very Negative	Very Negative	Very Negative	Medium Negative	None

Once the rules have been evaluated using the fuzzified inputs, implication is performed according to the modulation membership functions shown in Figure 4.22. Once again, the horizontal axis is undefined due to the dependence on the phenomenon and the system being compensated.

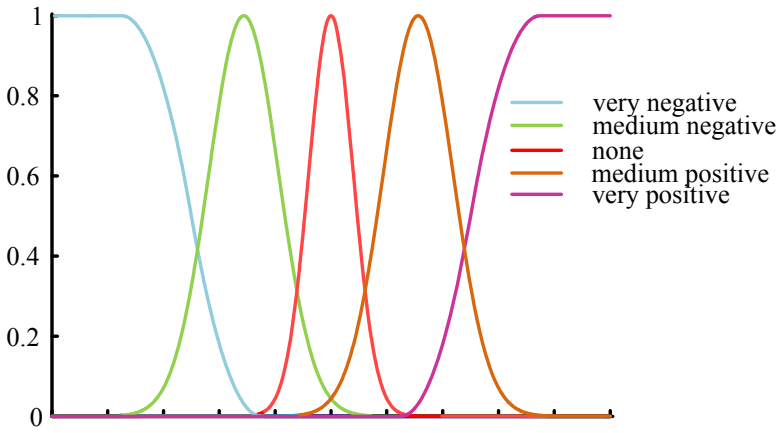

Figure 4.22: Modulation membership functions for the FIS

The results produced by the modulation membership functions are aggregated using the minimum method, and then a final modulation output value is determined by applying the centroid defuzzification calculation.

The membership functions employed vary according to the system being compensated in order to improve system response, but the general membership function shape and FIS rules are not manipulated. To illustrate this method, consider again a step change from 0.9 pu to 1.09 pu applied at $t = 0$ s to an underdamped second order system of damping ratio $\zeta = 0.5169$ and natural frequency $\omega_n = 82$ rad/s:

$$G(s) = \frac{6724}{s^2 + 84.7716s + 6724}$$

The FIS samples the slope and error of the response every millisecond and determines the timing and the modulation required to improve the system response. Figure 4.23 shows the set-point waveform provided to the system and the system's response both with and without fuzzy SPM.

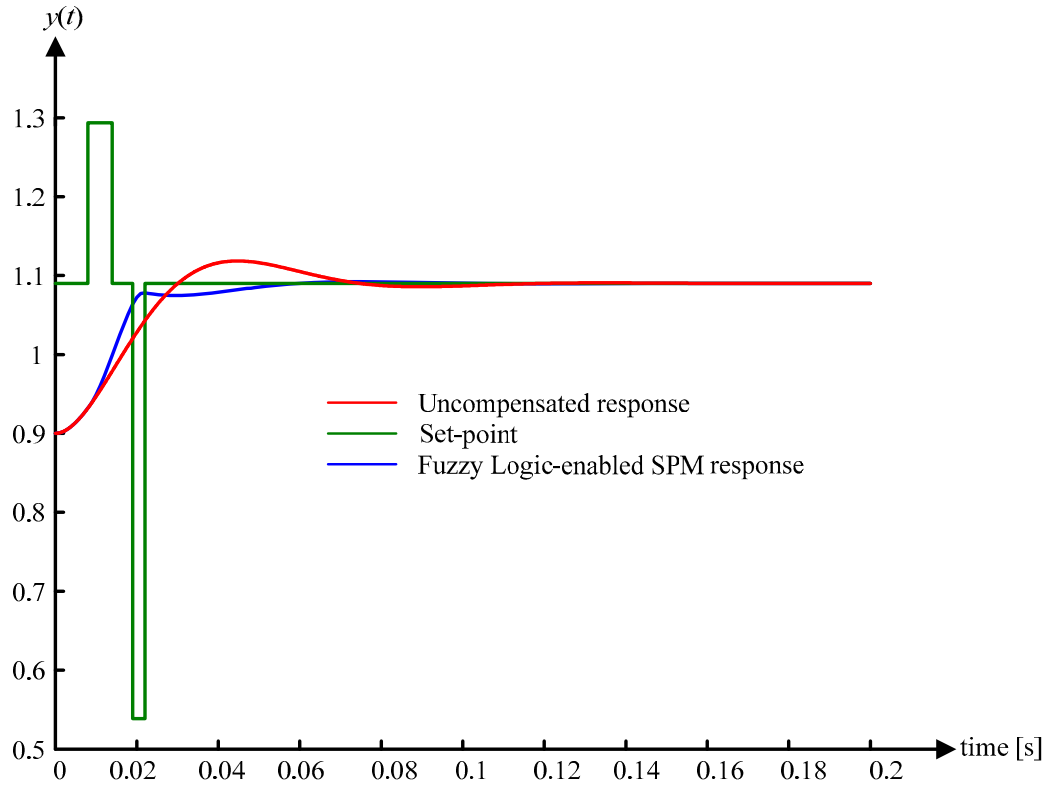

Figure 4.23: Fuzzy logic-enabled SPM applied to second order underdamped system

At t = 0.008 s, the FIS increases the set-point from 1.09 pu to 1.293 pu in order to increase the rate of rise of the underdamped second order system response and reduce the error magnitude. As the response approaches the desired value at a sufficient rate, the FIS reverts the set-point to 1.09 pu at t = 0.014 s. The FIS then determines that the magnitude of the error is too small for the slope at time t = 0.019 s, and it reduces the set-point to 0.5387 pu to mitigate or eliminate the overshoot. Once the slope and the error are sufficiently small to prevent significant overshoot from occurring, the FIS reverts the set-point back to 1.09 pu at t = 0.022 s. As illustrated in Figure 4.23, the fuzzy logic-enabled SPM control scheme decreases settling time and overshoot compared with an uncompensated system. This shows that in addition to SPAA and SPAACE, fuzzy logic-

enabled SPM can reduce underdamped second order system overshoots and settling times.

Different damping ratios are simulated to illustrate the robustness of applying the fuzzy SPM scheme to second order systems. Figure 4.24 illustrates the effect of reducing the above example's damping ratio by 10 percent to a value of $\zeta = 0.46521$. A small change in the damping ratio does not significantly affect the compensated system's response.

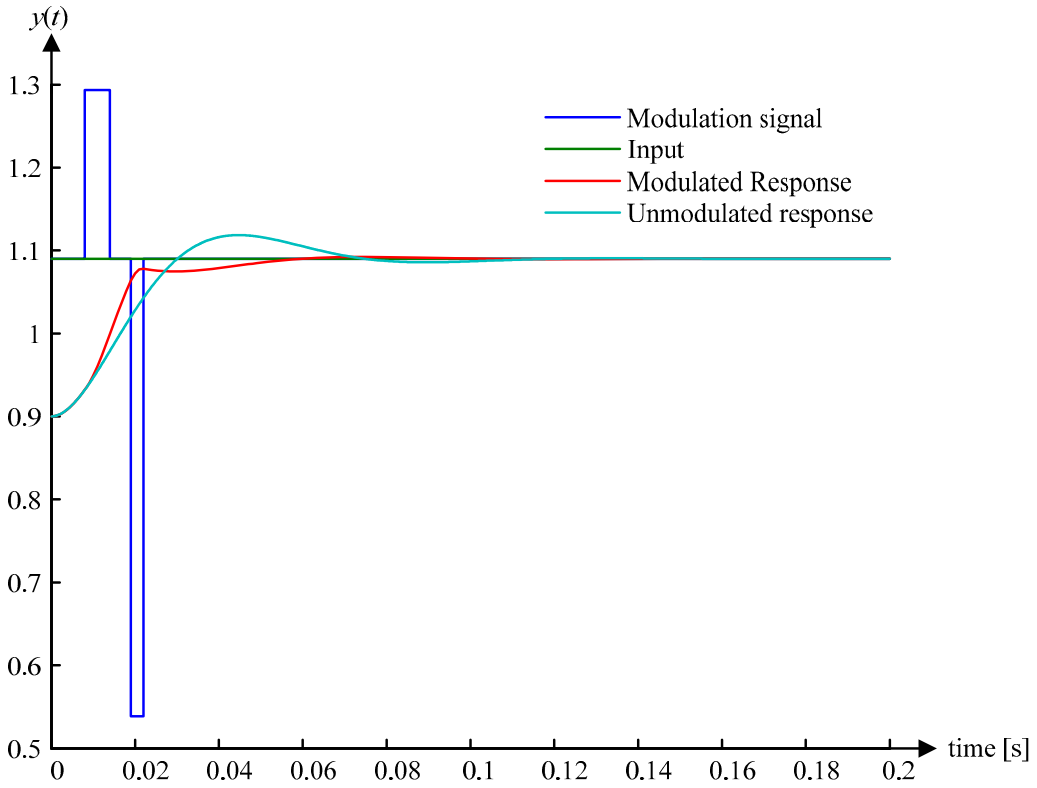

Figure 4.24: Response of second order system with 10% damping ratio change

Figure 4.25 shows a second order system response with the damping ratio changed from $\zeta = 0.5169$ to $\zeta = 0.2$.

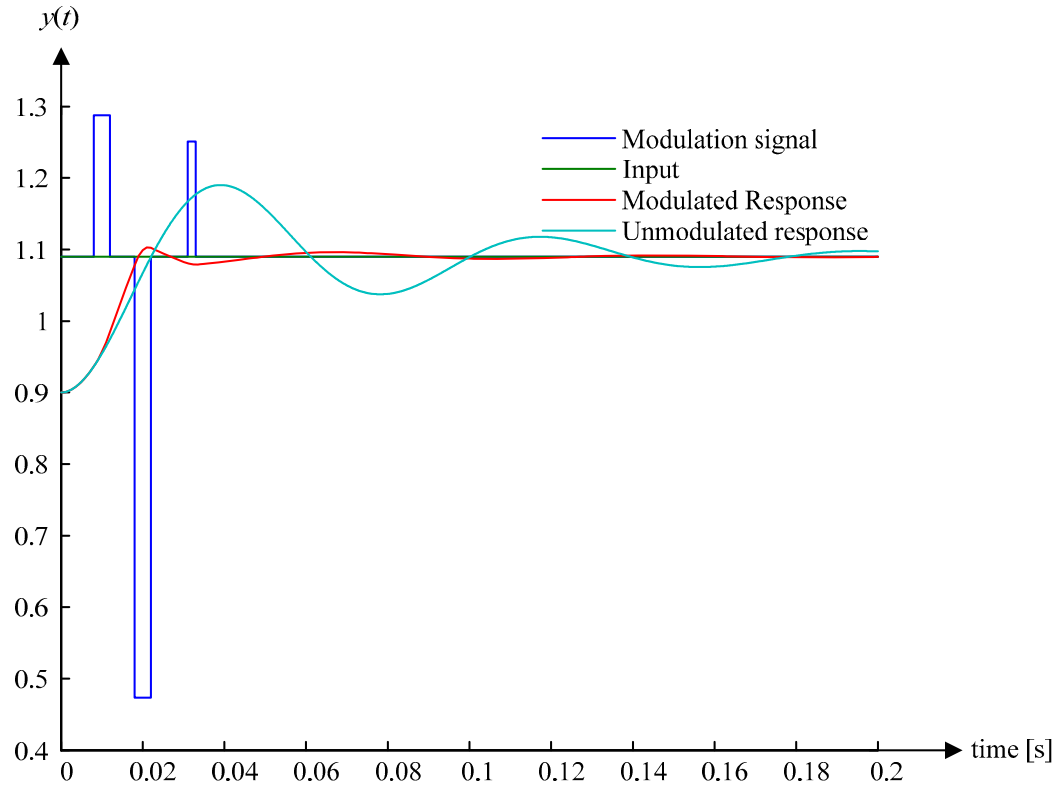

Figure 4.25: Response of second order system with damping ratio of 0.2

Finally, the fuzzy logic-enabled SPM method can even be used to stabilize unstable systems. Figure 4.26 illustrates the response of a second order system with a damping ratio of $\zeta = -0.1$

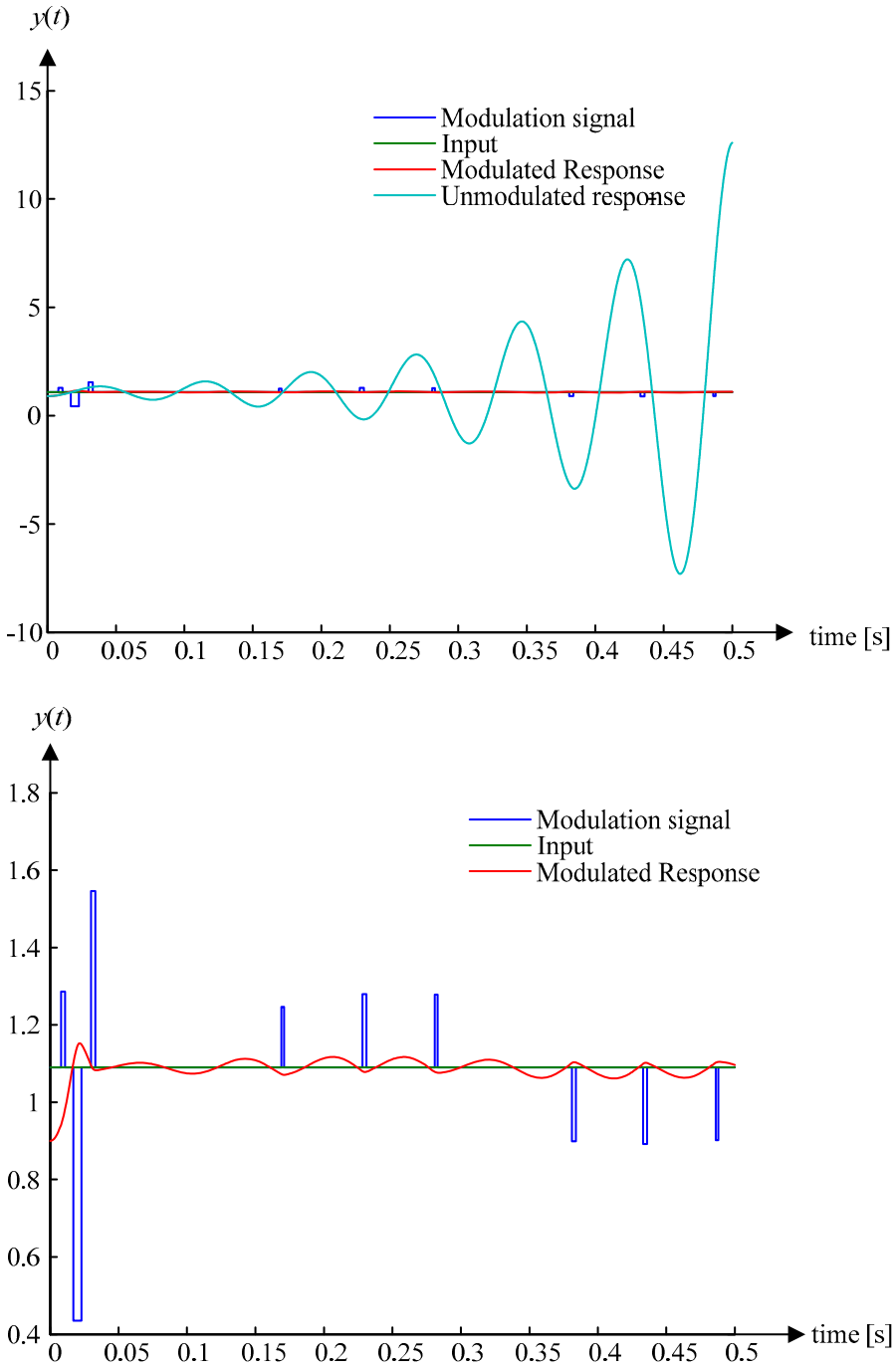

Figure 4.26: Response of a second order system with a negative damping ratio

Having demonstrated that the fuzzy SPM scheme improves underdamped second order system responses, it can now be applied to improve the Manitoba Hydro Ponton SVC control system's overshoot in response to control actions.

Chapter 5 Application of Fuzzy SPM to the Ponton SVC System

Chapter four limited its discussion of SPM's ability to improve control system responses to underdamped second order systems for simplicity. This chapter overviews the Ponton SVC control system as modeled in PSCAD/EMTDC and shows fuzzy SPM's ability to improve the Ponton SVC voltage control loop's response to overshoot to SVC voltage set-point changes. The fuzzy logic-based SPM algorithm developed in MATLAB/Simulink was interfaced with PSCAD/EMTDC in order to model step changes in the Ponton SVC and determine how fuzzy SPM improves the response.

5.1 Ponton SVC

The Ponton SVC is located in northern Manitoba, and its purpose is to increase the power transfer capability between Northern Manitoba and Southern Manitoba while maintaining the INCO mining company bus voltage level during transients [**31**]. The Ponton SVC consists of a 67.63 MVar delta-connected fixed capacitor bank, an 88.3 MVar delta-connected TCR and a 54.0 MVar delta-connected TSC, and it connects to the Manitoba Hydro 230 kV transmission network through a 230/9.3/13.8 kV transformer. A single line diagram of the Ponton SVC is shown in Figure 5.1.

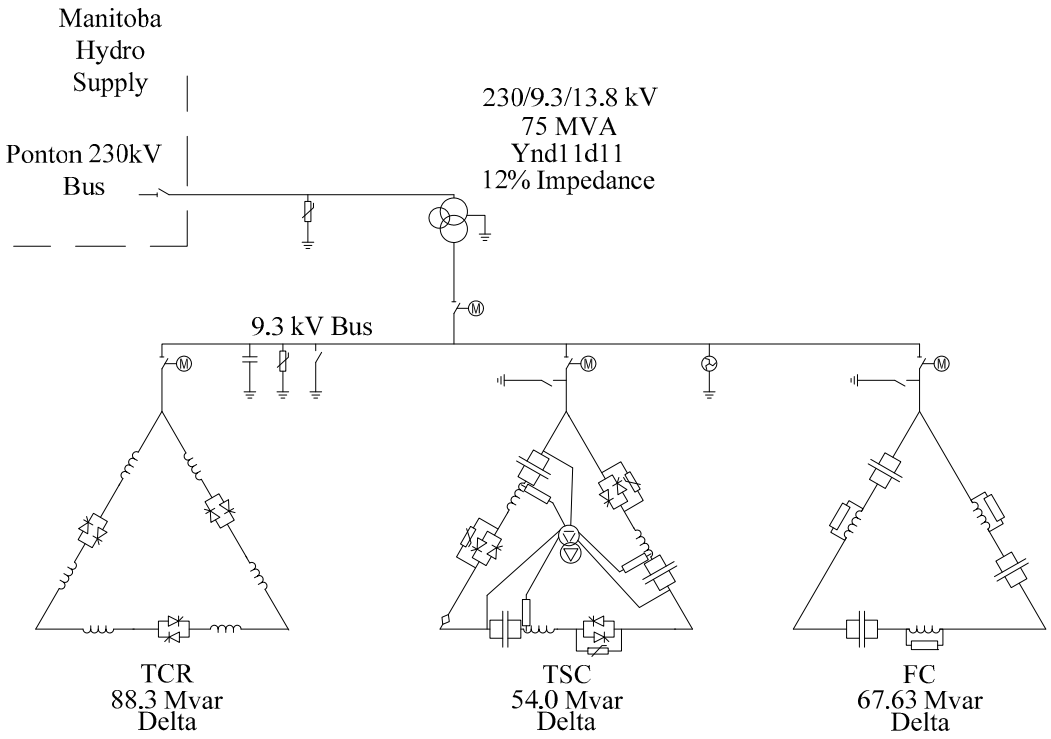

Figure 5.1: Ponton SVC single line diagram

5.2 Application of Fuzzy SPM to Ponton SVC Voltage Regulator

A fuzzy logic-based SPM scheme was added to the Ponton SVC's voltage regulator to improve its response to reference voltage step changes,.

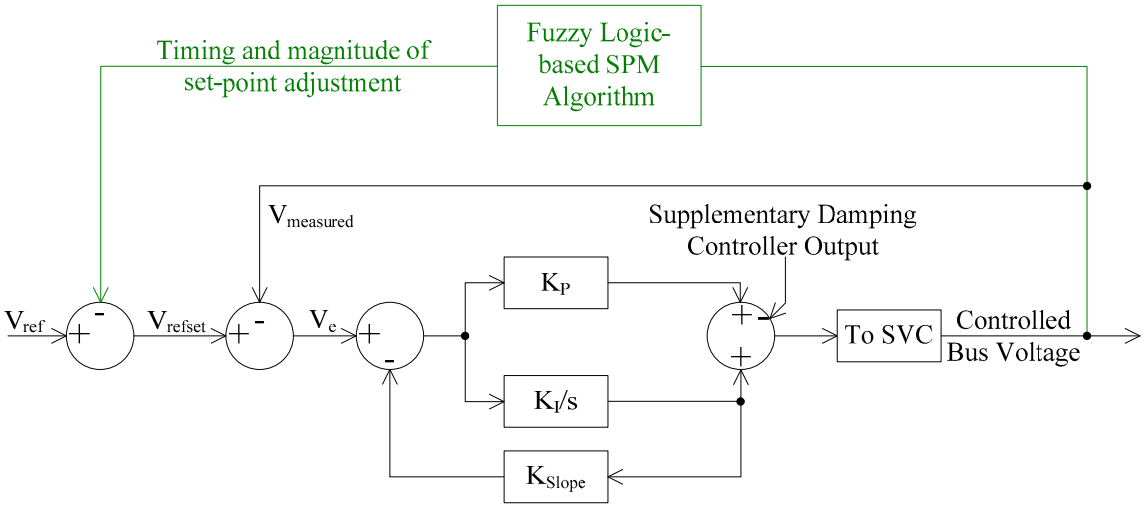

Figure 5.2: Ponton SVC voltage regulator with fuzzy logic-based SPM

5.2.1 System Characteristic

Tuning the fuzzy SPM algorithm and improving its response to set-point modifications requires a thorough understanding of the Ponton SVC system. Figure 5.3 illustrates the Ponton SVC's response to a reference voltage step change from 1.03 pu to 1.08 pu for a given system topology and PI controller gains.

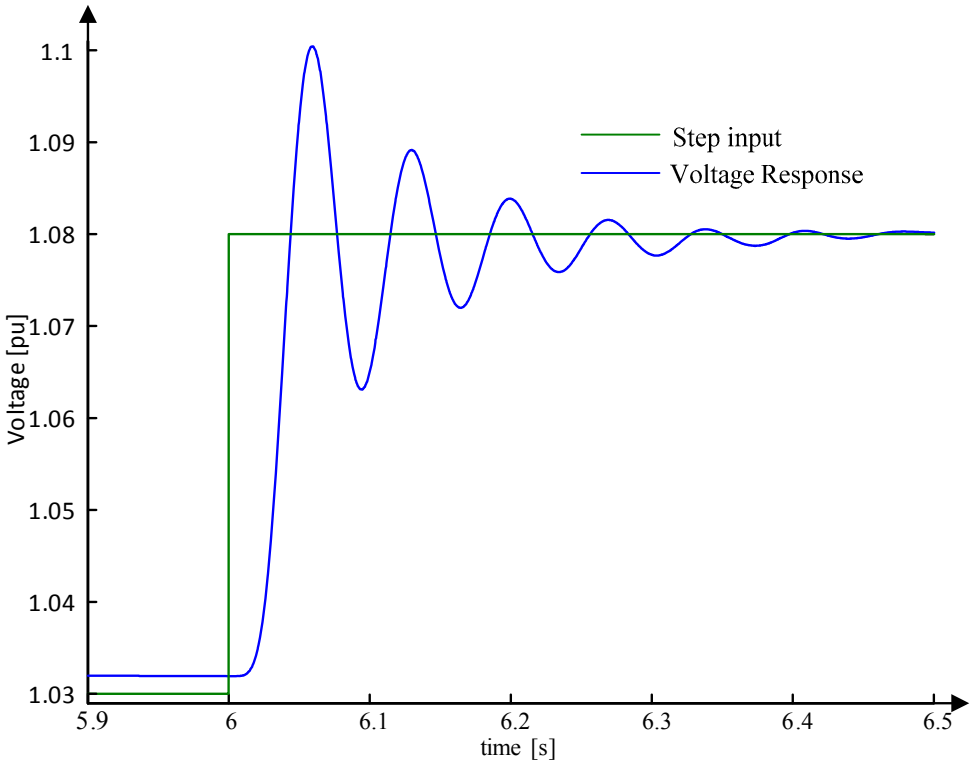

Figure 5.3: Response of Ponton SVC to a step change in reference voltage

The initial difference between the step-input voltage and the voltage response is due to the strong system voltage. This is because the modeled voltage level in the area is too high for the SVC to reduce to the desired set-point. The fuzzy SPM algorithm aims to reduce the maximum overshoot value of 1.1 pu. The relative slope and error magnitudes that can be expected from the step change must be obtained before tuning the SPM system. Figures 5.4 and 5.5 show the slope and error waveforms produced with a 1 ms

sampling interval. These figures also show that the maximum slope produced from a 0.05 pu step change in V_{ref} is approximately 3 and the maximum error is approximately 0.05 pu.

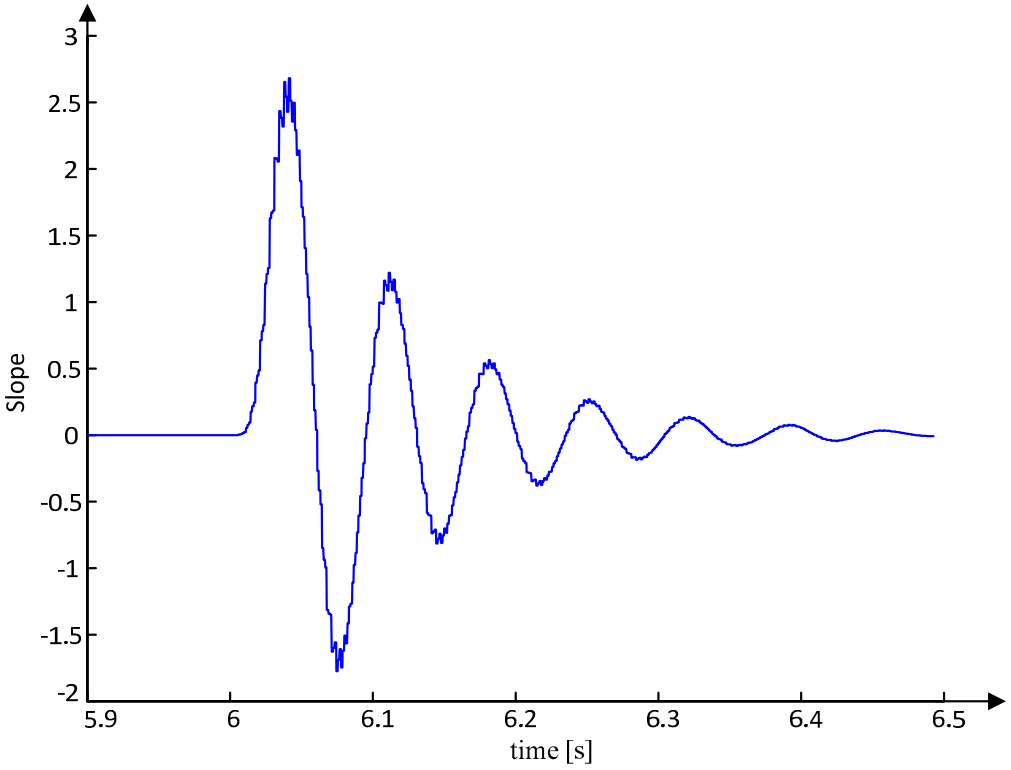

Figure 5.4: Slope waveform as a result of 0.05 pu step change in reference voltage

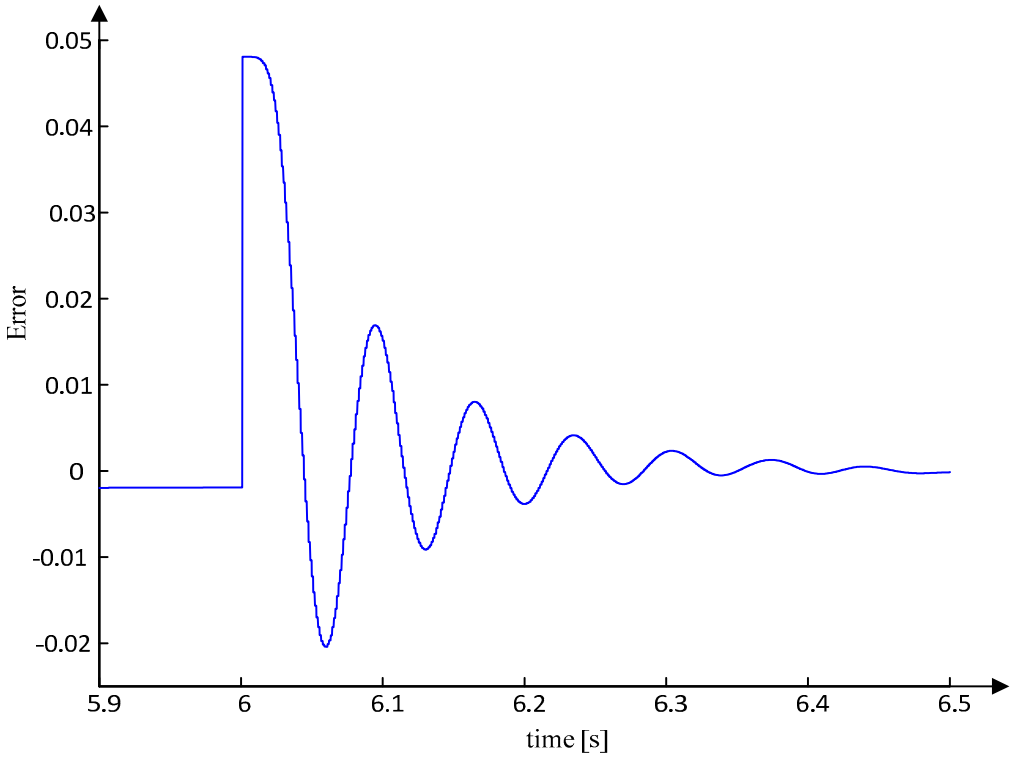

Figure 5.5: Error waveform as a result of 0.05 pu step change in reference voltage

Applying fuzzy if-then rules described in the previous chapter and knowing the above information, the prior chapter's membership functions can be scaled to produce fuzzy values that in turn produce acceptable modulation. The modulation membership functions are also scaled such that the algorithm does not excessively modulate the reference value. Figures 5.6 to 5.8 show the membership functions used to implement the fuzzy SPM.

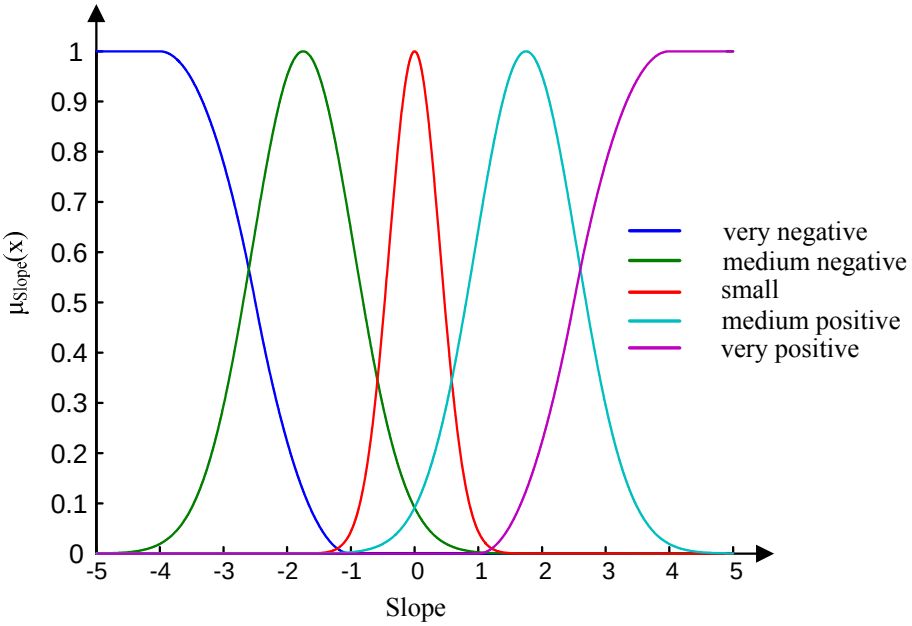

Figure 5.6: Slope membership functions used for initial attempt

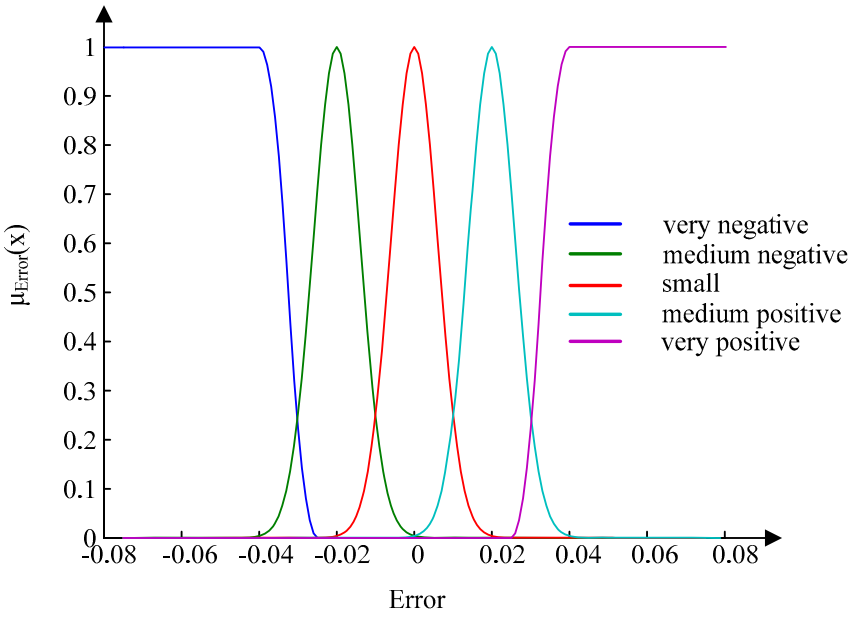

Figure 5.7: Error membership functions used for initial attempt

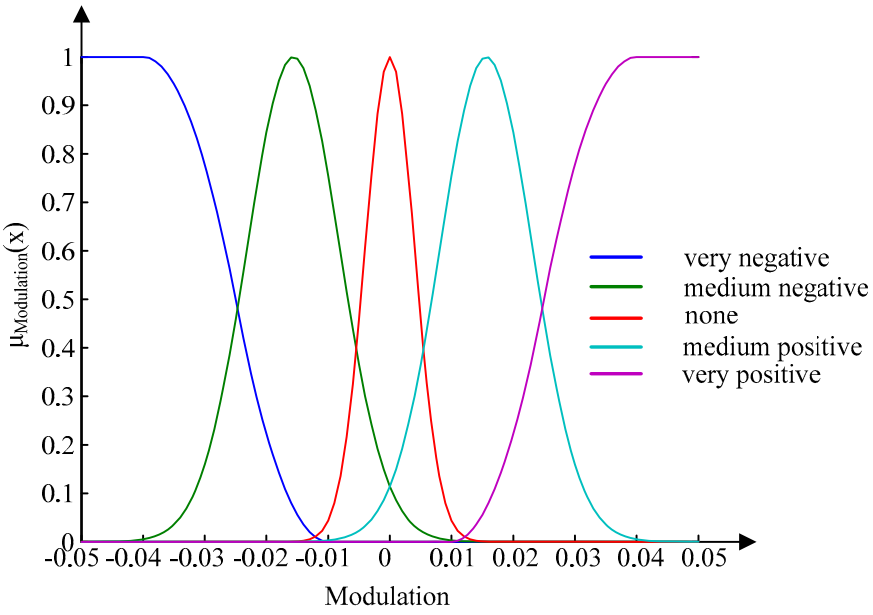

Figure 5.8: Modulation membership functions used for initial attempt

5.2.2 Initial Attempt

Once the membership functions are appropriately modified and incorporated into the algorithm, the step change shown in Figure 5.3 is applied to the Ponton SVC system, but this time with the fuzzy SPM algorithm applied. As Figure 5.9 illustrates, the algorithm has a negative effect on the Ponton voltage response compared to the uncompensated system shown in Figure 5.3.

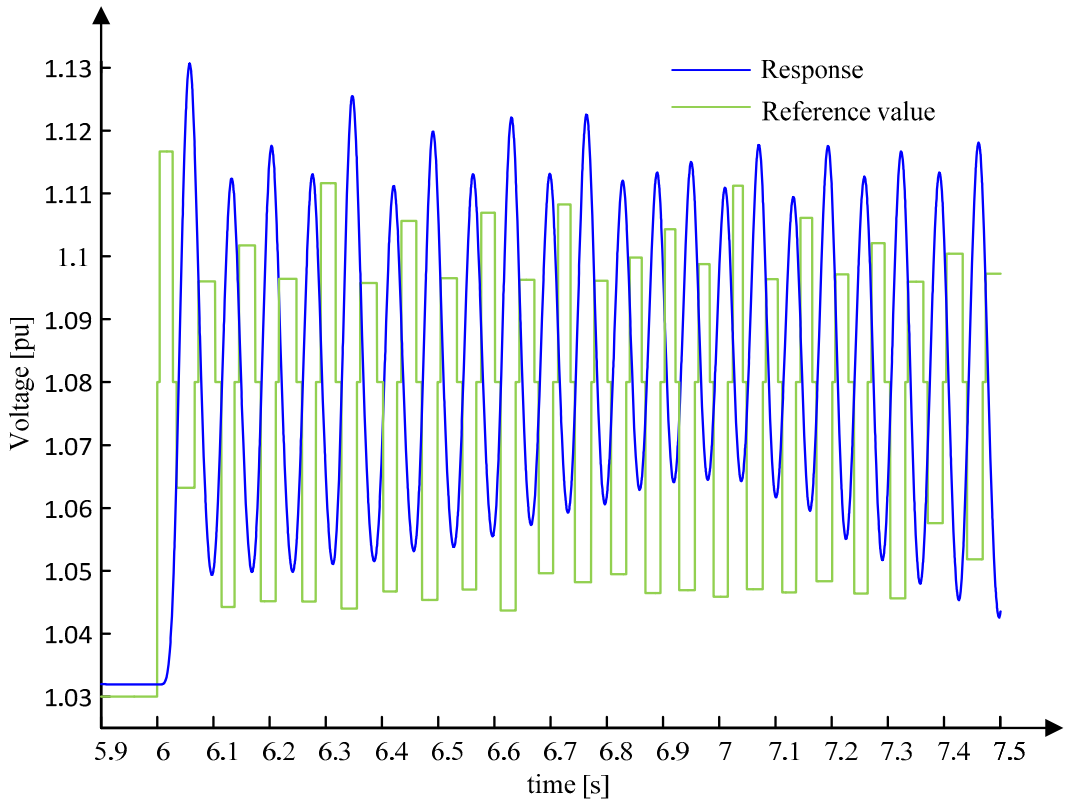

Figure 5.9: Initial attempt at improving step change performance

5.2.3 Membership Function Tuning

The response exhibits a sizeable and problematic delay 10 ms delay between the time that the Ponton SVC voltage regulator's step change occurs in reference value and the time at which the actual response of the controlled voltage begins to track the change. During this time, the algorithm receives large error values and small slope values and increases the set-point to increase the rate of rise in the Ponton voltage response. However, the delay in responding to set-point changes delays the effect of this modulation, thereby compounding the overshoot problem. Once the algorithm recognizes and attempts to compensate for this overshoot, the delayed action occurs too late to be effective.

An attempt to solve this problem involves modifying the membership functions and rules to modulate the set-point sooner in order to improve the timing of the set-point changes and the system response. The primary algorithm changes include altering the membership function shapes and reinterpreting the terms *large*, *medium*, and *small* to improve the system response. Because the delay essentially causes the slope to lag the error in time, smaller slope magnitudes must be reinterpreted as large in order to improve the fuzzy SPM algorithm's output. These resulting membership functions changes are depicted in Figures 5.10 to 5.12.

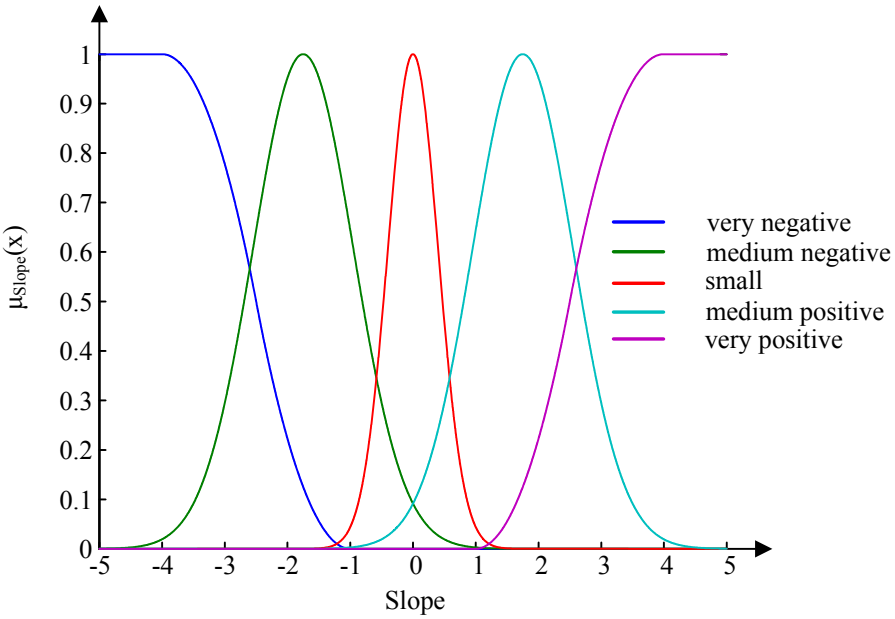

Figure 5.10: Modified slope membership functions

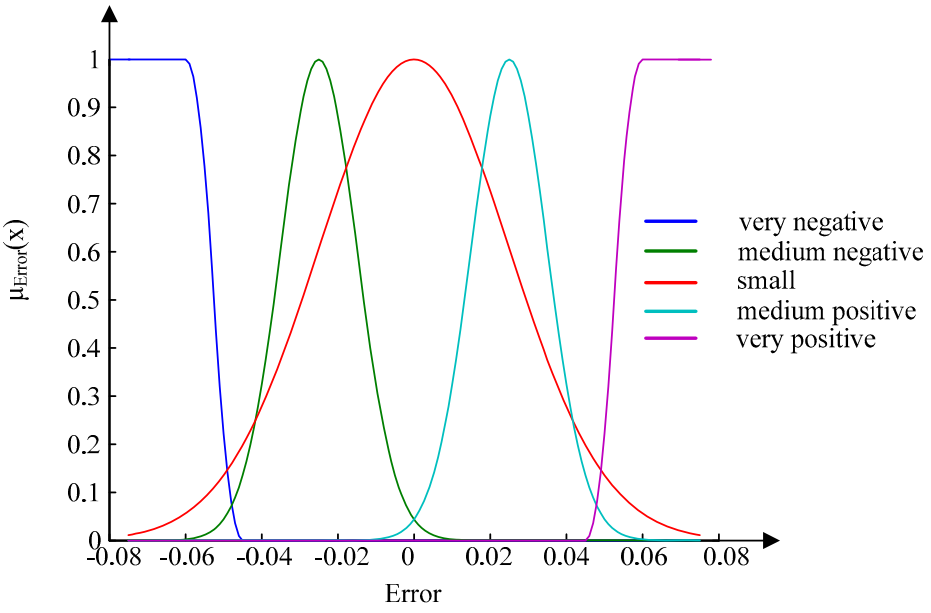

Figure 5.11: Modified error membership function

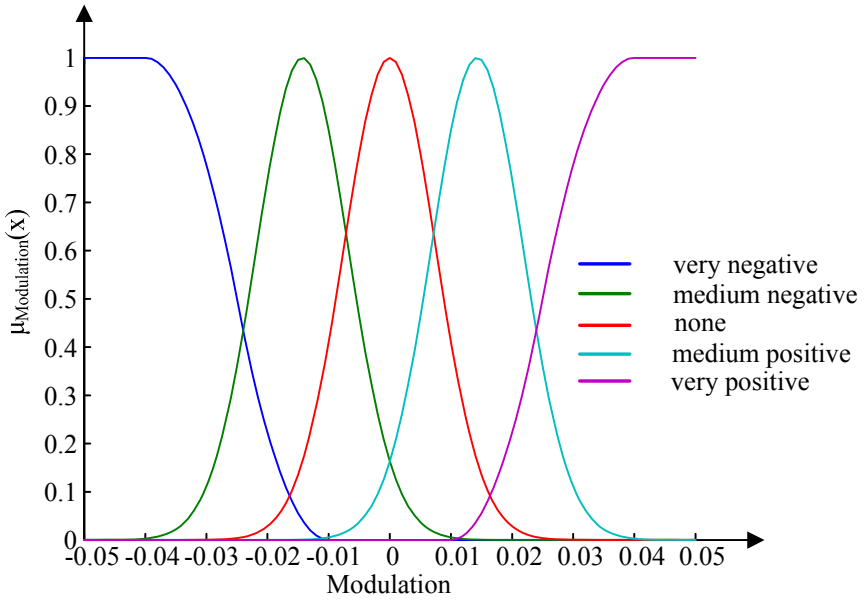

Figure 5.12: Modified modulation membership functions

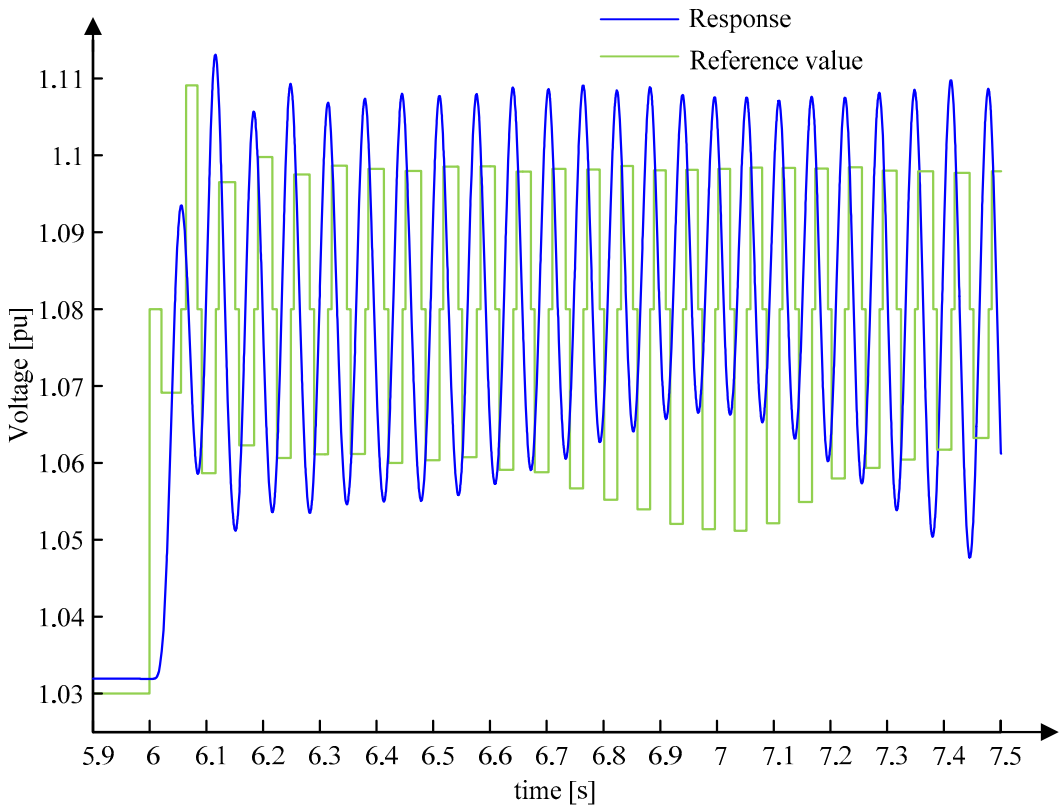

Figure 5.13: Results after re-tuning fuzzy logic-based SPM algorithm

The re-simulated results illustrated in Figure 5.13 shows a reduction of the initial peak of the uncompensated response from approximately 1.1 pu to approximately 1.095 pu, but the algorithm produced sustained non-decaying modulation changes resulting from the 10 ms controller delay. One option for eliminating this characteristic is to enable the fuzzy SPM algorithm for only a fixed time after the step change in the voltage reference value, as shown in Figure 5.14. This reduces the initial voltage peak and removes the sustained oscillations, but it requires advanced knowledge of the timing of the step change that would be required to properly enable the algorithm. Another attempt at retuning the membership functions of the fuzzy inference system and altering some fuzzy if-then rules are required to ensure the algorithm works for the step change without requiring enabling and disabling.

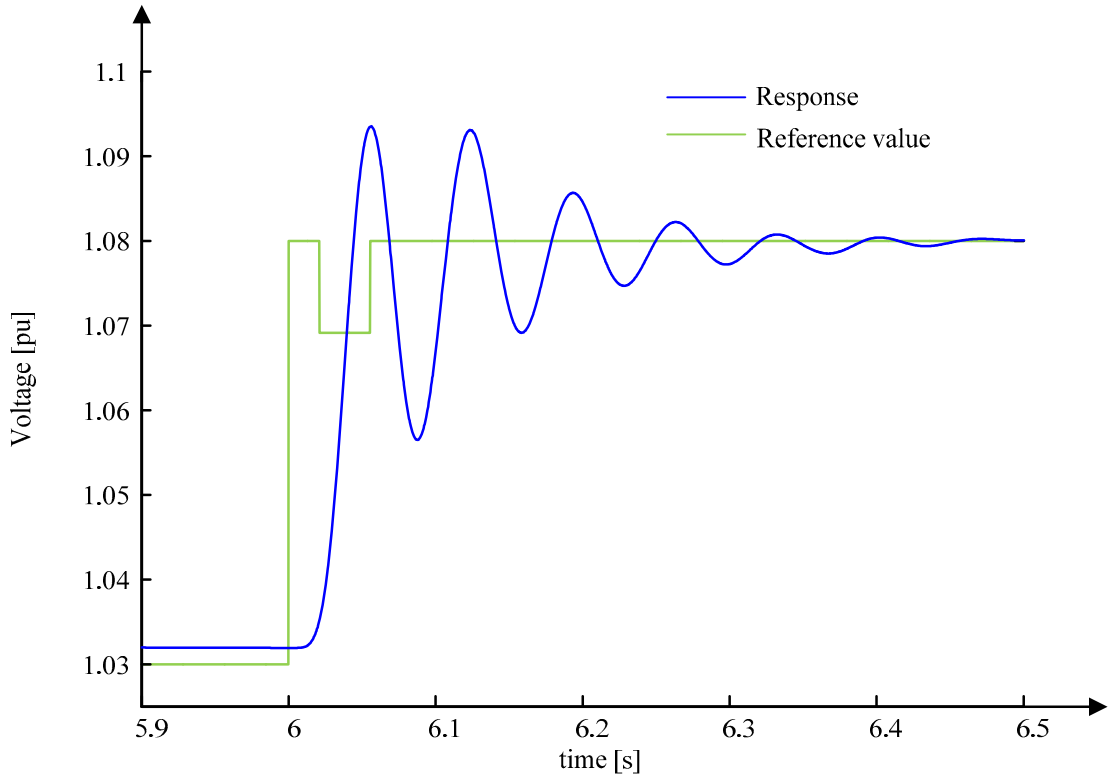

Figure 5.14: System response if SPM algorithm is enabled for a short duration after step change

5.2.4 Modifying Fuzzy Inference System

Accomplishing this requires changing both the membership functions and the rules that govern the Fuzzy Inference System itself. By emphasizing the error parameter over the slope parameter, the membership functions prevent the algorithm from modulating the set-point once the error reduces to a value below a critical threshold irrespective of the slope. This diminishes the effect of the other rules when the error is small, which allows the algorithm to stop modulating. Another change eliminates rules that were designed to quickly dampen oscillations, which are counterproductive due to the system delay and the relatively slow response when compared with the second order system

described in Chapter four. Table 5.1 shows the complete set of new rules utilized in the revised fuzzy inference system.

Table 5.1: Rules for modified fuzzy inference system

Slope \ Error	Very Negative	Medium Negative	Small	Medium Positive	Very Positive	Small
Very Negative	None	Medium Positive	None		Very Positive	None
Medium Negative	Medium Negative	None	Medium Positive	None	None	None
Small			None		Medium Positive	None
Medium Positive	Very Negative	Very Negative	Very Negative	Medium Negative	Medium Negative	None
Very Positive	Very Negative	None	None	Medium Negative	None	None

Gray boxes indicate rule changes

Figures 5.15 to 5.17 illustrate the retuned membership functions that accompany the new rules.

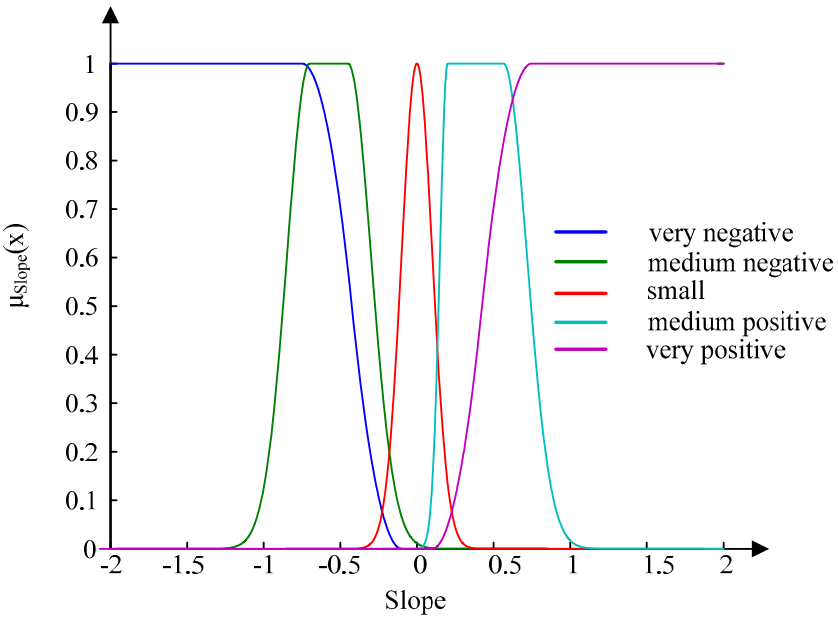

Figure 5.15: New slope membership functions

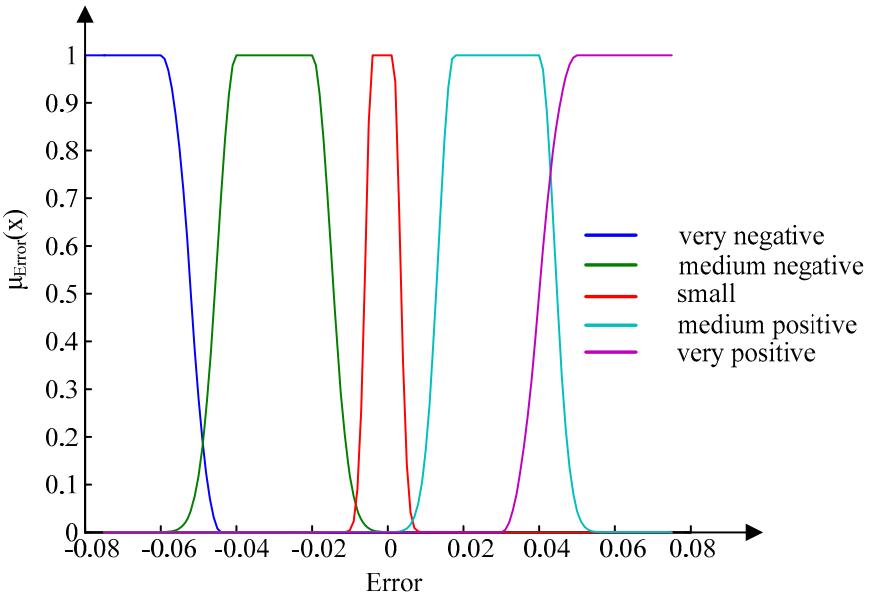

Figure 5.16: New error membership functions

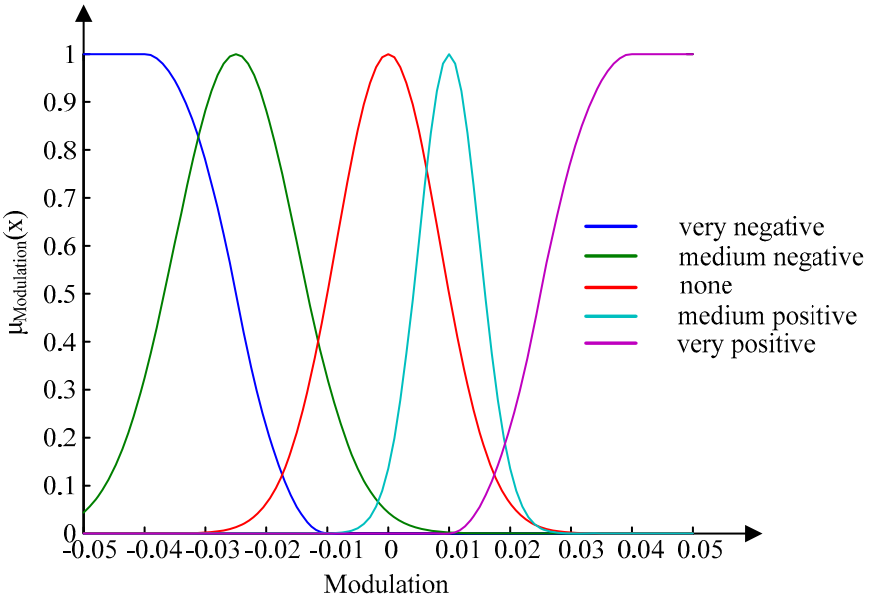

Figure 5.17: New modulation membership functions

5.2.5 Results

The results of the retuned algorithm are shown in Figure 5.18. The fuzzy SPM algorithm reduces the system overshoots and once the oscillation magnitudes reach a sufficiently small amplitude, the algorithm no longer modulates the reference voltage and the system

reaches a steady state operating point. Because the algorithm should be valid for different set-point magnitude changes, a step change from 1.03 pu to 1.05 pu is applied to the Ponton SVC system using the same FIS as above. The results with and without the SPM algorithm are shown in Figure 5.19.

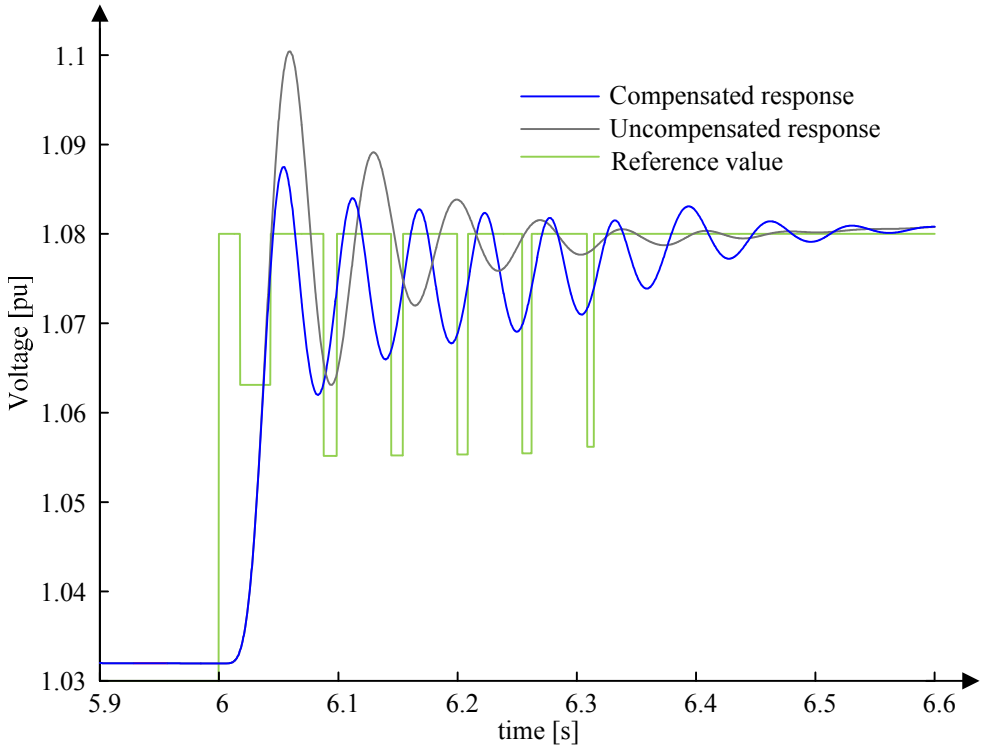

Figure 5.18: Results after major changes to the original fuzzy logic enabled SPM algorithm

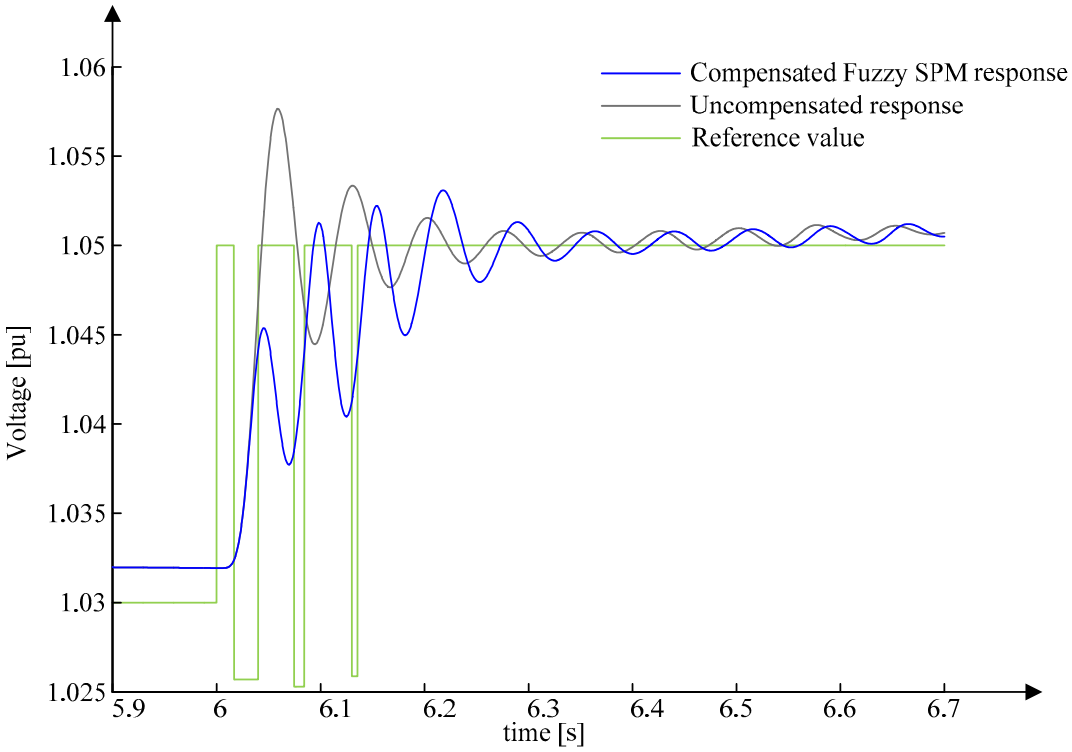

Figure 5.19: Different magnitude of step change with and without fuzzy logic based SPM algorithm

Figure 5.19 shows that the fuzzy SPM algorithm achieves its purpose of reducing the Ponton SVC system overshoot and demonstrates the ability of a fuzzy logic-enabled SPM algorithm to improve an SVC voltage regulator's performance in response to reference voltage step changes.

Chapter 6 Conclusion and Recommendations

6.1 Contributions and Conclusions

This thesis discusses several topics relating to fuzzy logic and set-point modulation and makes the following contributions:

1. Provides a comprehensive overview of existing set-point modulation techniques
2. Introduces a novel set-point modulation technique that improves control system performance by employing fuzzy logic to determine the timing and magnitude of the set-point modulation. Existing SPM methodologies have never been documented to have utilized fuzzy logic.
3. Develops and tests the fuzzy SPM algorithm in MATLAB/Simulink. The fuzzy SPM algorithm was initially developed and tested using second order systems. The results of these second order system tests include:
    - Development of a tuning procedure for the fuzzy SPM algorithm, which improves the performance of the system to which it was applied. This tuning procedure includes:
        - Observing the control system's response to set-point changes
        - Scaling the membership functions corresponding to the slope and error magnitudes so that the membership functions fuzzify the slope and error corresponding to the application
        - Scaling the modulation membership functions to provide acceptable range of modulations, and
        - Reviewing the fuzzy if-then rules to ensure adequate algorithm operation

- Once tuned, the fuzzy SPM algorithm showed insensitivity to both small and large changes in the damping ratio of the second order system to which it was applied
- The fuzzy SPM algorithm also showed an ability to stabilize an unstable second order system characterized by a negative damping ratio

4. Upon developing and testing in MATLAB/Simulink, the fuzzy SPM algorithm was developed and implemented in PSCAD/EMTDC
5. Upon implementation in PSCAD/EMTDC, the fuzzy SPM algorithm was applied to the model of Manitoba Hydro's Ponton SVC.
6. Once applied to the Ponton SVC model, the fuzzy logic-enabled SPM was shown to be capable of improving SVC control system performance in response to control changes such as set-point changes. However, the inherent delays in the control circuit made it difficult to tune the algorithm to satisfactorily improve SVC performance. As a result, this work shows that control systems that have large delays between changing reference values and system responses are unsuitable candidates for this application.

6.2 Future Work

The following future work suggestions may allow for ease of application of this idea and widen its possible applicability:

1. Create a Fuzzy Inference System component in PSCAD/EMTDC to enable easier investigations and eliminate concerns from having to interface MATLAB with PSCAD/EMTDC.

2. Quantitatively compare the fuzzy SPM to existing SPAA and SPAACE methods.
3. Investigate whether fuzzy SPM can be utilized in other applications such as HVDC, STATCOMs, and motor drive control systems.
4. Determine this approach's utility to other power system disturbances such as fault recovery or load shedding.

In summary, the implementation of a fuzzy-logic enabled SPM method allows for the intuitive modulation of a control system's set-point to obtain better performance of the control system to which it is applied.

References

[1] H. Saadat, *Power System Analysis*, 3rd ed. United States of America: PSA Publishing, 2010.

[2] P. Kundur, *Power System Stability and Control*, N. J. Balu and M. G. Lauby, Eds. New York, United States of America: McGraw-Hill, 1994.

[3] C. W. Taylor, *Power System Voltage Stability*, 1st ed., N. J. Balu and D. Maratukulam, Eds. United States: McGraw-Hill, 1994.

[4] T. J. E. Miller, *Reactive Power Control In Electric Systems*. United States of America: John Wiley & Sons, 1982.

[5] S. Filizadeh, A. M. Gole, D. A. Woodford, and G. D. Irwin, "An Optimization-Enabled Electromagnetic Transient Simulation-Based Methodology for HVDC Controller Design," *IEEE Transactions on Power Delivery*, vol. 22, no. 4, pp. 2559-2566, Oct. 2007.

[6] A. M. Gole, S. Filizadeh, R. W. Menzies, and P. L. Wilson, "Optimization-Enabled Electromagnetic Transient Simulation," *IEEE Transactions on Power Delivery*, vol. 20, no. 1, pp. 512-518, Jan. 2005.

[7] O. J. M. Smith, "Posicast Control of Damped Oscillatory Systems," *Proceedings of the IRE*, vol. 45, no. 9, pp. 1249-1255, Sep. 1957.

[8] G. H. Tallman and O. J. M. Smith, "Analog Study of Dead-Beat Posicast Control," *IRE Transactions on Automatic Control*, vol. 4, no. 1, pp. 14-21, Mar. 1958.

[9] A. Mehrizi-Sani and R. Iravani, "Online Set Point Adjustment for Trajectory Shaping in Microgrid Applications," *IEEE Transactions on Power Systems*, vol. 27,

no. 1, pp. 216-223, 2012.

[10] A. Mehrizi-Sani and R. Iravani, "Online Set Point Modulation to Enhance Microgrid Dynamic Response: Theoretical Foundation," *IEEE Transactions on Power Systems*, vol. PP, no. 99, pp. 1-8, 2012.

[11] G. Cook, "An Application of Half-Cycle Posicast," *IEEE Transactions on Automatic Control*, vol. 11, no. 3, pp. 556-559, Apr. 1966.

[12] L. Gyugyi and E. R. Taylor, "Characteristics of Static, Thyrsitor-Controlled Shunt Compensators for Power System Transmission Applications," *IEEE Transactions on Power Apparatus and Systems*, vol. PAS-99, no. 5, pp. 1795-1804, Sep. 1980.

[13] R. T. Byerly, D. T. Poznaniak, T. Jr., and E.R., "Static Reactive Compensation for Power Transmission Systems," *IEEE Transactions on Power Apparatus and Systems*, vol. PAS-101, no. 10, pp. 3997-4005, Oct. 1982.

[14] L. Gyugyi, R. A. Otto, and T. H. Putman, "Principles and Applications of Static, Thyristor-Controlled Shunt Compensators," *IEEE Transactions on Power Apparatus and Systems*, vol. PAS-97, no. 5, pp. 1935-1945, Sep. 1978.

[15] L. Gyugyi, "Reactive Power Generation and Control by Thyristor Circuits," *IEEE Transactions on Industry Applications*, vol. IA-15, no. 5, pp. 521-532, Sep. 1979.

[16] R. L. Hauth, S. A. Miske Jr., and F. Nozari, "The Role and Benefits of Static Var Systems in High Voltage Power System Applications," *IEEE Transactions on Power Apparatus and Systems*, vol. PAS-101, no. 10, pp. 3761-3770, Oct. 1982.

[17] N. G. Hingorani and L. Gyugyi, *Understanding FACTS Concepts and Technology of Flexible AC Transmission Systems*, 1st ed., M. El-Hawary, Ed. New York, United

States: IEEE Press, 2000.

[18] L. Gyugyi, "Power Electronics in Electric Utilities: Static Var Compensators," *Proceedings of the IEEE*, vol. 76, no. 4, pp. 483-494, Apr. 1988.

[19] A. Olwegard, K. Walve, G. Waglund, H. Frank, and S. Torseng, "Improvement of Transmission Capacity by Thyristor Controlled Reactive Power," *IEEE Transactions on Power Apparatus and Systems*, vol. PAS-100, no. 8, pp. 3930-3939, Aug. 1981.

[20] T. Ohyama, K. Yamashita, T. Maeda, H. Suzuki, and S. Mine, "Effective Application of Static Var Compensators to Damp Oscillations," *IEEE Transactions onPower Apparatus and Systems*, vol. PAS-104, no. 6, pp. 1405-1410, Jun. 1985.

[21] L. Gyugi, "Power Transmission Control: Basic Theory; Problems and Needs; FACTS Solutions," in *Flexible AC Transmission Systems (FACTS)*. Stevenage, United Kingdom: The Institution of Electrical Engineers, 1999, ch. 1, pp. 1-72.

[22] R. M. Mathur and R. K. Varma, *Thyristor-based FACTS Controllers for Electrical Transmission Systems*, 1st ed., M. E. El-Hawary, Ed. Danvers, United States of America: Wiley-Interscience, 2002.

[23] L. A. Zadeh, "Outline of a New Approach to the Analysis of Complex Systems and Decision Processes," *IEEE Transactions on Systems, Man, and Cybernetics*, vol. SMC-3, no. 1, pp. 28-44, Jan. 1973.

[24] R. M. Mathur, *Static Compensators for Reactive Power Control*, 1st ed. Winnipeg, Canada: Cantext Publications, 1984.

[25] L. A. Zadeh, "Fuzzy Sets," *Information and Control*, vol. 8, pp. 338-353, 1965.

[26] W. Pedrycz, *Fuzzy Control and Fuzzy Systems*, 2nd ed., M. J. H. Sterling, Ed.

Somerset, England: Research Studies Press LTD., 1993.

[27] E. H. Mamdani, "Application of Fuzzy Logic to Approximate Reasoning Using Linguistic Synthesis," *IEEE Transactions on Computers*, vol. C-26, no. 12, pp. 1182-1191, Dec. 1977.

[28] M. Inc., *Fuzzy Logic Toolbox User's Guide*, 5th ed. Natick, United States of America: Mathworks, 2010.

[29] H. P. Huang, M. L. Roan, and J. C. Jeng, "On-line Adaptive Tuning for PID Controllers," *IEE Proceedings, Control Theory and Applications*, vol. 149, no. 1, pp. 60-67, Jan. 2002.

[30] J. Y. Hung, "Feedback Control with Posicast," *IEEE Transactions on Industrial Electronics*, vol. 50, no. 1, pp. 94-99, Feb. 2003.

[31] D. A. N. Jacobson, "Northern AC Transmission System Requirements," Manitoba Hydro, Winnipeg, System Planning Report, 2002.